# CHARACTERIZATION OF RESISTANCE-WELDED THERMOPLASTIC COMPOSITE DOUBLE-LAP JOINTS

By

#### Aurélie Chazerain

Mechanical Engineering Department

McGill University, Montreal

June 2009

A thesis submitted to McGill University in partial fulfilment of the requirements of the degree of Aurélie Chazerain

© Aurélie Chazerain, 2009

# **Abstract**

An investigation of resistance welding of thermoplastic composite double-lap shear joints is presented. Double-lap shear specimens consisting of carbon fibre/poly-etherether-ketone (PEEK/CF), carbon fibre/poly-etherketone-ketone (PEKK/CF), carbon fibre/poly-ether-imide (PEI/CF) and glassfibre/poly-ether-imide (PEI/GF) were resistance-welded using a stainless steel mesh heating element. The objective of this work was to study the mechanical performances of the double lap shear resistance-welded joints and to compare them with the single lap shear resistance-welded joints. The welded specimens were analyzed using static and dynamic lap shear tests and optical and scanning electron microscopy. Lap shear strengths of 53 MPa, 49 MPa, 45 MPa and an extrapolated value of 34 MPa were obtained for PEEK/CF, PEKK/CF, PEI/CF and PEI/GF double-lap joints, respectively. Infinite fatigue lives were obtained at 30% for PEEK/CF and PEKK/CF, 25% for PEI/CF and 20% for PEI/GF. Resistance-welded double-lap joints were found to have equivalent static and fatigue mechanical properties compared with single-lap joints, for all materials tested.

## Résumé

Ce travail présente une étude des joints à recouvrement double de matériaux composites à matrice thermoplastique assemblés par soudage par résistance. Des échantillons de joints à recouvrement double constitués de fibre de carbone/polyéther éther cétone (PEEK/CF), fibre de carbone/polyéther cétone cétone (PEKK/CF), fibre de carbone/polyéther imide (PEI/CF) et fibre de verre/polyéther imide (PEI/CF), ont été assemblés pas soudage par résistance à l'aide d'un élément chauffant en acier inoxydable. L'objectif de ce travail est d'étudier les performances mécaniques des joints à recouvrement double soudés pas résistance et de les comparer avec celles des joints à recouvrement simple. Les échantillons soudés ont été analysés à l'aide de tests de chargement statiques et dynamiques, ainsi que pas microscopie optique et par microscopie électronique à balayage. Une résistance au cisaillement de 53 MPa, 49 MPa, 45M Pa, et une valeur extrapolée de 34 MPa ont été obtenues pour les joints à recouvrement double de PEEK/CF, PEKK/CF, PEI/CF et PEI/GF, respectivement. Une durée de vie indéterminée en fatigue de 30% du chargement statique pour les joints de PEEK/CF et PEKK/CF, de 25% pour les joints de PEI/CF, et de 20% pour les joints de PEI/GF ont été obtenues. Pour chacun des matériaux testés, les joints à recouvrement double soudés par résistance ont donné lieu à des propriétés mécaniques en statique et en fatigue équivalentes à celles des joints à recouvrement simple.

# **Acknowledgements**

I would like to express my gratitude to all those who gave me the possibility to complete this thesis.

I would like to gratefully acknowledge my supervisor, Pr Pascal Hubert, for his support and the valuable advice and guidance he provided me during the completion of my thesis. I would also like to thank him for giving me the opportunity of going to the SAMPE conference in Baltimore. A special thanks for the warm welcome and the barbecue parties with his family!

I would like to acknowledge with gratitude Dr Ali Yousefpour for allowing me to work with the Aerospace Manufacturing and Technology Center, and for his priceless advice and assistance. I would like to thank him for taking the time to help me, despite his very busy schedule.

I would also like to acknowledge the Design and Production of Composite Structures group in Delft University, especially Dr Hararld Bersee, Dr Irene Fernandez and Shafqat Rasool. Thank you for welcoming me in the Netherlands and for the technical assistance.

I would like to thank all my fellow students in McGill Structures and Composite Materials Laboratory for their help, their advice, and their friendship. Special thanks to Jonathan Laliberté for his technical assistance, and to Meysam Rahmat for helping me with the SEM.

Finally, I would like to convey thanks to the Canadian Research Chair in Advanced Composites and to the National Research Council of Canada for providing the financial means and laboratory facilities.

# **Table of Contents**

Al	ostract.		2
Ré	ésumé		3
A	knowle	edgements	4
Ta	ble of (	Contents	5
Li	st of Fig	gures	8
Li	st of Ta	ıbles	12
1	Intro	ductionduction	13
	1.1 G	eneral objective	15
	1.2 Oı	rganisation of the work	15
2	Litera	ature Review	16
,	2.1 Re	esistance welding process	16
	2.1.1	Heating element	17
	2.1.2	Insulating blocks	18
	2.1.3	Adherends	19
	2.1.4	Geometry of the joint	19
,	2.2 M	echanical performances of resistance-welded joints	20
	2.2.1	Lap shear static tests	20
	2.2.2	Lap shear dynamic tests	24
	2.2.3	Other characterization methods	24

	2.3	Joi	nt design	25
	2	.3.1	Influence of the geometry: single and double-lap joints	. 25
	2	2.3.2	Stress analysis of the joint	. 31
		2.3.2	.1 Adhesive joints	. 31
		2.3.2	.2 Other types of joints	. 35
	2.4	Su	mmary	36
	2.5	Spe	ecific research objectives	37
3	F	Exper	imental procedures	38
	3.1	Spe	ecimens preparation	38
	3	.1.1	High performance thermoplastic composites	. 38
	3	.1.2	Material used and experimental set-up	. 40
	3	.1.3	Resistance welding process	. 43
	3.2	Me	echanical testing	47
	3	.2.1	Tensile static testing	. 47
	3	.2.2	Tensile fatigue testing	. 49
	3.3	Int	erface characterization and fracture analysis	50
	3	.3.1	Optical microscopy	. 50
	3	.3.2	Scanning electron microscopy	. 51
4	F	Exper	imental results	52
	4 1	Sta	itic tests results	52

4.1.1	Double-lap joints results	52
4.1.2	Comparison with single-lap joints	55
4.2 Fa	atigue test results	58
4.2.1	Double-lap results	58
4.2.2	Comparison with single-lap joints	61
4.3 O	bservation of the fracture surfaces	64
4.3.1	Failure modes	64
4.3.2	Fracture surfaces from static tests	65
4.3.3	Fracture surfaces from fatigue tests	68
4.4 In	terface quality characterization	72
4.4.1	Scanning electron microscopy (SEM)	72
4.4.2	Optical microscopy	77
5 Discu	ission and stress analysis	80
5.1 G	eometry and material properties	81
5.2 Be	oundary Conditions	81
5.3 Ro	esults	82
6 Conc	clusions and future work	89
6.1 Co	onclusions	89
6.2 Ft	uture work	90
Reference	es	91

# **List of Figures**

Figure 1: Typical experimental resistance welding set-up [9]
Figure 2: Skin/stringer geometry with square-ended (a) and tapered (b) flanges [36]20
Figure 3: Fatigue results of PEKK/CF, PEI/CF and PEI/GF resistance-welded single-
lap joints [43]
Figure 4: Joint configurations: (a) single-lap, (b) double-lap, (c) scarf, and (d) strap
[48]
Figure 5: Strength of single-lap and double-lap bolted joints, under various
environmental conditions [51]
Figure 6: Internal bending in double-lap joint [54]
Figure 7: Maximum bond stresses in single and double lap joints, for a fixed loading
stress $\sigma x = 10[56]$
Figure 8: Shear strength of double-lap bonded joints [57]
Figure 9: Shear strength of single-lap bonded joints [58]
Figure 10: Configurations and deformations of theoretical models: (a) 1-D bar model
(Volkersen, 1938; de Bruyne, 1944) for double-lap joint; (b) 1-D bar model
(Volkersen, 1938) for single-lap joint; and (c) I-D beam model (Goland and
Reissner, 1944) for single-lap joint[64].
Figure 11: Configurations and deformations of theoretical models including the shear
deformations of adherends: (a) 1-D bar model for double-lap joint; (b) I-D bar model
for single-lap joint; and (c) 1 -D beam model for single-lap joint.[64]
Figure 12: Schematics of the geometry and material parameters of the overlaminated
double-lap joint[74]

Figure 13: Normalized interfacial shear stresses (a) and peel stresses (b) along the	ne
overlap of an overlaminated double-lap joint[74].	36
Figure 14: Chemical structure of PEEK [78]	39
Figure 15: Chemical structure of PEKK [78]	39
Figure 16: Chemical structure of PEI [79]	39
Figure 17: Resistance welding experimental set-up	13
Figure 18: Temperature at the weld interface for each material	14
Figure 19: Different steps followed for the first weld	15
Figure 20: Different steps followed for the second weld	16
Figure 21: Double-lap sample clamped in the MTS 100kN machine	18
Figure 22: Schematic of the tested sample	19
Figure 23: Influence of the cooling rate on properties of PEEK/CF [80]	53
Figure 24: Coupon failure of a PEI/GF sample	54
Figure 25: Static load-Displacement curve for double-lap PEEK/CF, PEKK/C	F,
PEI/CF and PEI/GF joints	54
Figure 26: Static lap shear strength of resistance-welded double-lap PEEK/C	F,
PEKK/CF and PEI/CF joints	55
Figure 27: Static load-displacement curves of PEEK/CF [40]	56
Figure 28: Static load-displacement curves of PEKK/CF [18]	57
Figure 29: Static load-displacement curves of PEI/CF [18]	57
Figure 30: Static load-displacement curves of PEI/GF[18]	58
Figure 31: Lap shear strength values for single-lap and double-lap joints [18; 40] 5	58
Figure 32: Fatigue performance of double-lap specimens for PEEK/CF, PEKK/C	F,
PEI/CF and PEI/GF	50

Figure 33: Fatigue performance of double-lap specimens for PEEK/CF, PEKK/CF	,
PEI/CF and PEI/GF (% LSS)6	0
Figure 34: Fatigue performance and modes of failure of double-lap PEI/GF	1
Figure 35: Fatigue performance of PEEK/CF (%LSS)[40]	2
Figure 36: Fatigue performance of PEKK/CF (% LSS)[43]6.	3
Figure 37: Fatigue performance of PEI/CF (% LSS)[43]	3
Figure 38: Fatigue performance of PEI/GF (% LSS)[43]6	4
Figure 39: Schematic of the failure modes [9]	5
Figure 40: Fracture surfaces from PEEK/CF static tests	6
Figure 41: Fracture surfaces from PEKK/CF static tests	7
Figure 42: Fracture surfaces from PEI/CF static tests	7
Figure 43: Fracture specimen of PEI/GF from static tests	8
Figure 44: Schematics of the double-lap specimen	8
Figure 45: Fracture surfaces from fatigue tests for the two welds for: (a) PEEK/CF	,
(b) PEKK/CF, (c) PEI/CF, (d) PEI/GF69	9
Figure 46: Schematics of the welding configuration for (a) the first weld and (b) the	e
second weld	0
Figure 47: Schematics of the suggested welding configuration for the second weld. 7	1
Figure 48: Heating element deterioration	1
Figure 49: Temperature distribution along the length of the weld as predicted by 3I	)
model[21]	2
Figure 50: Fracture surface of fatigue tested PEKK/CF (SEM x40)	3
Figure 51: SEM image of (a): Polymer-rich region (450x), (b): Heating element	ıt
(406x)	3

Figure 52: SEM image of (a): Inner laminate fibres (1490x) and (b): Outer laminate
fibres (1500x)
Figure 53: SEM pictures of the heating element impregnation for (a) PEI/CF, (b)
PEEK/CF, (c) PEI/GF and (d) PEKK/CF
Figure 54: Typical fracture surface of fatigue tested PEI/GF (30×)
Figure 55: Heating element impregnation for a fatigue tested PEI/GF specimen
(350×)
Figure 56: Fracture surface of fatigue tested PEEK/CF (30×)
Figure 57: Micrographs 25× and 100× of the cross-section at the center (a) and edge
(b) of a double-lap PEKK/CF specimen
Figure 58: Micrographs 25x and 100x of the cross-section at the center (a) and edge
(b) of a double-lap PEI/CF specimen
Figure 59: Boundary conditions for (a): single-lap joint and (b): double-lap joint 82
Figure 60: Deformed shape of single-lap joint
Figure 61: Deformed shape of double-lap joint
Figure 62: Shear stresses $\tau_{xy}$ in (a) single-lap joint and (b) double-lap joint
Figure 63: Normal stresses in (a) single-lap joint and (b) double-lap joint 85
Figure 64: Stresses along the interface for the single-lap joint
Figure 65: Stresses along the interface for the double-lap joint

# **List of Tables**

Table 1: Reported lap shear strengths for APC-2/AS4 resistance-welded s	ingle-lap
joints	21
Table 2: Reported lap shear strengths of UD-16 plies APC-2/AS4 resistance	e-welded
single-lap joints	22
Table 3: Reported lap shear strengths for resistance-welded PEKK/CF, PE	I/CF and
PEI/GF single-lap joints	23
Table 4: Material properties of PEEK, PEKK and PEI [76]	40
Table 5: Materials used and their characteristics	42
Table 6: Welding conditions	47
Table 7: Polishing method used for cross-section observation of the de	ouble-lap
samples	50
Table 8: APC2/AS4 Mechanical properties [82]	81

#### 1 Introduction

High-performance thermoset matrix composites are typically used in aircraft structures. However, in the late 1980s, high performance thermoplastic matrix composites were introduced. These materials had similar mechanical properties but superior impact resistance and toughness compared to thermoset matrix composites. Another advantage of thermoplastics is their ability to be melted and reshaped, allowing them to be welded.

In the aerospace industry, the complexity of the structures requires cost-effective, reliable joining methods. The classical joining methods are mechanical fastening and adhesive bonding. Mechanical fastening has many drawbacks as it involves the drilling of a hole that introduces stress concentrations, and the insertion of rivets, that add cost and weight to the structure. Adhesive bonding provides more uniform stress distribution compared to mechanical fastening and can be used to join any materials. However, it requires a careful surface preparation that can be complex and time-consuming. Moreover, airworthiness authorities still require adhesive bonded structural composites on aircraft to be riveted, so adhesive bonding is not a very good alternative. On the other side, riveting is not required for welded joints[1], which eliminates time and labour of drilling and riveting, as well as the extra weight and cost introduced by the rivets.

Several welding methods are available to join thermoplastic composites and can be classified in 3 types based on the approach used to heat the weld interface: thermal, friction and electromagnetic. One of the most promising methods, resistance welding, was selected by Airbus for the assembly of the leading edge of the A380. This

electromagnetic welding method is fast and simple and can be automated to weld large parts together.

A large number of experimental investigations have been performed on resistance welding of thermoplastic composites. These investigations mostly focused on two geometries, the single-lap shear and the double cantilever beam geometries, that were used to study and optimize the welding parameters. Significant efforts focused on the modelling the heat transfer and consolidation process where the influence of the various welding parameters on the weld quality and the mechanical performance of single-lap joints was investigated. However, the influence of the joint configuration, and the stress distribution in the joint was not systemically studied for resistance welding. Studies on adhesive bonding have shown that the peel stresses are critical in adhesive joints, and that the joint configuration has a major influence on the stress distribution and the mechanical performances of the joint. In particular, the double-lap configuration was found to reduce peel stresses and improve the joint's strength.

# 1.1 General objective

In light of the above, the main objective of this work was to investigate and characterize the double-lap configuration for resistance-welded thermoplastic composite joints.

# 1.2 Organisation of the work

The thesis is organized as followed:

- Chapter 2 will provide a general overview of the resistance welding process, with a focus on the mechanical performances of the resistance welded-joints and the design of the joint.
- Chapter 3 will present the experimental procedures used for the characterization of the resistance-welded thermoplastic composite double-lap joints.
- Chapter 4 will present the experimental results on the double-lap joint and compare them with the results obtained with the single-lap configuration.
- Chapter 5 will focus on a stress analysis of the resistance-welded joints and a discussion of the numerical results.
- Chapter 6 will highlight the findings of this work and propose future work.

## 2 Literature Review

# 2.1 Resistance welding process

Resistance welding has been identified as being one of the most promising techniques for joining thermoplastic composites [2]. It offers a number of advantages compared with other joining methods: unlike mechanical fastening it creates a uniform joint with no stress concentration and no damage or distortion induced to the fibres; unlike adhesive bonding it requires little or no surface preparation. It is a fast, inexpensive technique that requires simple, low-cost equipment, which could be made portable for repair purposes [3]. It also offers a possibility of reprocessing if flaws or defects were detected at the joint interface [4][5]. Moreover, resistance welding can be applied to weld large components [6]. It has been applied to complicated joints in automotive applications, plastic pipes [7], containers and medical devices [8], and more recently, aerospace applications, the most common example being the J-nose of Airbus A340 and A380 [1].

The working principle of the resistance welding process is rather simple. The heat is provided by an electrically resistive implant, also called the heating element, which is trapped between the parts to be joined, under the application of pressure. When electrical current passes through the heating element, heat is generated due to Joule's heating effect. The temperature increases at the interface between the two parts, and the polymer surrounding the heating element starts to melt. When nominal melting is achieved, the current is stopped and the joint is allowed to cool while the pressure is maintained, until it solidifies and form the weld. The heating element remains trapped in the joint, allowing reprocessing by applying electrical current again. However, its

presence in the joint might affect the strength of the structure, so compatibility with the joint material is critical [9].

A typical experimental set-up for resistance welding is shown in Figure 1. It consists of several basic components: the laminates to be joined, the heating element, an electrical power supply with voltmeter and ampere meter, electrical connectors and wires, insulating blocks to avoid thermal losses and a pressure application system. Thermocouples may also be used for temperature measurements purpose.

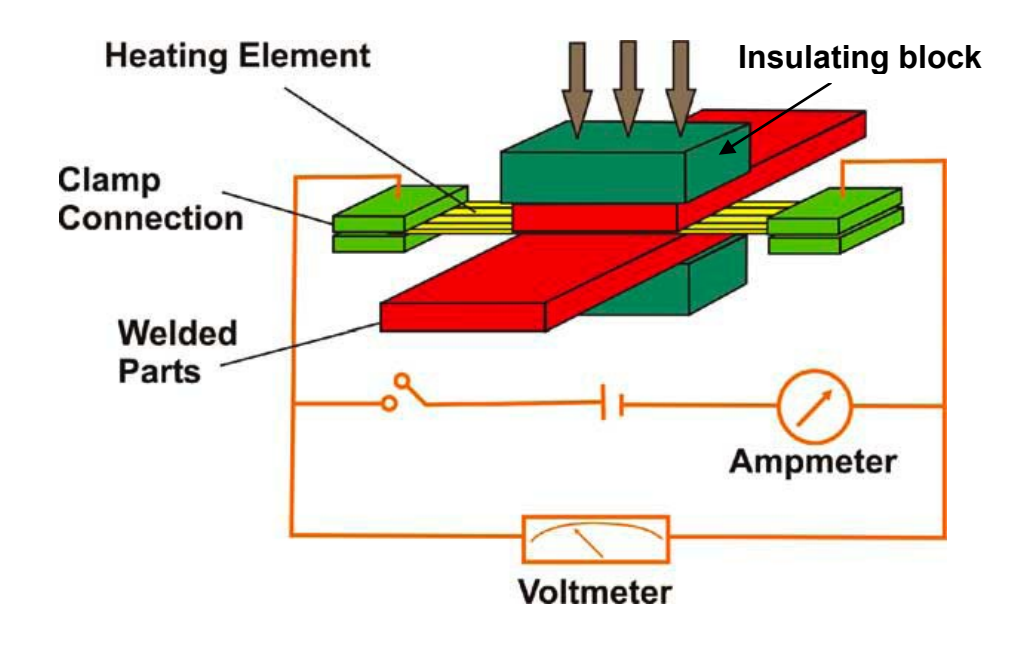


Figure 1: Typical experimental resistance welding set-up [9]

#### 2.1.1 Heating element

The heating element is one of the most critical components of the resistance-welding set-up, as it provides the heat to melt the polymer, and remains embedded in the weld afterwards. The main parameters that affect the choice of the heating element are the thermal behaviour and the mechanical performance that might be affected by the introduction of a foreign material. The heating element can be made of any electrically conductive material, such as metal mesh, carbon trip or conductive prepreg thermoplastic composite are usually chosen [10]. In the nineties and twenties,

carbon fibre prepreg were used as heating element because of their compatibility with carbon fibre reinforced laminates [11][12]. Heating element were produced from a single layer of unidirectional or fabric prepreg carbon fibre. The heat efficiency proved to be similar for fabric and unidirectional heating elements, however the temperature uniformity was better for the fabric elements, as the heat transfer was very poor in the transverse direction for unidirectional elements. Another problem that arose was the brittleness of the carbon fibres that resulted in the reduction of the connection efficiency with the power supply for both types of heating elements [13]. Another type of heating element, consisting of a stainless steel mesh, was thus introduced. A more homogeneous temperature distribution was generated by the metal mesh at the bonding surface, resulting in better quality welds [14]. Although the metal mesh induced a lower resistance to galvanic corrosion, it was more resistant to the clamping pressure from the electrical connectors and it improved the temperature homogeneity of the weld area, leading into better overall performance of the weld [15]. The wire diameter and open gap width of the metal mesh were found to affect the polymer diffusion and mechanical interlocking in the weld, and hence the quality of the weld [16][17]. Therefore, the optimization of the heating element size was conducted on three different materials (CF/PEKK, CF/PEI and GF/PEI), and a stainless steel mesh with a wire diameter of 0.04 mm and open gap width of 0.09 mm was found be the optimum one, for all three materials [18].

#### 2.1.2 Insulating blocks

The choice of the insulation material is critical in the resistance welding process as it determines how much heat is lost during the process. Different kinds of materials have been investigated, such as ceramics, Maronite [19], asbestos [3], spruce wood [10] and [12], oak wood [13], high-density fibre wood [15], and silicon rubber [20]. It

was shown that the choice of insulating material influences greatly the resistance welding process. Talbot [21] compared the effect of different types of insulating material (free convection, ceramic tooling-plates and stainless steel tooling plates) in a numerical model. It was shown that the thermal properties of the tooling-plates have significant effects on the welding time and temperature gradient through the weld thickness, and ceramic tooling-plates were shown to be a good choice as insulation tooling-plates.

#### 2.1.3 Adherends

Resistance welding can be used to weld dissimilar materials, including thermoplastics, thermoplastic composites, metals and some thermosets. However, it was originally developed for high performance thermoplastic composites [22], such as carbon fibre reinforced polyetheretherketone (PEEK/CF) [3] [8] [11] [19] [23], or polyetherimide reinforced with carbon or glass fibre (PEI/CF or PEI/GF) [4] [12] [14] [24] [25]. Resistance welding was also used to weld polypropylene reinforced with carbon or glass fibres (PP/CF and PP/GF) [26] [27], and a dual-polymer composite system, graphite-polyarylsulfone/polysulfone [28]. Resistance welding of dissimilar materials including metals and thermosetting composites has also been investigated: L113 Aluminum/APC-2 [29], Steel [30], Aluminum-GF/PP [31], 7075-T6 Aluminum -PEEK/CF [32], 7075-T6 Aluminum-CF/PEI [33], PSU-CF/BMI [34], and CF/epoxy-CF/PEI [35].

#### 2.1.4 Geometry of the joint

Only two-types of joint geometry were extensively investigated for the resistance welding process: the single-lap shear and the double cantilever beam (DCB) configurations [9] [11] [12] [19] [22] [26] . These are very simple configurations, which are very well suited for evaluation and optimization of resistance welding

parameters. However, they are not always representative of the geometries that are used in real industrial applications. Dubé *et al* investigated a skin/stringer configuration in order to better represent the loading cases of a real-life situation, in the case of the aerospace industry. Two specimen geometries were used: square-ended and tapered flanges, in order to study the effect of both specimen types on stress concentration [36] [37]. They are shown in Figure 2.

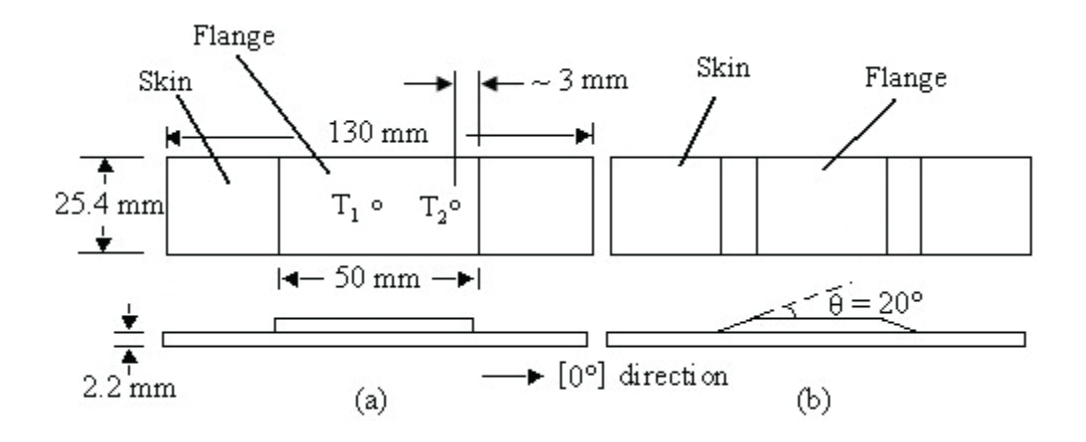


Figure 2: Skin/stringer geometry with square-ended (a) and tapered (b) flanges [36]

# 2.2 Mechanical performances of resistance-welded joints

The joints performances are usually evaluated using the lap shear or double cantilever beam (DCB) testing methods. The failure modes can then be characterized by looking at the fracture surfaces with optical microscopy or scanning electron microscopy (SEM). Non-destructive evaluation methods such as ultrasonic C-scan inspections can also be used to determine the weld quality.

#### 2.2.1 Lap shear static tests

The lap shear tests are performed according to the ASTM D1002 standard test method, with a weld area of 25.4mm by 12.7mm. Lap shear strengths are calculated simply by dividing the maximum load by the weld area. Many materials with different lay-ups have been tested in various studies, as well as many types of heating

elements. The reported results for APC-2/AS4 single-lap joints are shown in Table 1 for various lay-ups and Table 2 for unidirectional 16-plies. Reported results for other materials are shown in Table 3.

Table 1: Reported lap shear strengths for APC-2/AS4 resistance-welded single-lap joints

Author	Material	Heating element	Layup	Lap shear strength (MPa)
Bastien[38]	Commingled NCS/PEEK	UD APC- 2/AS4	Quasi-isotropic. 16 plies	_
	Commingled NCS/PEEK	Thermabond	Quasi-isotropic. 16 plies	
	APC-2/AS4	UD APC- 2/AS4	Quasi-isotropic. 16 plies	30
<b>Don</b> [39]	Commingled NCS/PEEK	UD APC- 2/AS4	Quasi-isotropic. 16 plies	29
	Commingled NCS/PEEK	Thermabond	Quasi-isotropic. 16 plies	29 27.5 30 29
Xiao[23]	APC-2/AS4	UD APC- 2/AS4	Cross-ply. 16 plies	34

Table 2: Reported lap shear strengths of UD-16 plies APC-2/AS4 resistance-welded single-lap joints

Author	Material	Heating element	Layup	Lap shear strength (MPa)
	APC-2/AS4	Stainless steel mesh	UD. 16 plies	50
Yousefpour[40]	APC-2/AS4	Commingled CF	UD. 16 plies	33
	APC-2/AS4	UD APC- 2/AS4	UD. 16 plies	24.5
Taylor[41]	APC-2/AS4	Stainless steel mesh	UD. 16 plies	44
v E 3	APC-2/AS4	UD APC- 2/AS4	UD. 16 plies	43
<b>Don</b> [39]	APC-2/AS4	Thermabond	UD. 16 plies	34
	APC-2/AS4	UD APC- 2/AS4	UD. 16 plies	37
Silverman[42]	APC-2/AS4	UD APC- 2/AS4	UD. 16 plies	25.5

Table 3: Reported lap shear strengths for resistance-welded PEKK/CF, PEI/CF and PEI/GF single-lap joints

Author	Material	Heating element	Layup	Lap shear strength (MPa)
	PEKK/CF	Stainless steel mesh	UD. 16 plies	52
<b>Dubé</b> [18]	PEI/CF	Stainless steel mesh	UD. 16 plies	47
	PEI/GF	Stainless steel mesh	Fabric 8 plies	33
Hou[14]	PEI/CF	Stainless steel mesh	Cross-ply 10- plies	34.5
Ageorges[24]	PEI/CF	UD PEI/CF	Cross-ply 10- plies	25
8 8[ ]	PEI/CF	Fabric PEI/CF	Cross-ply 10- plies	30
Stavrov[15;	PEI/GF	Stainless steel mesh	Cross-ply 6 plies	25
20]	PEI/GF	Fabric PEI/CF	Cross-ply 6 plies	

The best lap shear strengths are obtained with stainless steel meshes as heating element. Dubé *et al* [18] reported the highest values for PEKK/CF, PEI/CF and PEI/GF with respectively 52MPa, 47MPa and 33MPa. The best value for UD-16 plies APC-2/AS4 was reported by Yousefpour *et al* [40] with 50 MPa.

#### 2.2.2 Lap shear dynamic tests

Fatigue testing was only performed by Dubé *et al* [43], for resistance-welded single-lap joints, with PEKK/CF, PEI/CF and PEI/GF adherends. The results are shown in Figure 3. Infinite fatigue lives (more than 1 million cycles without failure) were reported at 25% of the static lap shear strengths for both the PEKK/CF and PEI/CF specimens and at 20% of the static lap shear strength for the PEI/GF specimens. The heating element used for the specimens' preparation was a stainless steel mesh, the same that was used to obtain the static shear strength values reported in the previous section.

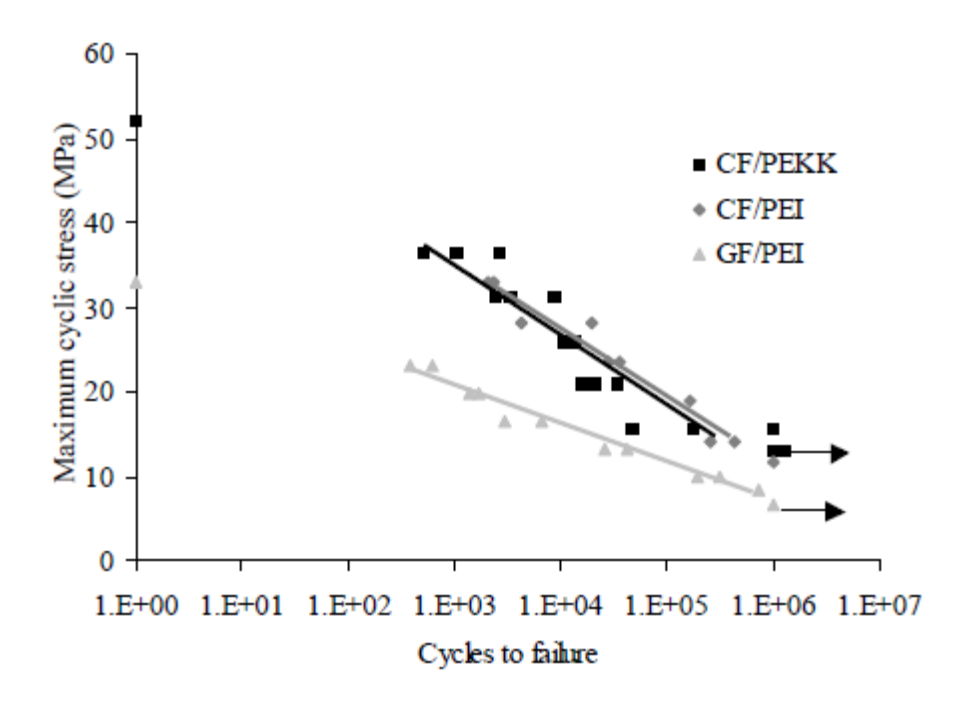


Figure 3: Fatigue results of PEKK/CF, PEI/CF and PEI/GF resistance-welded single-lap joints [43]

#### 2.2.3 Other characterization methods

Another method to characterize the resistance-welded joints is the double cantilever beam (DCB) test. It is not very well suited for resistance-welded specimens, but it can provide information on the weld quality. DCB tests are performed according to the ASTM D5528 standard test method and give the weld toughness under mode I crack propagation (G<sub>IC</sub>) as a result. Ageorges *et al* [24] used the DCB testing method on PEI/CF and PEI/GF composites and obtained good results, with the G<sub>IC</sub> approaching or exceeding the values of compression-moulded benchmarks of the laminates. Dubé *et al* [36] used the three-point and four-point bending tests to characterize skin/stringer specimens and find the optimal welding parameters. Ultrasonic C-scan inspection was also used as a non-destructive method to evaluate the quality of the weld by revealing the defect and porosities inside the weld and helped determining the ideal parameters without breaking the specimens. Most investigations also include observation of the fracture surfaces, by optical or scanning electron microscopy, to characterize the mode of failure.

# 2.3 Joint design

The joint is often the weakest point of a structural assembly, and a careful design of the joint is necessary in order for it to resist the operational conditions. Various geometrical configurations are available, each of which having a complex stress distribution that needs to be taken into account in order to design the optimum joint.

#### 2.3.1 Influence of the geometry: single and double-lap joints

The most commonly used configuration is the single-lap joint. It is a very simple geometry, which requires no machining of the adherends. The single-lap joint is the most popular joint, due to its ease of manufacturing and relatively low cost [44]. However, it is a non symmetric configuration and the stress state is complex. Studies on adhesively bonded joints have shown that the single-lap configuration is not the best one in terms of load-bearing capability. The main issue with single-lap shear joints is the out-of-plane moment caused by the eccentricity of the load path. The out-

of-plane moment promotes peel stresses and non-uniform shear stresses at the weld interface which can reduce the mechanical performance of the joint [45; 46]. In the case of adhesive joints, different alternative configurations have been developed to improve the stress distribution within the joint [47]. A few examples are shown in Figure 4.

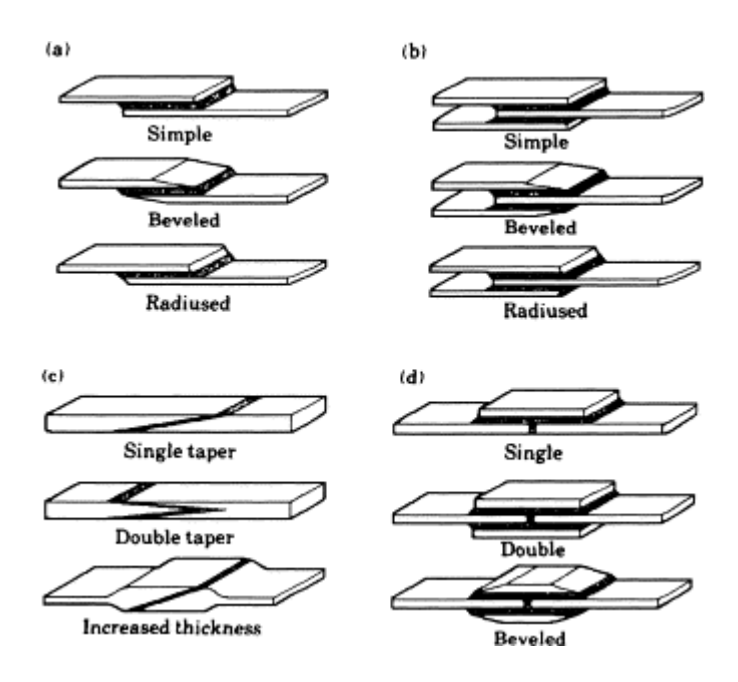


Figure 4: Joint configurations: (a) single-lap, (b) double-lap, (c) scarf, and (d) strap [48]

Minimizing peel stresses is particularly important in structures involving composite materials, as their transverse modulus and strength are generally low compared with their longitudinal modulus and strength. Therefore, if the joint experiences transverse (peel) loading, it is likely to fail due to transverse tension rather than in shear [49].

In 1969, Lehman and Hawley [50] were the first to show that double-lap joints were more than twice as strong as single-lap joints of the same lap length. For the same material, they reported a load to failure for the double-lap joint around 3 times higher than the one for the single-lap joint. Therefore, the double-lap joint was around 1.5 times stronger than the single-lap joint, in terms of joint's strength.

This observation was found to be true for adhesive bonding as well as mechanical fastening. Parida *et al* [51] showed that single-lap quasi-isotropic laminates with titanium fastener bolts had around 1.5 times lower strengths than their double-lap counterparts, under various environmental conditions (RT/AR: room temperature/as received, H/W: hot/wet). Their results are shown in Figure 5

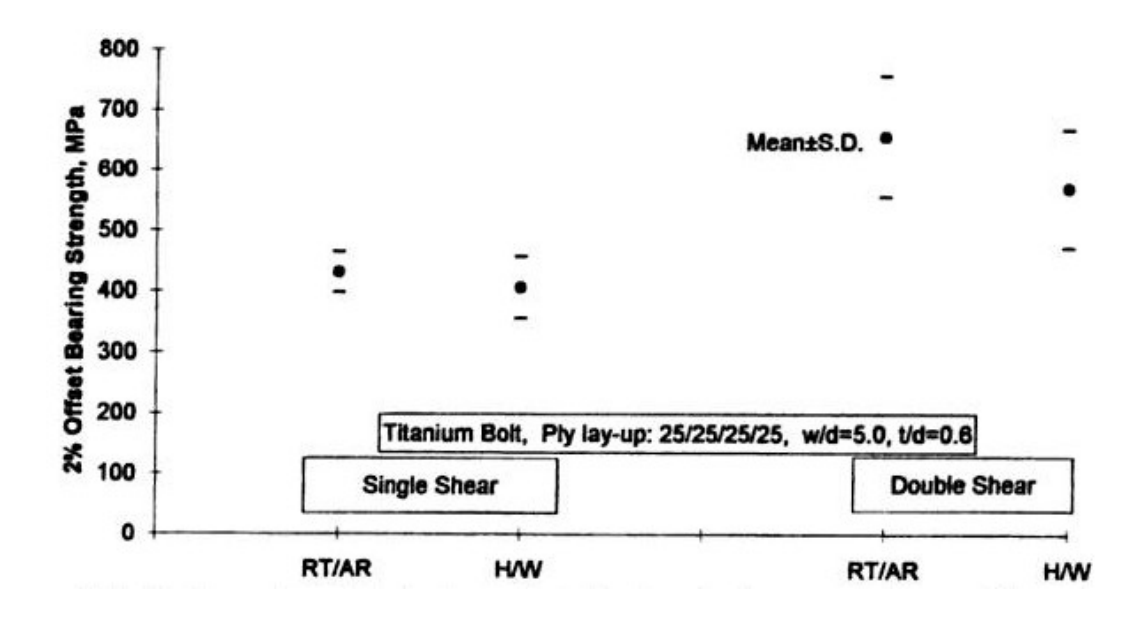


Figure 5: Strength of single-lap and double-lap bolted joints, under various environmental conditions [51]

Many analyses have been performed in the case of adhesive bonding to explain this effect. The double-lap configuration, due to its symmetry, reduces bending in the adherends and transverse (peel) stresses in the adhesive, leading to higher joint strengths [52; 53]. Although double-lap joints have no bending moments, they still undergo internal bending, as shown in Figure 6 [54].

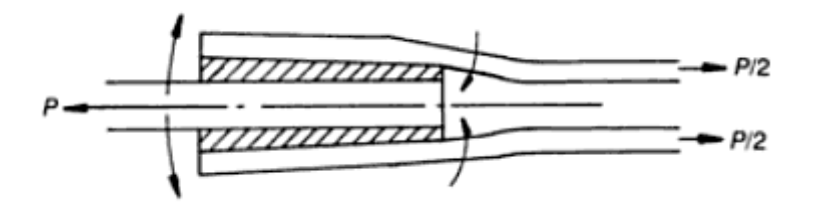


Figure 6: Internal bending in double-lap joint [54]

Therefore, peel stresses cannot be fully removed from the joint and can still be high, especially at the edges were they are maximum. However, double-lap adhesive joints have proven to have significantly better mechanical performances than single-lap joints, in particular in dynamic loading [44; 55].

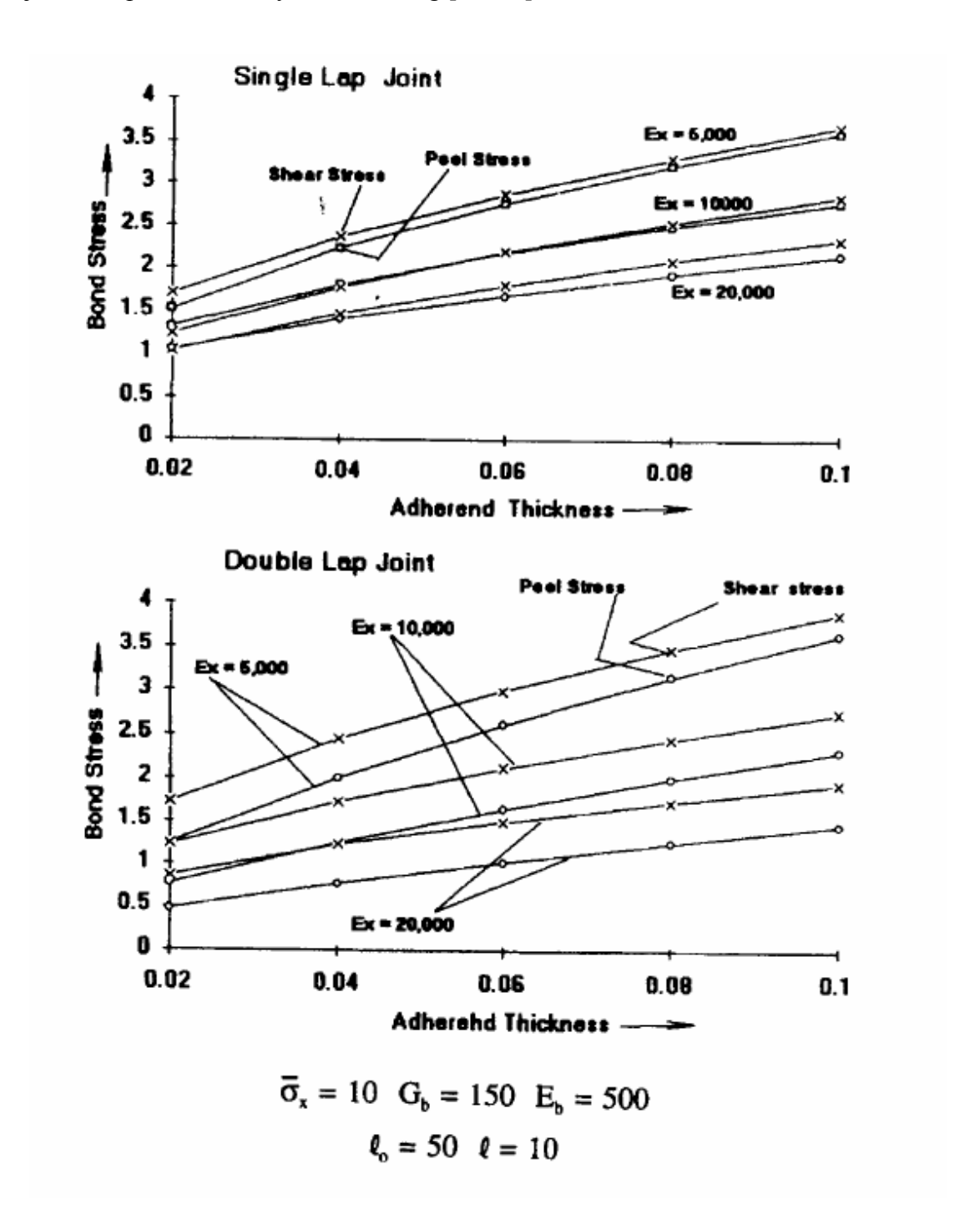


Figure 7: Maximum bond stresses in single and double lap joints, for a fixed loading stress  $\sigma x = 10[56]$ 

Figure 7 gives a comparison of the maximum bond stresses in single and double lap joints for a fixed value of the loading stress  $\sigma_x$ . In the case of the double lap joint, there is a considerable separation between the peel and shear stresses, the peel stresses being smaller, while they are comparable to the shear stresses in the case of single lap joints. Thus peel stresses for double lap joints are not as much of a factor in joint failure as they are in single lap joints, although they are still large enough relative to the shear stresses that they can not be ignored [56].

In both cases, the strength of the joint is strongly influenced by the adhesive's properties and the length of the overlap, as shown in Figure 8 and Figure 9. The more ductile the adhesive is, the lower the peel stresses are, and thus the stronger the joint will be. The ductile response of the adhesive provides additional structural capability of the joint over its limit load capacity. However, some damage to the adhesive probably occur in the ductile regime which would degrade the long term response, so it is advisable to keep the applied load low enough to stay in the elastic regime of the adhesive. The main benefit of ductile behaviour is to provide a better tolerance with regards to peak loads and flaws in the adhesive layer. Some plastic deformation in the adhesive will also reduce the stress concentration at the corners.

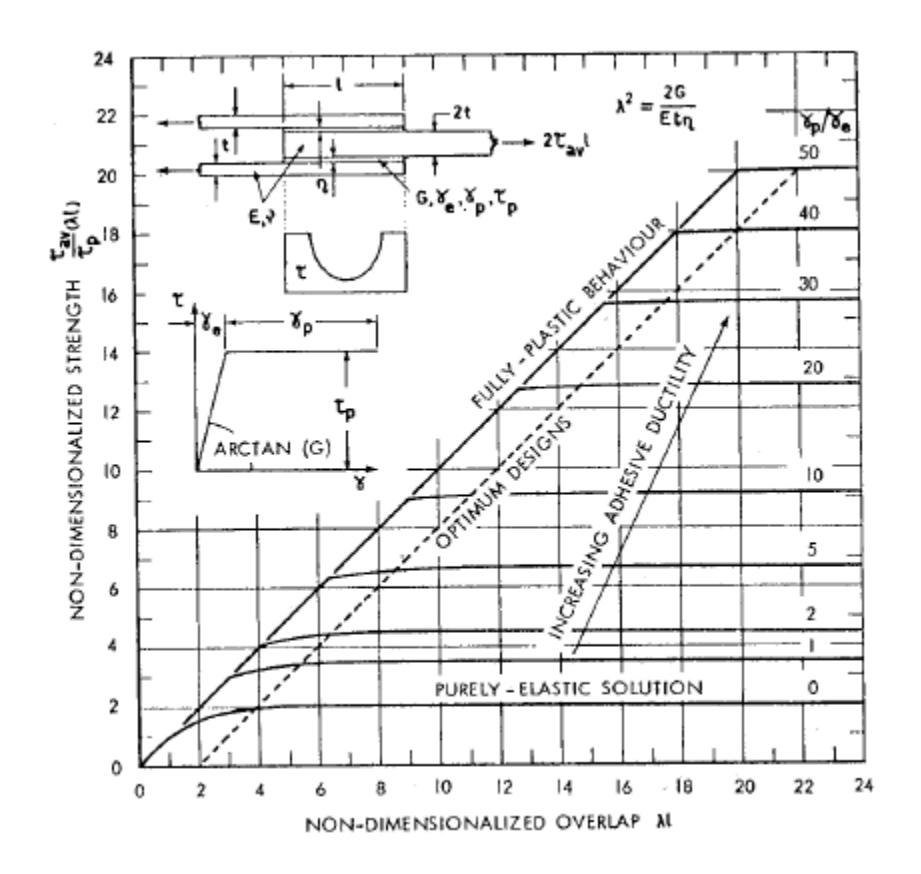


Figure 8: Shear strength of double-lap bonded joints [57]

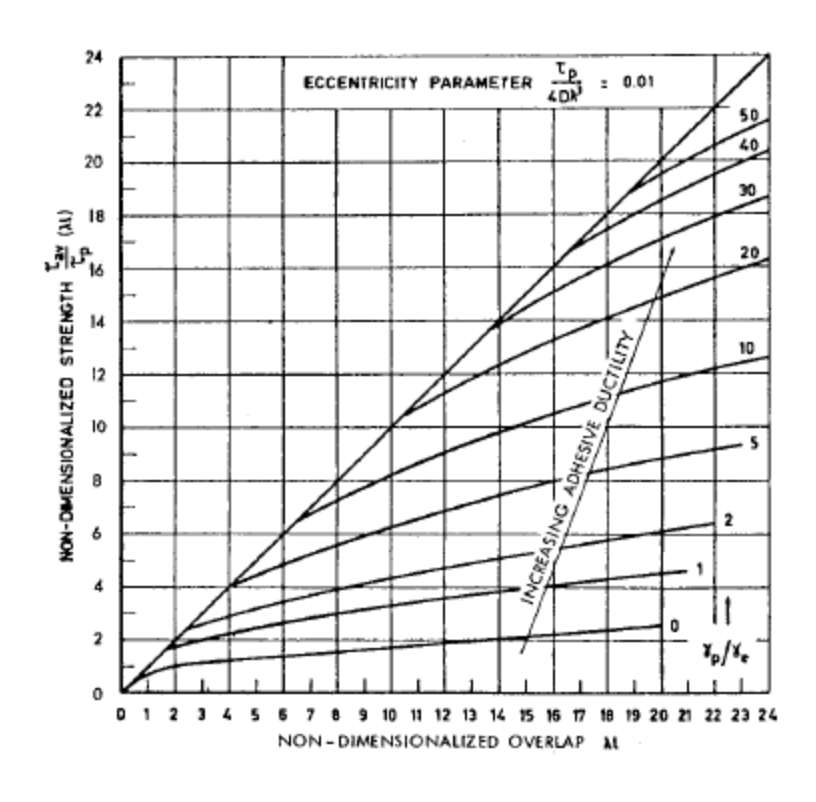


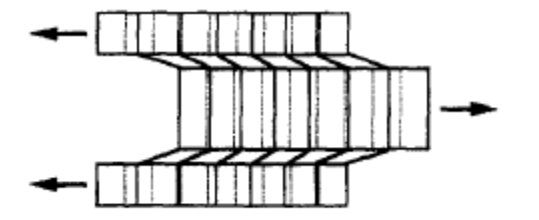
Figure 9: Shear strength of single-lap bonded joints [58]

#### 2.3.2 Stress analysis of the joint

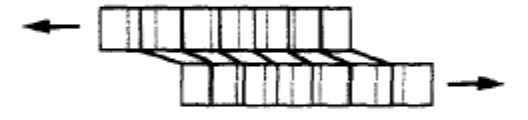
Stress analysis is a key step to provide information on distribution of stress or strain in structures subjected to specified loading and service conditions, enabling the prediction of the strength and service life of the designed structures [59]. A very large amount of information is available on stress analysis and strength prediction of adhesively bonded joints. However, other types of joints like welds have considerably less been investigated in terms of stress analysis.

#### 2.3.2.1 Adhesive joints

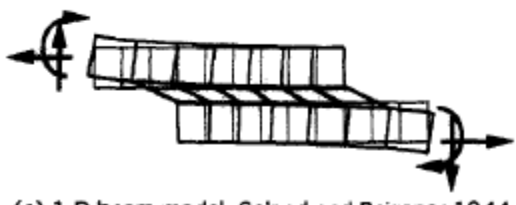
Single-lap adhesive joints have been thoroughly investigated, since the earliest development from Volkersen [60] in 1938. Volkersen's analysis was a simple shear lag model based on the assumptions of a perfectly elastic adherend that deforms only in tension, with only shear deformation in the adhesive layer. This model did not take into account the non-colinearity of the applied forces and thus the induced bending moment was ignored. It also ignored the bending of the adherends that allows a rotation of the joint and gives rise to a non-linearity of the problem [61]. De Bruyne [62] adapted this model in 1944 for the double-lap configuration. The same year, Goland and Reissner improved Volkersen's model by introducing a cylindrically bent-plate analysis [63]. In their formulation, they used a bending moment factor to take into account the effects of the joint edge moment, assuming that the adhesive layer could be neglected because it is very thin compared with the adherend thickness. Under these assumptions, the critical effect of the peel stresses at the free end of the adhesive layer was demonstrated. The configurations used in these theoretical models are presented in Figure 10.



(a) 1-D bar model, Volkersen 1938/de Bruyne 1944



(b) 1-D bar model, Volkersen 1938



(c) 1-D beam model, Goland and Reissner 1944

Figure 10: Configurations and deformations of theoretical models: (a) 1-D bar model (Volkersen, 1938; de Bruyne, 1944) for double-lap joint; (b) 1-D bar model (Volkersen, 1938) for single-lap joint; and (c) I-D beam model (Goland and Reissner, 1944) for single-lap joint[64].

In 1973, Hart-Smith [58] extended Goland and Reissner's model to include adhesive plasticity and adherend thermal mismatch, and coupled the determination of the bending edge moment and the adhesive stresses. Hart-Smith has also investigated the double-lap configuration [57] and developed an analysis for balanced double-lap joints with an elastic-plastic adhesive. Peel and shear stresses were decoupled based on the assumptions that the shear stress near the overlap end becomes constant after yielding and that the peak peel stress occurs at the overlap end, and the nonlinear equation for adhesive shear stress was solved. For both configurations, Hart-Smith has developed a peel stress coefficient,  $k_{peel}$ , to determine the maximum peel stress,  $\sigma_{peak}$  [65].

$$k_{\text{peel}} = \frac{3E_c t}{E\eta} \tag{5}$$

Where  $E_c$  is the effective transverse adhesive Young's modulus, E is the transverse adherend Young's modulus, t is the adherend thickness, and  $\eta$  is the adhesive thickness.

The same peel stress coefficient appears in the calculation of  $\sigma_{peak}$  for both configurations, but with different powers: for the single-lap joint,  $\sigma_{peak}$  is proportional to  $k_{peel}^{1/2}$ , while, for the double-lap joint, it is proportional to  $k_{peel}^{1/4}$ . This theory predicts a more powerful peel stress effect for single-lap joints, which explains the better performances of the double-lap joints.

Hart-Smith has done very extensive work on the analysis of adhesive joints and published many papers [65; 66; 67; 53; 57; 58], trying to improve the strength of the joints by removing peel stresses with different methods, such as tapering or scarfing the adherends [68], or using alternative configurations to the single-lap joint. Hart-Smith has used a continuum mechanics approach, allowing a parametric investigation concerning the effects of adhesive thickness, overlap length, stiffness unbalance and so on. A further development was introduced in 1991 by Oplinger [69], taking into account the large deflection effect in the single-lap joint overlap that Hart-Smith had neglected.

Finite elements models have also been developed to predict the stress distributions of the joints, because of the complexity induced by the non-linearity of the problem. Adams and Peppiatt (1974) developed a two-dimensional finite-element method to analyse lap joints by treating the adhesive spew as a triangular fillet instead of a square edge [70]. Lin and Lin (1993) derived a finite element model of single-lap

adhesive joints [71]. Tsai and Morton (1994) evaluated theoretical solutions using nonlinear finite element analyses [72]

Due to the high stiffness of the adherends compared with the adhesive, none of the mathematical models mentioned above included shear deformations in the adherends. Tsai *et al* .[73] showed that these deformations are not always negligible and that they should be taken into account in the theoretical model. Tsai *et al*. improved the classical solutions by incorporating the adherends shear deformations assuming a linear shear stress (strain) through the thickness of the adherends. The joints configurations of Tsai *et al*. theoretical models are presented in Figure 11.

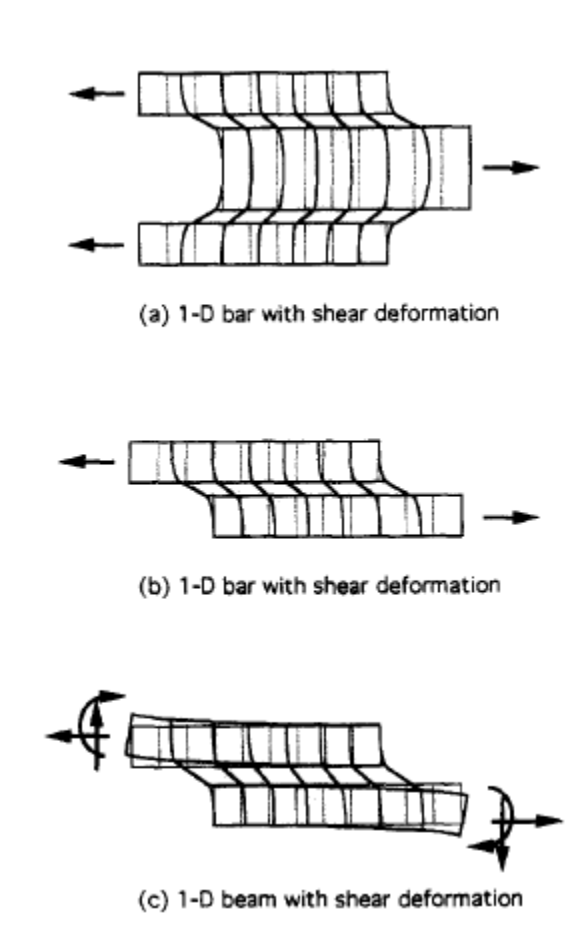


Figure 11: Configurations and deformations of theoretical models including the shear deformations of adherends: (a) 1-D bar model for double-lap joint; (b) I-D bar model for single-lap joint; and (c) 1 -D beam model for single-lap joint.[64]

### 2.3.2.2 Other types of joints

The well-known models used for adhesive bonding are not applicable in the case of welding, as they assume that shear deformations are confined to a thin adhesive layer that separates the adherends. This is not the case for welded joints, where the surfaces of the two adherends are in direct contact with each other and fused together. The problem of shear and peel stresses is not critical in the case of metals, because of their isotropy. However, for composite materials, which can have relatively low transverse shear modulus or transverse tensile modulus, the question of the stress distribution in the weld area is not trivial. Fusion bonding of composite materials is relatively new, and the focus so far has been on the thermal analysis of the process rather than the stress distribution.

Another type of composite joints has been investigated by Osnes and McGeorges [74]. The classical works from Hart-Smith and Goland and Reissner were adapted in the case of overlaminated double-lap joints, where the second laminate adherend is manufactured directly onto the first adherent by wet hand lay-up.

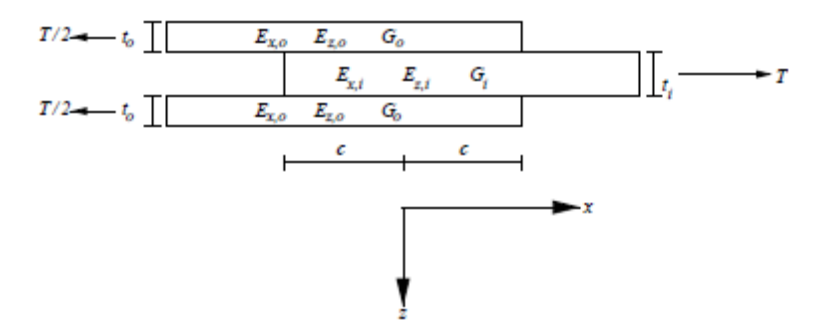


Figure 12: Schematics of the geometry and material parameters of the overlaminated double-lap joint[74] Like in the welded joints, there is no adhesive layer with that type of joint, and hence the classical solution cannot be used. A new simple closed-form solution for the stress distribution in overlaminated joints, based on the ideas of Tsai *et al.* including

shear deformations in the adherends, was derived, and showed good accuracy when compared with numerical results. Some results are shown in Figure 13.

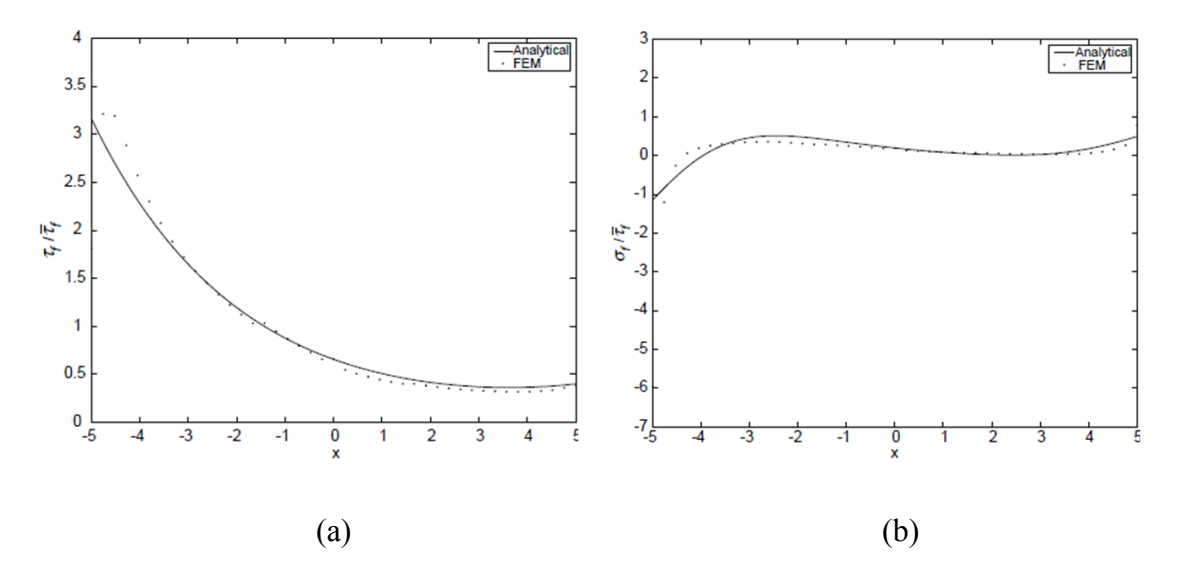


Figure 13: Normalized interfacial shear stresses (a) and peel stresses (b) along the overlap of an overlaminated double-lap joint[74]

# 2.4 Summary

Various welding parameters have been investigated to optimize the resistance welding process. Many studies have been conducted to characterize the single-lap geometry and find the ideal welding conditions to obtain the better mechanical performances. The best results have been obtained with a stainless steel mesh for which size has been optimized to give the best static lap shear strength. Only one work has been focusing on the dynamic performances of the joint, every other study has been using static testing.

Previous work with adhesive bonding and mechanical fastening has shown that a double-lap configuration leads to better mechanical performances of the joint, due to the change in the stress distribution. Adhesive joints have been thoroughly investigated and stress analyses have been performed for the single-lap joints as well as for the double-lap joints, to predict the stress distribution and the failure of the

joints. No such work has been done in the case of resistance welding, and no alternative configuration has been studied.

# 2.5 Specific research objectives

Considering the work that has been done on adhesive bonding and the improvement obtained with the double-lap configuration, the following objectives were specified:

- Investigate the mechanical performances of the resistance-welded double-lap
  joints in static and in fatigue, for various materials.
- Characterize the quality of the joints
- Compare the results with the single-lap ones to study the influence of the joint configuration

# 3 Experimental procedures

This chapter will present all the experimental procedures that were used for the characterization of the resistance-welded thermoplastic composite double-lap joints, including the specimens' preparation, the mechanical testing, the interface characterization and the fracture surface observation.

# 3.1 Specimens preparation

### 3.1.1 High performance thermoplastic composites

The laminates used as the adherends were high performance thermoplastic composites. High performance thermoplastics, as opposed to engineering thermoplastics, are polymers based on highly aromatic molecular structures, with improved mechanical properties, high temperature capabilities and solvent resistance [75]. They are mostly used in aircraft structural applications.

PEI, on the other side is an amorphous polymer [76]. It is appreciated for its good mechanical and electrical properties, high service temperature (up to 170°C), rigidity, good creep behaviour, fatigue endurance, low shrinkage and moisture uptake, resistance to UV, transparency to visible light, IR and microwaves. Its main drawbacks are the cost, a high density and an insufficient chemical resistance [77]. The high performance thermoplastics selected for this work were PEEK, PEKK and PEI. Their chemical structures are shown in Figure 14, Figure 15 and Figure 16, and their properties are summarized in Table 4.

Figure 14: Chemical structure of PEEK [78]

Figure 15: Chemical structure of PEKK [78]

Figure 16: Chemical structure of PEI [79]

Table 4: Material properties of PEEK, PEKK and PEI [77]

	PEEK	PEKK	PEI
Miscellaneous properties:			
• Density (g/cm <sup>3</sup> )	1.27-1.32	1.28-1.31	1.27-1.3
• Shrinkage (%)	1.1	0.5-1	0.7-0.8
• Absorption of water (%)	0.1-0.5	0.2	0.2-0.3
Mechanical properties:			
Tensile strength (MPa)	100-107	90-110	90-100
• Elongation at break (%)	30-150	12-80	60
Tensile modulus (GPa)	3.6-3.9	3.4-4.4	3
Flexural modulus (GPa)	3.7-3.9	3.4-1.6	3-3.3
Notched impact strength ASTM D256 (J/m)	80-85	50-63	50-60
Thermal properties:			
Glass transition temperature(°C)	143	155-160	215
Melting temperature (°C)	334	306-360	
Thermal conductivity (W/m.K)	0.25	0.25	0.22
• Specific heat (cal/g/°C)	0.32		
Coefficient of thermal expansion	4-6	2.1-7.7	5-6
(10 <sup>-5</sup> /°C)			
Electrical properties:			
<ul> <li>Volume resistivity (Ω.cm)</li> </ul>	10 <sup>16</sup> -10 <sup>17</sup>	$10^{16}$	10 <sup>15</sup> -10 <sup>17</sup>
Dielectric constant	3.2	3.3	3.1-3.2
• Loss factor (10 <sup>-4</sup> )	30	40	13-25
Dielectric strength (kV/mm)	20	24	28-33

## 3.1.2 Material used and experimental set-up

The power was supplied by a Xantrex XPR (150-40 DC, 0-150V, 0-40A). Data acquisition was performed using Labview. Pressure was applied during the welding process using a pneumatic system, providing a constant pressure throughout the process. The tooling plates were ceramic insulators. The heating element was a

stainless steel mesh with 0.066 mm wire diameter, 0.104 mm open gap width and a linear wire density of 5.8 wires/mm. The mesh size was chosen according to the mesh optimization performed by Dubé [18]. It was cut to dimensions 12.7 mm x 76.2 mm, and clamped between two copper electrodes. The adherends were thermoplastic composite laminates with 2.3 mm average thickness, cut with a water-cooled diamond saw to dimensions 101.6 mm x 25.4 mm. The laminates were provided by Cytec Engineered Material Inc. Four different materials were used: 16 plies of unidirectional carbon fibre polyether-ether-ketone (PEEK/CF [0]<sub>16</sub>), 16 plies of unidirectional carbon fibre reinforced polyether-ketone-ketone (PEKK/CF [0]<sub>16</sub>), and 8 plies of 8-harness satin weave glass fabric polyether-imide (PEI/GF). Polymer films were introduced between the adherends and the heating element to make sure no void was left during the welding. They were cut from polymer sheets to the dimensions of the overlap: 25.4 mm x 12.7 mm. The materials used and their characteristics are summarized in Table 5. The experimental set-up is shown in Figure 17.

Table 5: Materials used and their characteristics

	Material	Characteristics	Dimensions (mm) (Length × width × thickness)
Adherends	PEEK/CF PEKK/CF PEI/CF	Unidirectional 16 plies	102 x 25 x 2.3
	PEI/GF	8 plies of 8-harness satin weave	102 x 25 x 2.0
Heating element	Stainless steel mesh	0.04 mm wire diameter 0.09 mm open gap width 76 x 13 x 0.08	
Polymer films	PEEK PEEK PEI		25 x 13 x 0.01

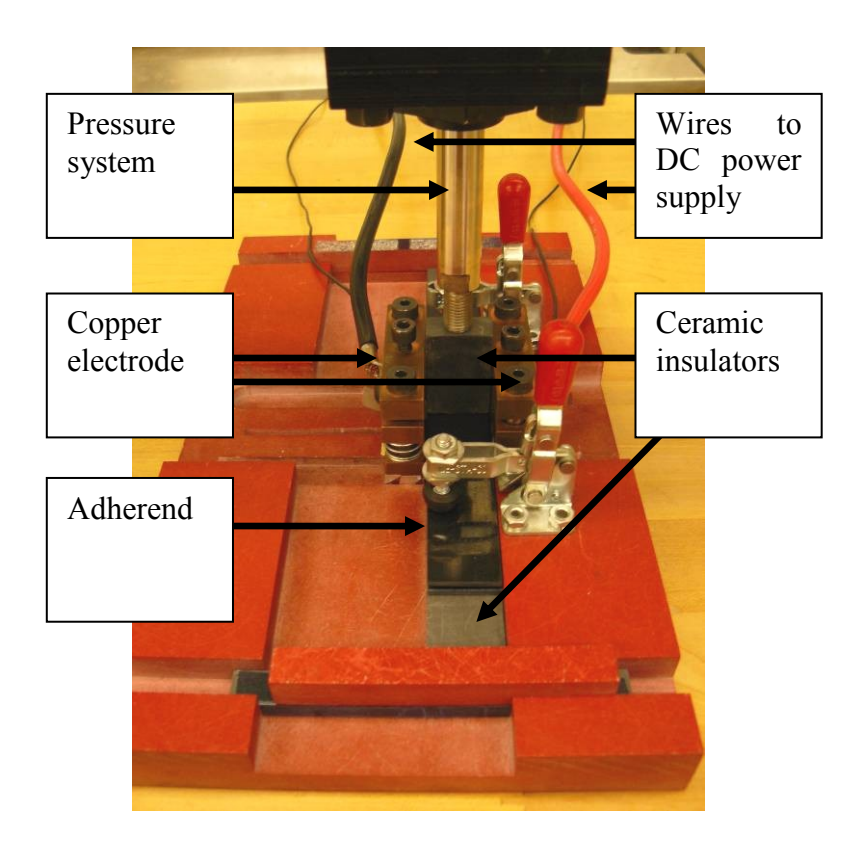


Figure 17: Resistance welding experimental set-up

## 3.1.3 Resistance welding process

The carbon fibre adherends were welded using the ramped voltage input power method developed by Yousefpour [40], with an initial voltage of 2V and an input voltage rate of 10V/min, while the glass fibre adherends were welded under constant voltage input. Lookup tables were established prior to the samples preparation to determine the ideal welding parameters: different welding temperatures (maximum reached temperature) and welding pressures were tried and the quality of the obtained joints was established, based on visual observation of fractured samples (uniform weld, unwelded zones, overheated zones). The temperature was monitored during the welding process using a K-type thermocouple placed at the centre of the weld interface, between the polymer film and the laminate to avoid any current leakage in the heating element. A welding temperature of 445°C was selected for PEEK/CF specimens, along with a welding pressure of 110 kPa. The same pressure was selected

for PEKK/CF and PEI/CF, with respective welding temperatures of 410°C and 390°C. For the PEI/GF specimens, a constant voltage of 4.5V was used, for a maximum welding temperature of 345°C and a pressure of 60 kPa. A comparison between the temperatures vs. time curves for each material is shown in Figure 18.

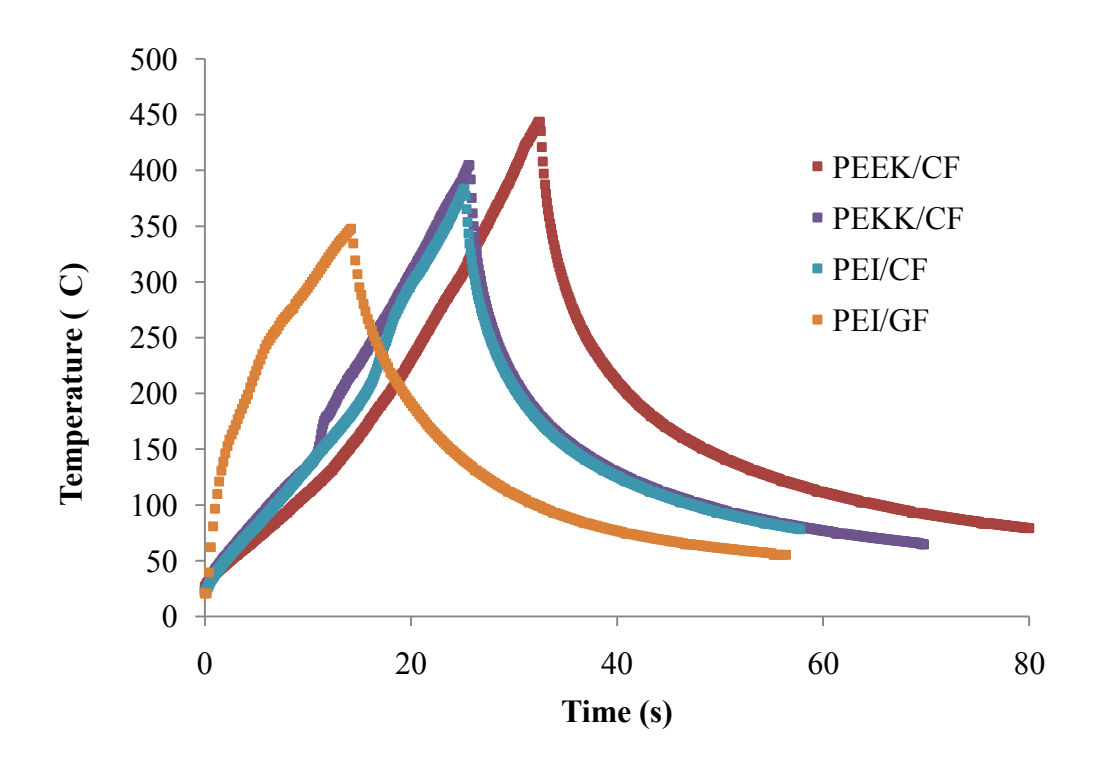


Figure 18: Temperature at the weld interface for each material

The double-lap-shear specimens were processed in two sequential welds. Figure 19 shows the different steps of the resistance welding followed for the first weld:

- 1) a laminate was placed on the bottom ceramic insulator
- 2) a polymer film was placed on the laminate on the weld area
- 3) the heating element was placed beneath the polymer film and clamped between the copper electrodes
- 4) a second polymer film was placed on top of the heating element
- 5) a second laminate was placed overlapping the other
- 6) the top ceramic insulator was placed on the overlap area
- 7) pressure was applied using a pneumatic pressure system
- 8) voltage was applied to the heating element

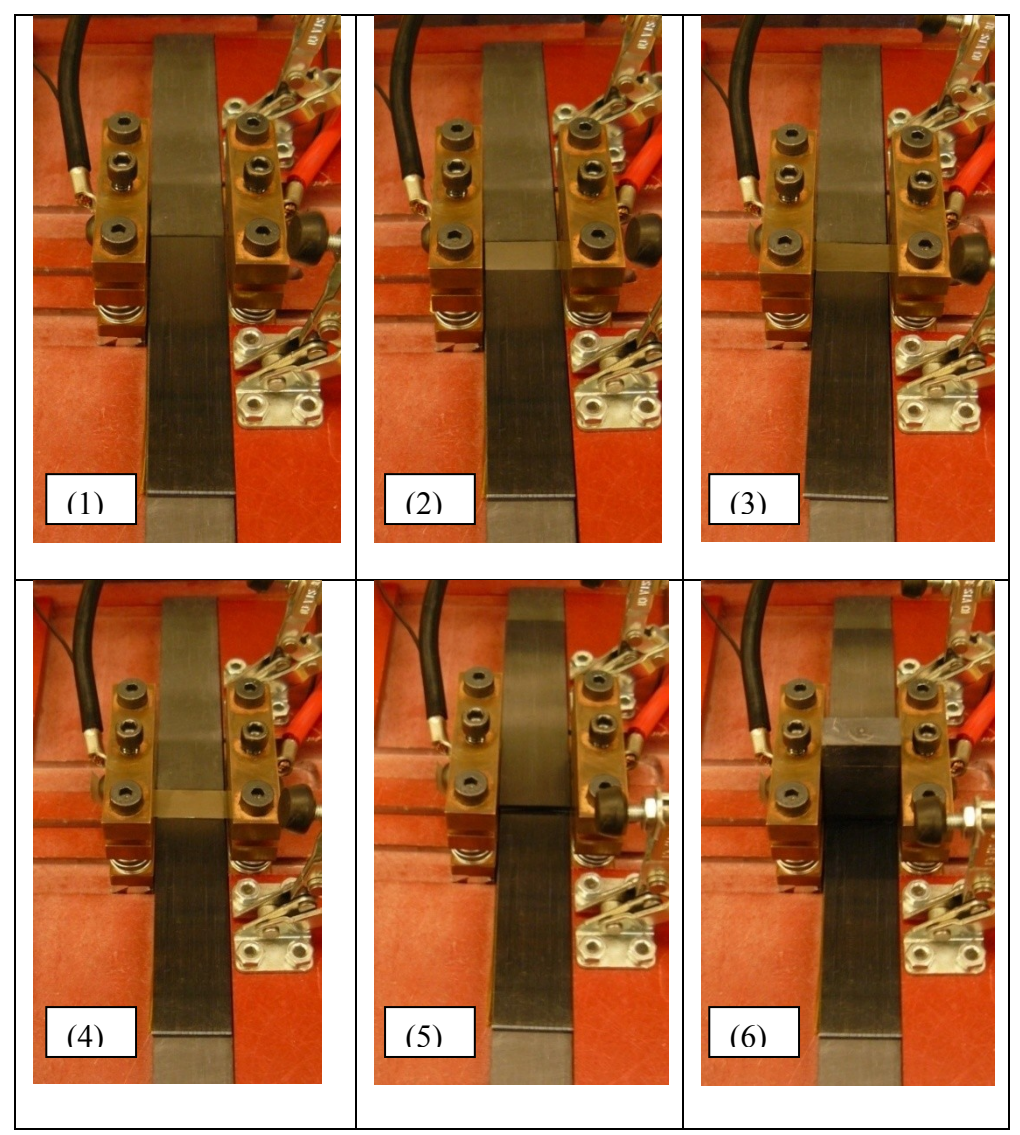


Figure 19: Different steps followed for the first weld

The same steps were repeated to obtain a double-lap shear joint, shown in Figure 20:

- 1) a polymer film was placed on the upper laminate of the joint on the weld area
- 2) the heating element was placed beneath the polymer film and clamped between the copper electrodes
- 3) a second polymer film was placed on top of the heating element
- 4) a spacer was placed on the lower laminate to avoid bending
- 5) a second laminate was placed overlapping the single-lap joint
- 6) the top ceramic insulator was placed on the overlap area
- 7) pressure was applied using a pneumatic pressure system
- 8) voltage was applied to the heating element

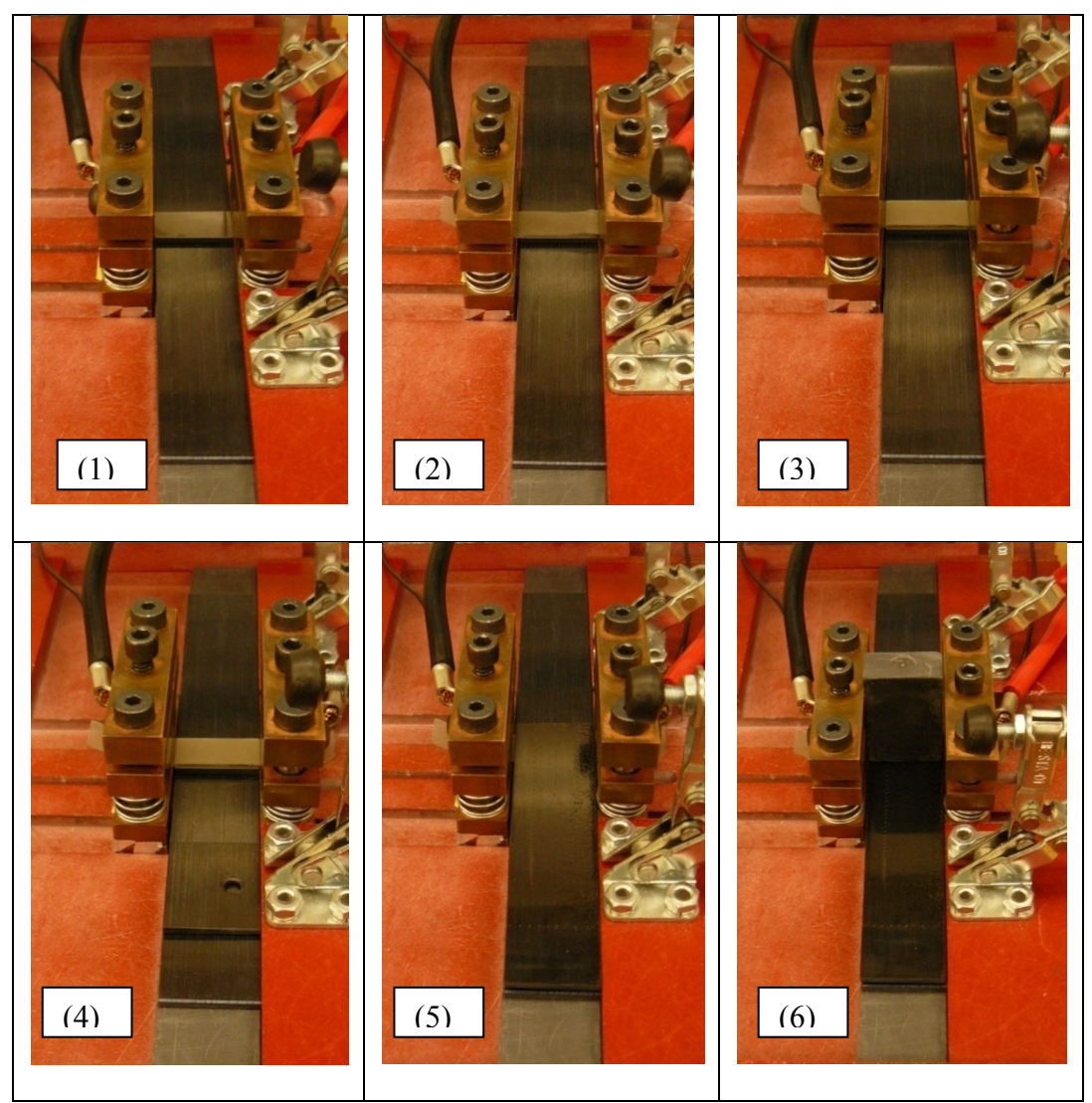


Figure 20: Different steps followed for the second weld

Between 20 and 25 double-lap shear specimens of each material were welded following these steps, to be tested in tensile static and fatigue loading. A summary of the welding conditions as well as the characterization methods is shown in Table 6.

**Table 6: Welding conditions** 

	PEEK/CF	PEKK/CF	PEI/CF	PEI/GF
Welding temperature	445°C	410°C	390°C	345°C
Welding pressure	110kPa	110kPa	110kPa	60kPa
Power input	Ramped (10V/min)	Ramped (10V/min)	Ramped Constant (10V/min) (4.5V)	

All samples were then characterized using static testing, dynamic testing, optical microscopy and fracture surface observation.

## 3.2 Mechanical testing

### 3.2.1 Tensile static testing

The strength properties of the double-lap shear resistance welded joints were determined in accordance with the ASTM D3528 standard method. This standard tensile test involves applying a uniaxial tensile load to the sample and increasing the load until the sample breaks, and is used to determine the lap shear strength (LSS). The LSS is calculated by dividing the maximum load obtained before failure by the overlap area, using the following formula:

$$LSS = \frac{L_m}{l \times w \times 2} \tag{1}$$

where  $L_m$  is the maximum load (N), l is the overlap length (mm) and w is the overlap width (mm).

The samples were 190.5 mm long and 25.4 mm wide, with two overlap surfaces, each 12.7 mm long. They were clamped at each end between the hydraulic grips of a MTS 100 kN machine, with a clamped length of 25.4 mm at each end and a clamping pressure of 15 MPa. A tab made of the same material and the same thickness as the laminate to be tested was inserted between the two outer laminates in order to avoid bending from the clamping as shown in Figure 21 and Figure 22. The free length between the grips was 139.7 mm. The crosshead speed was 1.3 mm/min and the samples were tested under standard conditions with a room temperature of 23°C and a relative humidity of about 50%. Five replicated samples of each material were tested. Fracture surfaces were then observed with an optical microscope to determine the failure mode.



Figure 21: Double-lap sample clamped in the MTS 100kN machine

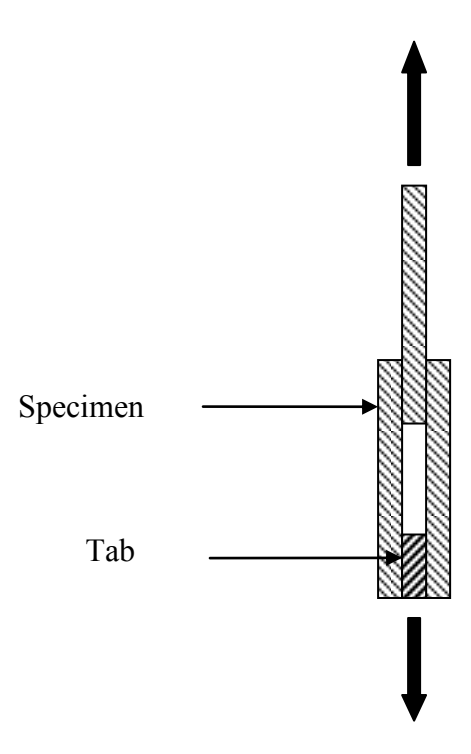


Figure 22: Schematic of the tested sample

#### 3.2.2 Tensile fatigue testing

The results of the static tests were used to design fatigue tests in order to investigate the fatigue performance of the resistance-welded double-lap shear joints. Between 13 and 20 specimens were tested at various stress levels between 70% and 20% of the lap shear strength determined with the static tests. Specimens were loaded with a sinusoidal waveform, at a frequency of 5 Hz and a load ratio of 0.1. All fatigue tests were performed at Delft University of Technology, in the Faculty of Aerospace Engineering. MTS 100kN and 60kN servo-hydraulic machines were used to conduct the tests, with a clamping distance of 25.4 mm and a clamping pressure of 10 MPa. An insert was used to avoid any bending of the specimen as shown in Figure 22. The sample was carefully aligned using an angle bracket to make sure only an axial force would be applied. The tests were stopped when the specimen failed and the number of cycles until failure was noted down. An infinite fatigue life was reported when a

specimen survived more than a million cycles and the test was stopped. The failure surfaces were then examined visually and using an optical microscope.

## 3.3 Interface characterization and fracture analysis

## 3.3.1 Optical microscopy

In order to inspect the quality of the weld, the cross-section of the joint was examined by optical microscopy. New specimens were welded and then cut vertically at the middle of the overlap with a water-cooled diamond saw to have a cross-sectional view of the weld. They were then embedded into epoxy resin and polished before being observed at 25x and 100x magnitudes with an Olympus microscope. The method used for the polishing is described in Table 7.

Table 7: Polishing method used for cross-section observation of the double-lap samples

Step	Abrasive	Lubricant	Speed (RPM)	Time (s)
1	Sand paper (SiC) 200	water	300	300
•	Sand paper (SIC) 200	Water		
2	Sand paper (SiC) 600	water	300	300
3	Sand paper (SiC) 800	water	300	300
4	Sand paper (SiC) 1200	water	300	300
5	9 microns diamond	DP red	150	150
6	3 microns diamond	DP red	150	150
7	1 micron diamond	DP red	150	150

## 3.3.2 Scanning electron microscopy

The fracture surfaces of the fractured specimens were observed using scanning electron microscopy (SEM). The surfaces to be observed were coated with a thin layer of gold-palladium with a Hummer VI sputter coater (Anatech LTD), and then they were observed using a FE-SEM Hitachi S-4700 at magnitudes varying between  $100 \times$  and  $2000 \times$ .

## 4 Experimental results

The results will be presented in this chapter: first, the results from the mechanical testing from both static and fatigue tests will be analyzed and compared with single-lap results. Then the fracture surfaces observation will be shown, and finally the interface quality will be characterized.

#### 4.1 Static tests results

### 4.1.1 Double-lap joints results

The load-displacement curves from double-lap-shear specimens are presented in Figure 25. The PEI/CF and PEI/GF exhibited a linear behaviour up to the maximum load, followed by a brittle fracture. On the other side, the PEEK/CF and PEKK/CF exhibited a linear behaviour corresponding to the elastic region in the first part of the curve, then followed by a non-linear curve before reaching the maximum load. A plateau can be observed before the fracture, in the plastic region. This plateau is due to the higher ductility of PEEK and PEKK polymer, compared with PEI. Unlike what was expected, PEKK/CF specimens did not break at a much higher load than PEI/CF. It can be explained by the fact that the better mechanical properties of the PEKK material are mainly due to the high crystallinity of this polymer, which was not controlled during the process. The very fast cooling of the weld resulted in an amorphous state at the weld interface, leading to a lower strength of the joint. Typical cooling rates used to produce highly crystalline polymers are around 10°C/min, while the cooling rate obtained with resistance welding was around 1500°C/min. Gao et al [80] showed the influence of the cooling rate on the degree of crystallinity and the mechanical properties of the material, including interfacial shear strength (IFSS) and interlaminar shear strength (ILSS). Their results for PEEK/CF are shown in Figure 23.

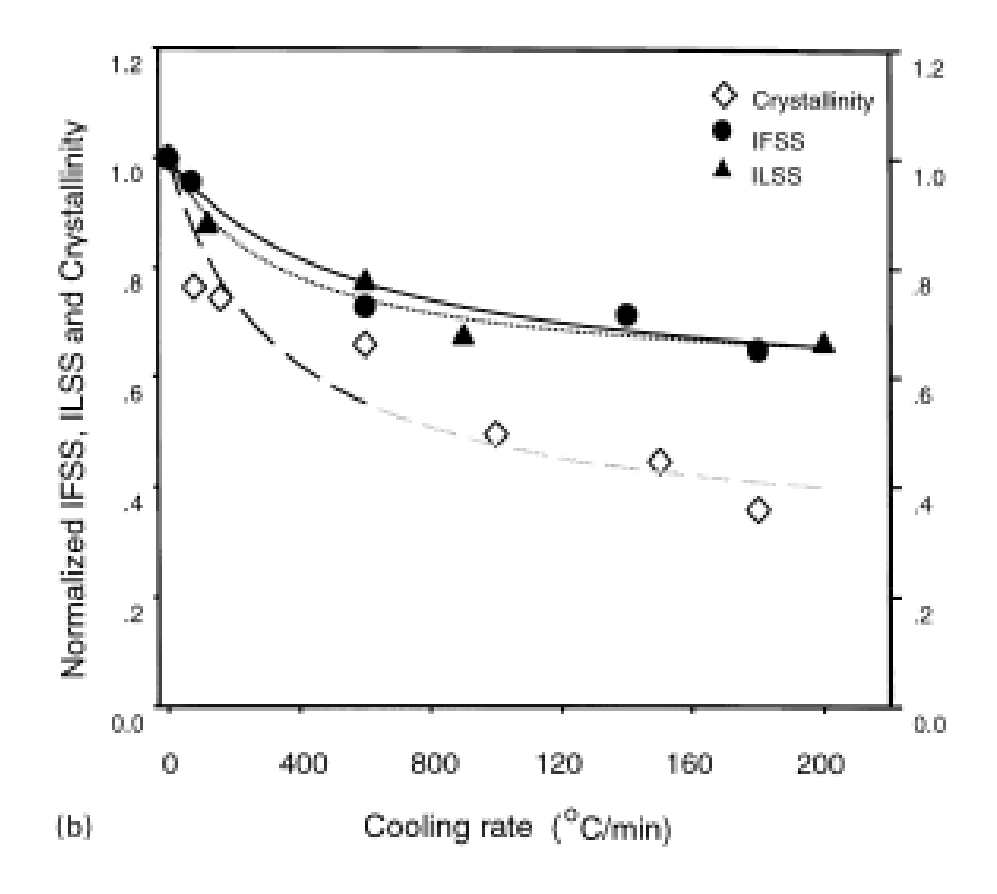


Figure 23: Influence of the cooling rate on properties of PEEK/CF [80]

The PEI/GF showed a much lower strength and higher displacement to failure than the other materials. The use of weaker glass fibre instead of carbon fibre, and the different lay-up (fabric versus unidirectional) is responsible for this different behaviour. Both welds seemed to have failed at the same time. This can be explained by the fact that if one weld failed first, the entire load was transferred on the other weld, leading to its immediate failure almost simultaneously. However, it is important to note that for the PEI/GF specimens, the failure did not occur in the joint, but in the laminate itself, as shown in Figure 24.

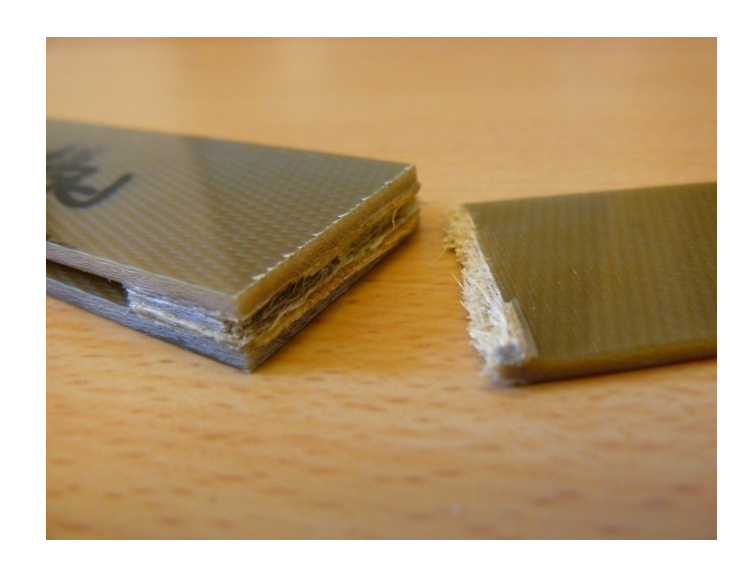


Figure 24: Coupon failure of a PEI/GF sample

Consequently, the lap shear strength (LSS) could not be calculated for this material, and can only be assumed to be the same or higher than the laminate strength. The LSS of the other materials are shown in Figure 26. LSS of 53MPa, 49MPa and 45MPa were obtained for PEEK/CF, PEKK/CF and PEI/CF, respectively.

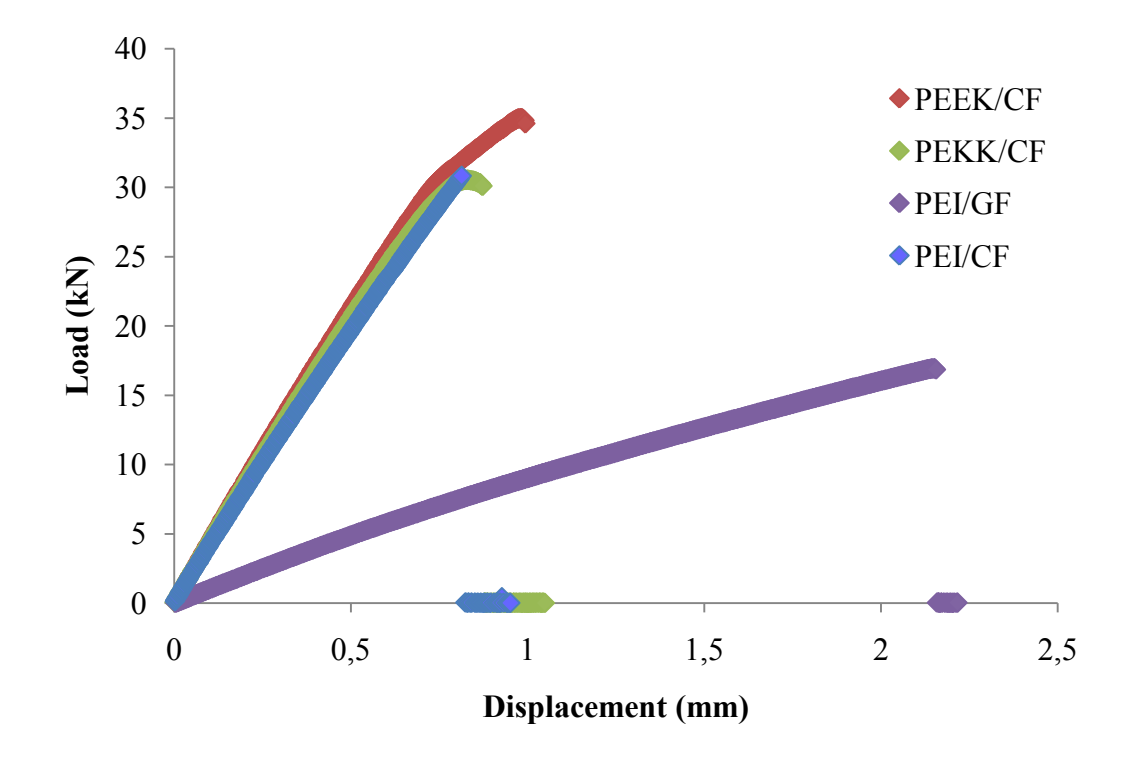


Figure 25: Static load-Displacement curve for double-lap PEEK/CF, PEKK/CF, PEI/CF and PEI/GF joints

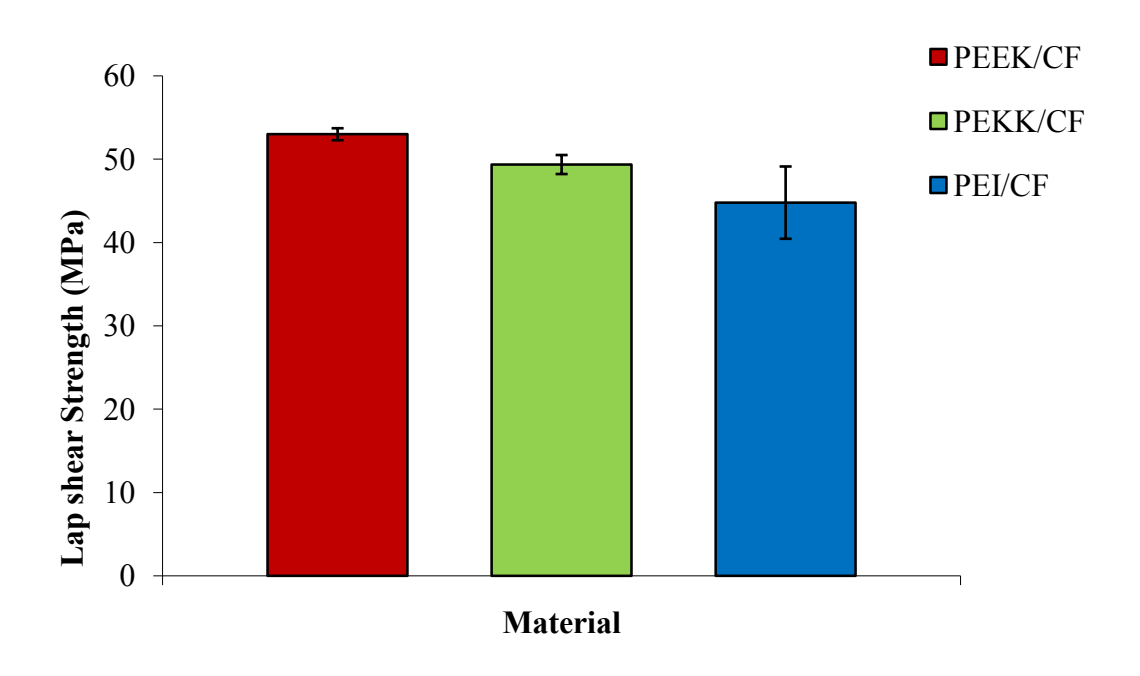


Figure 26: Static lap shear strength of resistance-welded double-lap PEEK/CF, PEKK/CF and PEI/CF joints

#### 4.1.2 Comparison with single-lap joints

The results obtained for double-lap samples for PEKK/CF, PEI/CF and PEI/GF were compared with single-lap joints [18]. The PEEK/CF results were compared with the data from Yousefpour *et al* [40]. The load-displacement curves for PEEK/CF, PEKK/CF, PEI/CF and PEI/GF are presented in Figure 27, Figure 28, Figure 29 and Figure 30, respectively. The LSS values for single-lap and double-lap samples are shown in Figure 31. The shapes of the curves are the same for the single and double-lap samples (linear for PEI, linear followed by a plateau for PEKK and PEEK), however some differences can be noted. For PEI/CF and PEI/GF, the displacement to failure is smaller for the single-lap specimens than for the double-lap specimens, while for PEEK/CF and PEKK/CF it is the opposite. This is explained by the different material behaviours: for PEEK/CF and PEKK/CF, there is a plastic deformation whereas for PEI/CF and PEI/GF the deformation is elastic only. The

plastic region is larger in the case of the single-lap specimens, while the elastic region is smaller. This is a result of the change of configuration: in the double-lap specimens, the apparent Young modulus is higher due to the added laminate, which affects the elastic behaviour. The plastic deformation mainly occurs in the areas where the stresses are maximum, i.e. the overlapped areas, which are twice bigger in the case of double-lap joints. The comparison of the LSS values for the single-lap and the double-lap joints shows that very similar results are obtained in both configurations. Less than 5% difference could be observed between the single-lap and the double-lap samples, for every material tested, except PEI/GF where no value could be obtained for the double-lap configuration. This similarity was unexpected, as the double-lap specimens were expected to lead to better mechanical performances than the single-lap ones, based on results from adhesive bonding (section 2.3.1).

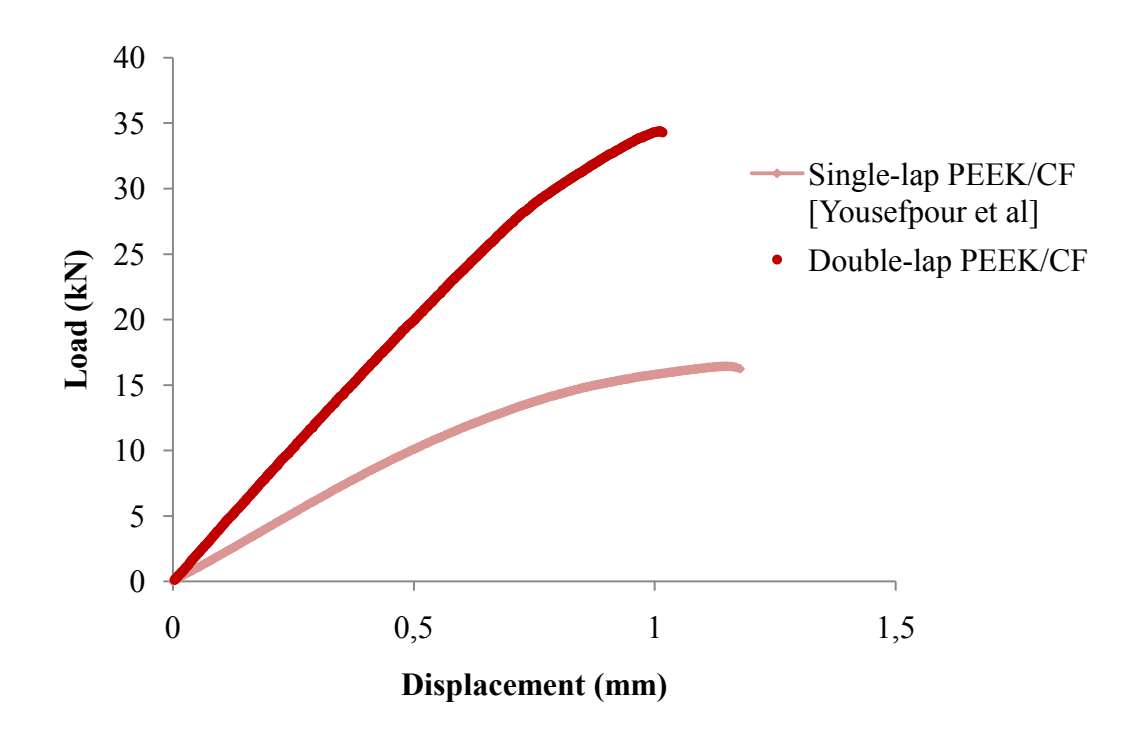


Figure 27: Static load-displacement curves of PEEK/CF [40]

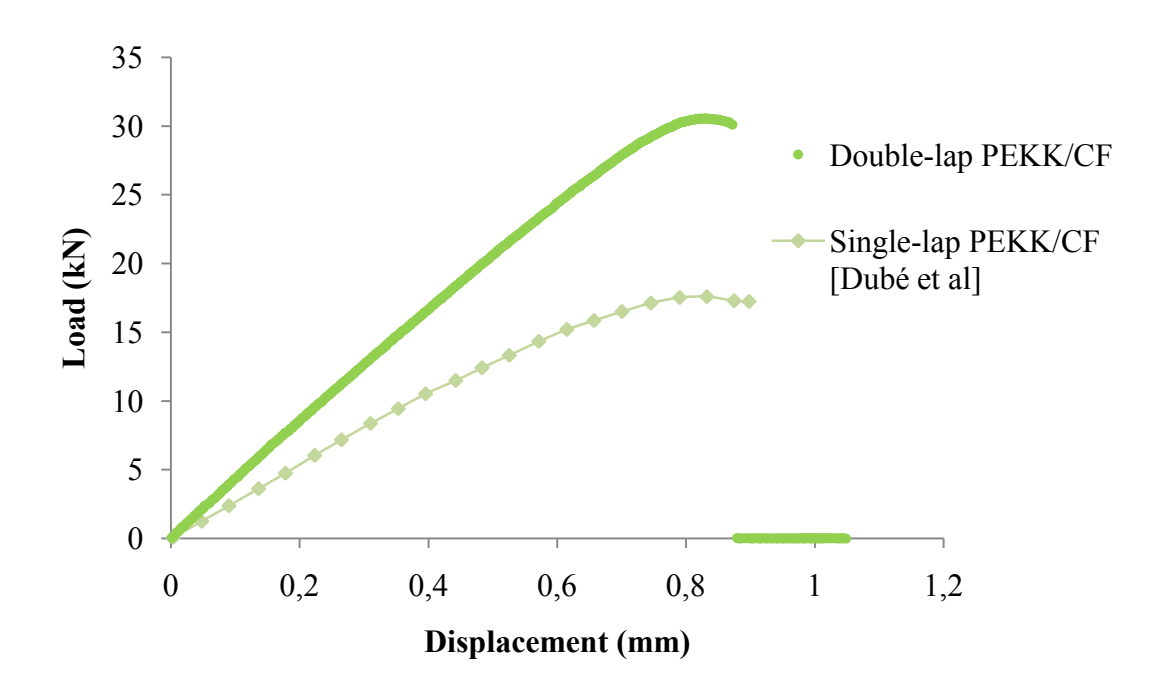


Figure 28: Static load-displacement curves of PEKK/CF [18]

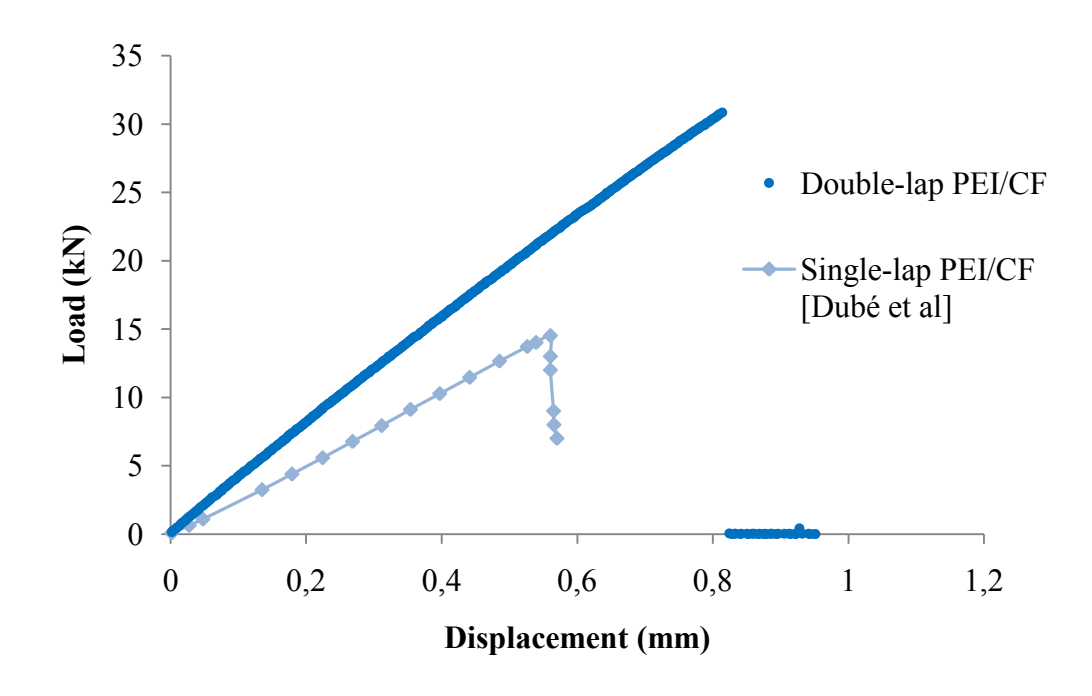


Figure 29: Static load-displacement curves of PEI/CF [18]

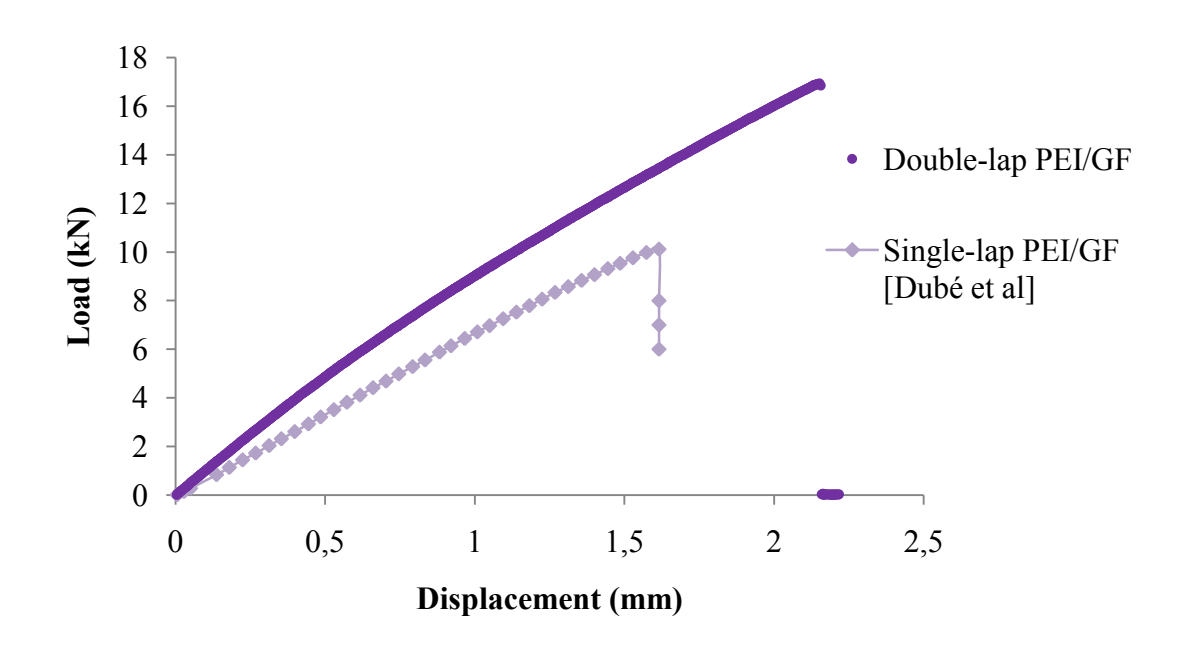


Figure 30: Static load-displacement curves of PEI/GF[18]

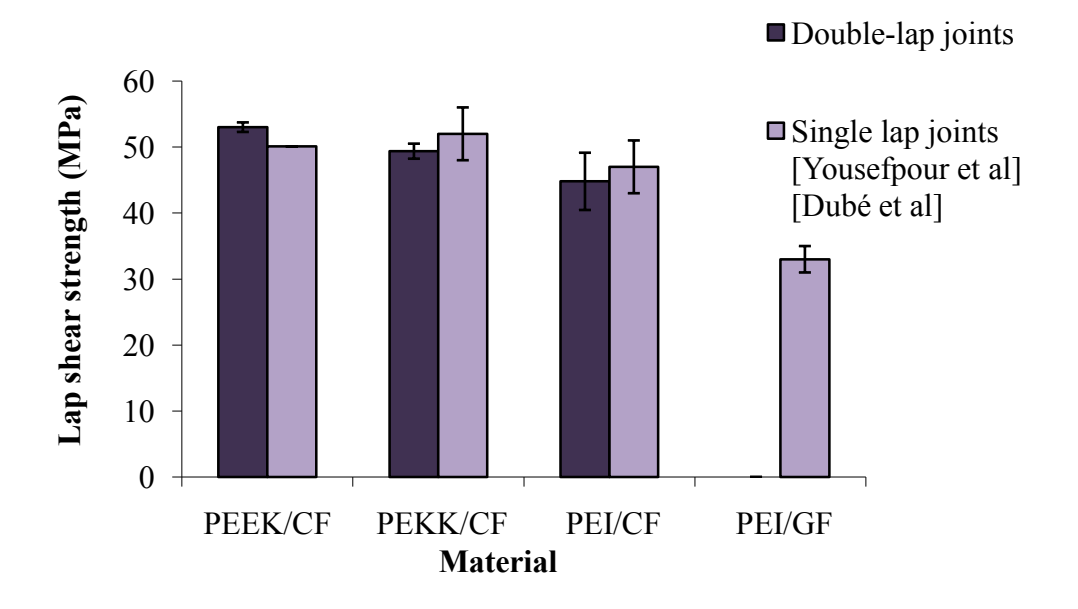


Figure 31: Lap shear strength values for single-lap and double-lap joints [18; 40]

# 4.2 Fatigue test results

## 4.2.1 Double-lap results

The fatigue performances of the double-lap specimens are presented in Figure 32 as a plot of the maximum cyclic stress versus the number of cycles before failure. The

fatigue performances of PEKK/CF and PEI/CF specimens were very similar; the PEKK/CF maximum cyclic stresses were slightly higher but both curves followed the same trend. PEEK/CF specimens exhibited better performances, while PEI/GF performances were much lower, due to the weakness of the material and configuration. These differences could be expected, considering the static strengths found previously. Since no LSS could be found from the static tests for PEI/GF, it was extrapolated from the curve, as shown with the dashed line in Figure 32. A value of 34 MPa was found, which was very close to the LSS of 33 MPa of the single-lap PEI/GF specimens. It is consistent with the observation made with the other materials, which had similar LSS values for the single-lap and the double-lap configuration. In Figure 33 the fatigue performances of the double-lap specimens are presented in terms of the percentage of the static lap shear strength (% LSS). The same observations as in terms of maximum cyclic stress could be made, with a reduction of the differences between the materials. Infinite fatigue lives were reported at 30% for PEEK/CF and PEKK/CF, 25% for PEI/CF and 20% for PEI/GF. The curves for PEKK/CF and PEI/CF could almost be superposed, which was unexpected, as PEKK/CF is supposed to have better mechanical performances. However, as it has already been said for static loading, the crystallinity of the specimens was probably very low in the weld area because of the very fast cooling rate (the interface was actually amorphous, like PEI). This indicates that the morphology of the material was not optimized, and crystallinity should probably be controlled through the processing temperature and the cooling rate in order to obtain better results. Instead of turning the current off when the maximum temperature is reached, a decreasing ramped voltage should be applied in order to obtain slower cooling rates, and hence higher degrees of crystallinity. However this would considerably increase the time necessary to achieve the welding.

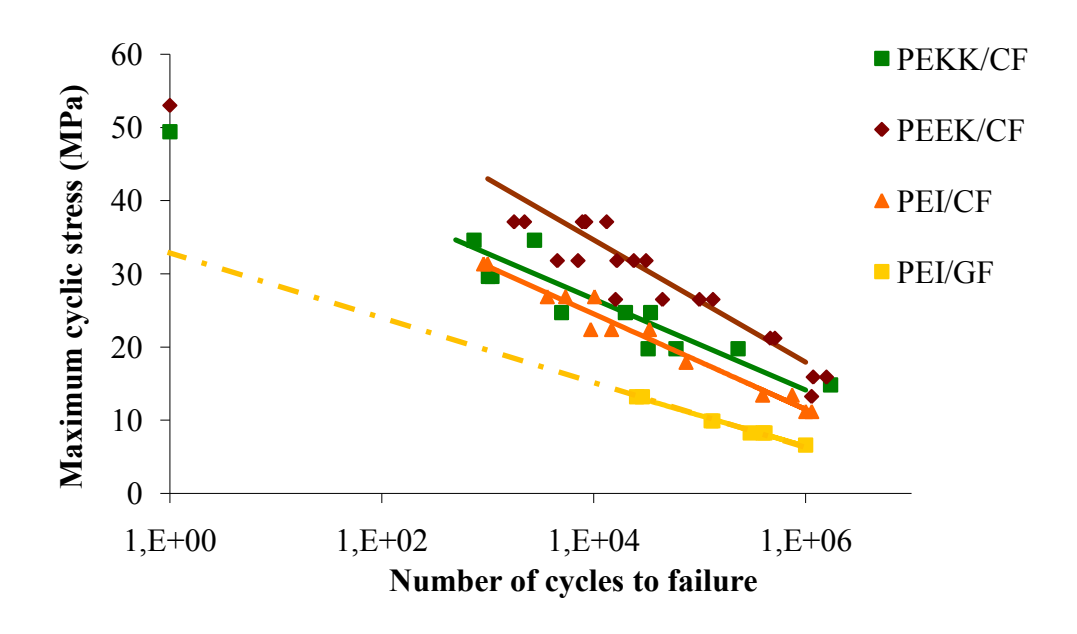


Figure 32: Fatigue performance of double-lap specimens for PEEK/CF, PEKK/CF, PEI/CF and PEI/GF

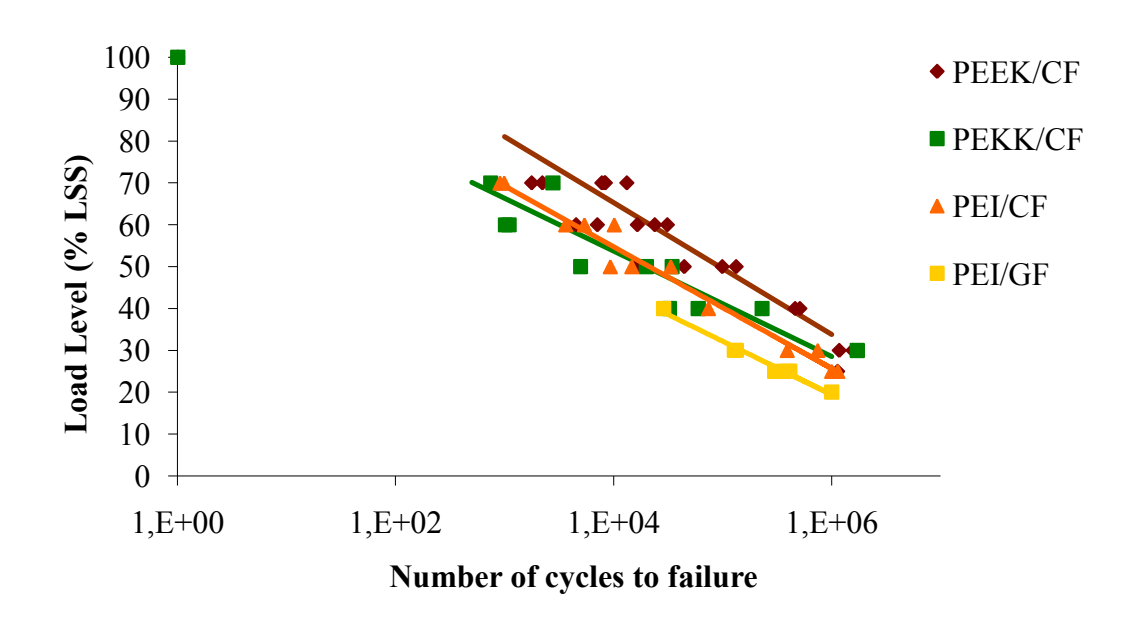


Figure 33: Fatigue performance of double-lap specimens for PEEK/CF, PEKK/CF, PEI/CF and PEI/GF (% LSS)

A remark should be made about the PEI/GF specimens: for about half the tests, coupon failure occurred instead of weld failure, indicating that the weld was roughly

the same strength as the material itself. The same problem had been encountered for the static tests, preventing the calculation of the lap shear strength of the specimens. However, when adding in the plot the results from the coupon failures, as presented in Figure 34, , they match the curve perfectly, with very few scatter, showing that the mechanical performances of the weld could be deducted from a simple coupon test instead of testing the double-lap specimens, in that particular case.

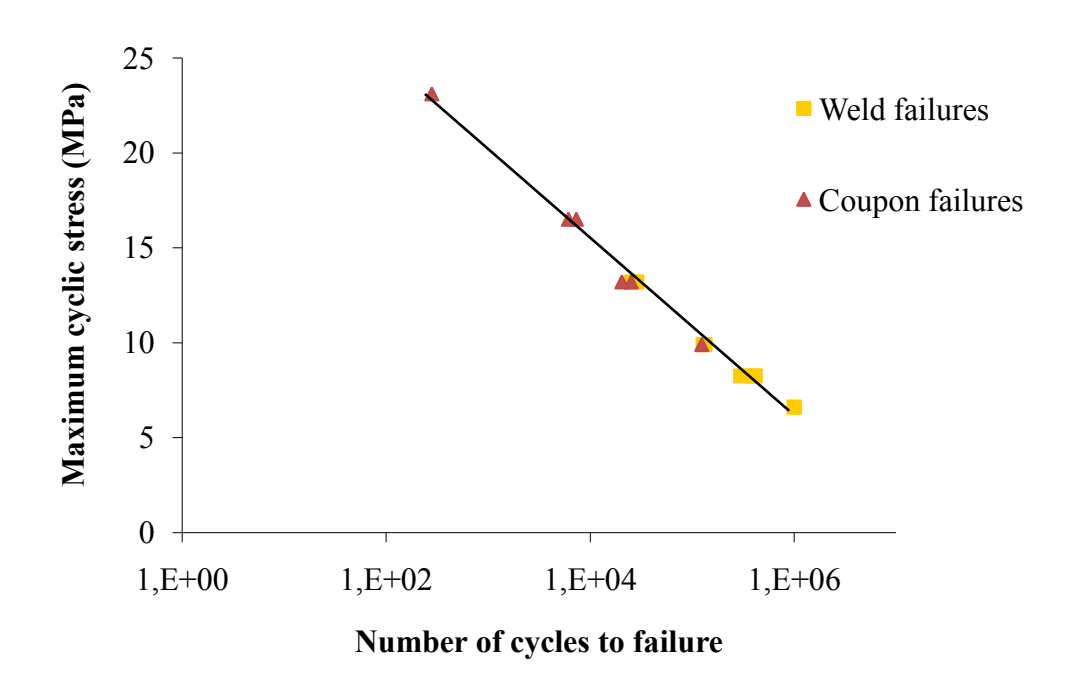


Figure 34: Fatigue performance and modes of failure of double-lap PEI/GF

### 4.2.2 Comparison with single-lap joints

Very few investigations have been conducted on dynamic behaviour of resistance-welded joints. The only information available are fatigue data on PEKK/CF, PEI/CF and PEI/GF single-lap joints by Dubé *et al* [81], and PEEK/CF single-lap joints by Yousefpour *et al* [40]. Fatigue results for each material were thus compared with the results obtained in these two studies for single-lap joints. They are plotted in terms of percentage of static strength in Figure 35, Figure 36, Figure 37 and Figure 38. Since

the static lap shear strengths were very similar for the double-lap and the single-lap configurations, there is no major difference between plotting in terms of percentage of LSS or in terms of maximum cyclic stress. Very similar fatigue behaviours could be observed for PEEK/CF, PEKK/CF, PEI/CF and PEI/GF single-lap and double-lap specimens. In particular, for PEI/GF, the curves could almost be superposed. For PEI specimens, for both configurations, the same infinite fatigue life was reported: 25% for PEI/CF and 20% for PEI/GF. On the other hand, the same was not true for PEKK/CF specimens, for which infinite fatigue life was reported at 30% for the double-lap configuration, and at 25% for the single-lap configuration. However, the scatter of the data is sufficient to explain that difference. In the case of PEEK/CF, infinite fatigue life was reported at 35% for the single-lap joint and 30% for the double-lap joint, but the double-lap specimens were not tested at 35%, which could explain that difference.

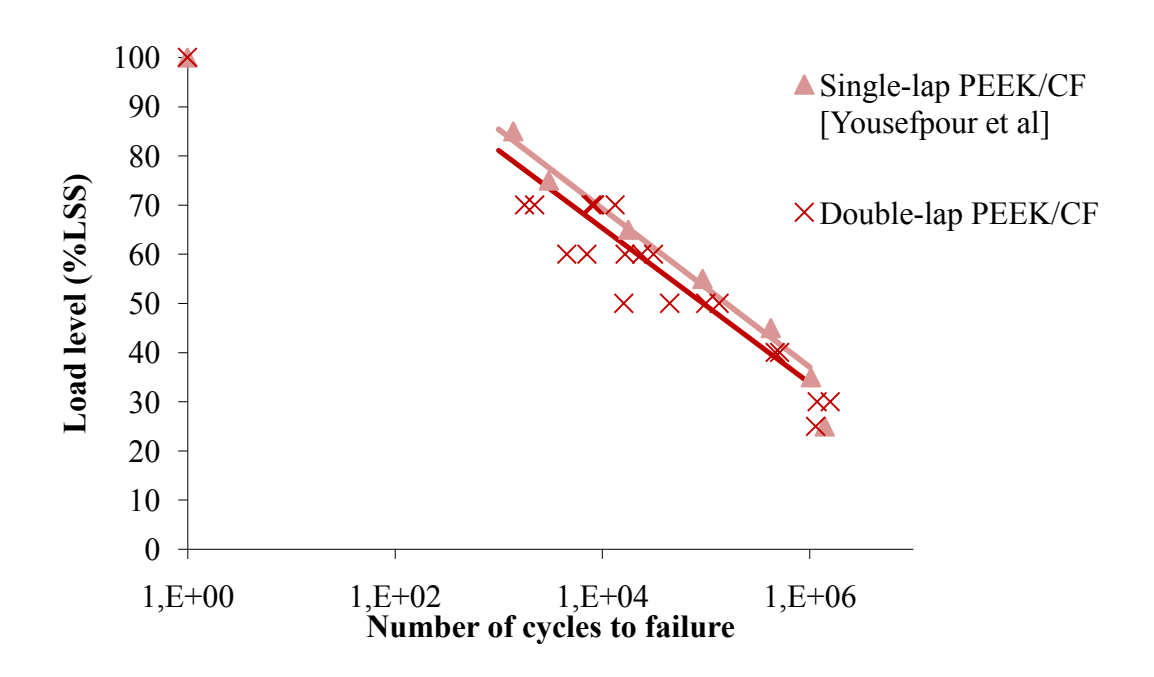


Figure 35: Fatigue performance of PEEK/CF (%LSS)[40]

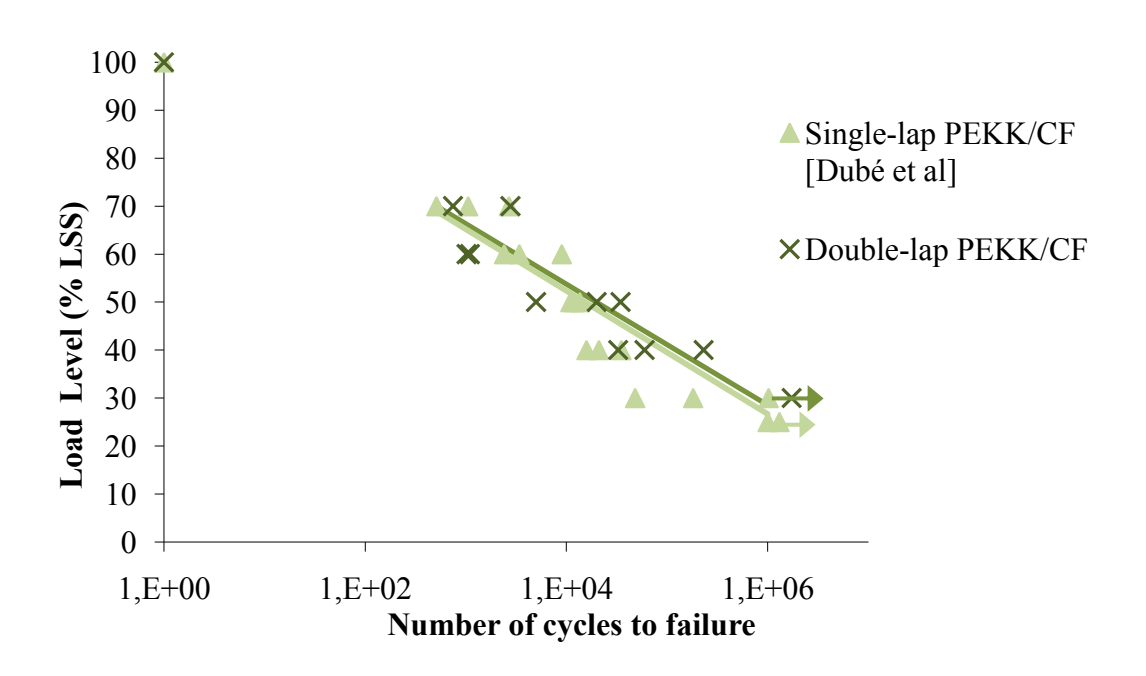


Figure 36: Fatigue performance of PEKK/CF (% LSS)[43]

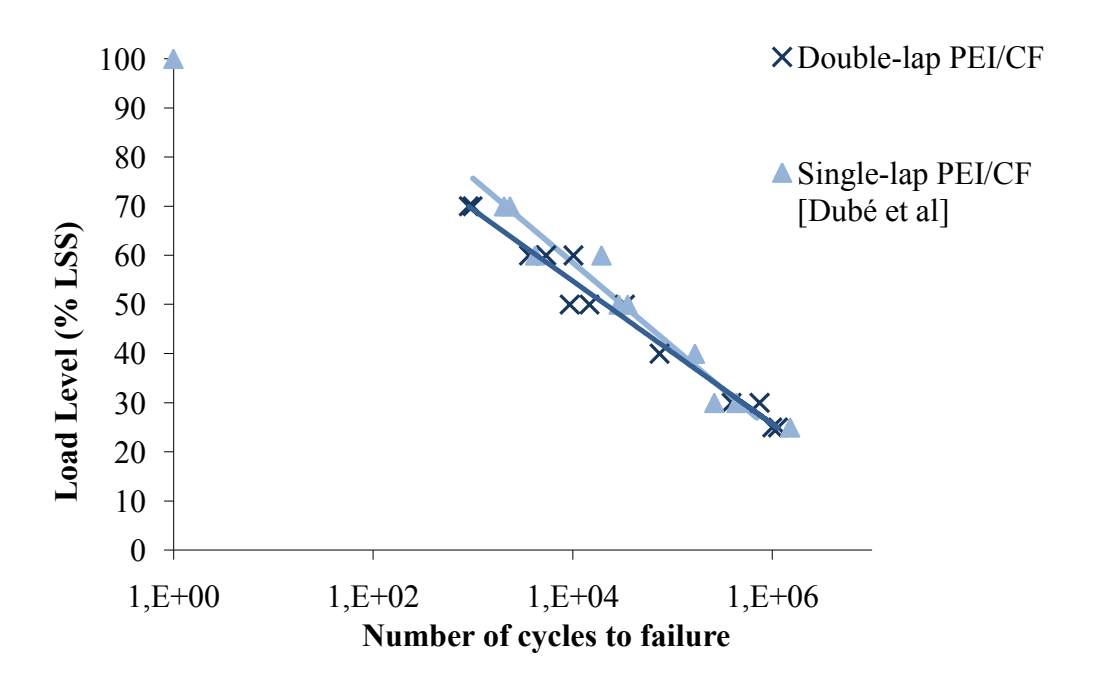


Figure 37: Fatigue performance of PEI/CF (% LSS)[43]

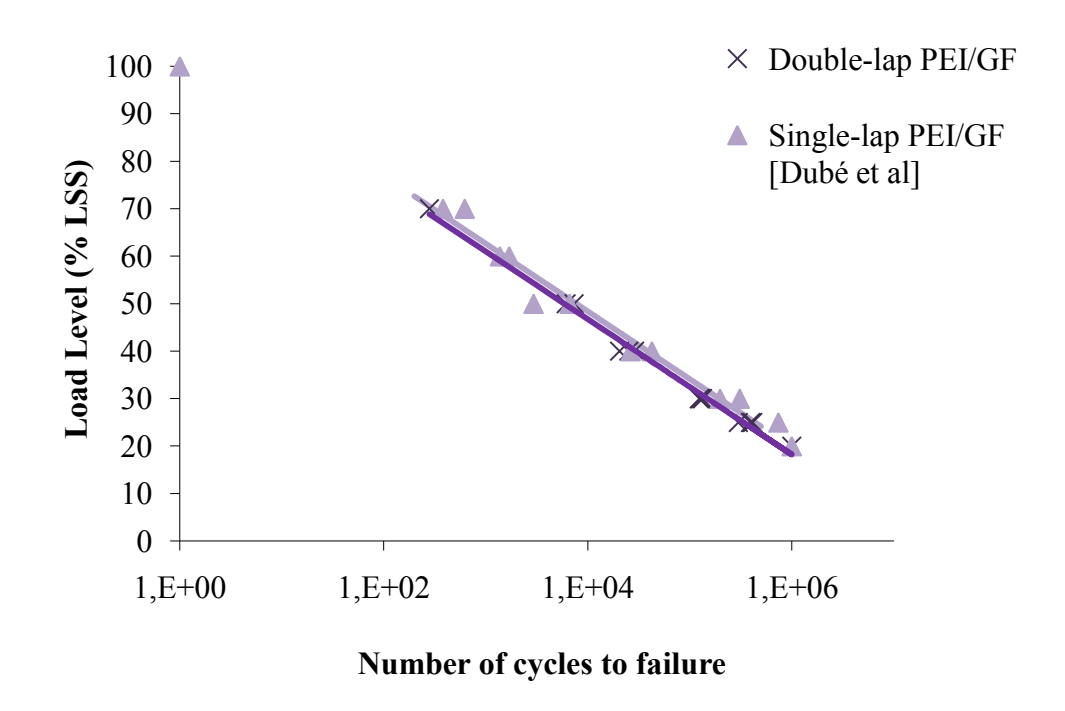


Figure 38: Fatigue performance of PEI/GF (% LSS)[43]

The similarity between the double-lap and the single-lap configuration for each material is striking, and unexpected, as these results are very different from those obtained for adhesive bonding (section 2.3.1).

## 4.3 Observation of the fracture surfaces

#### 4.3.1 Failure modes

The quality of the weld can be evaluated by mechanical testing, but also by an examination of the fracture surfaces. Visual observation of these surfaces can give information about the mode of failure of the specimen. In the case of lap shear testing, three different modes of failure can be observed [9]: interlaminar, interfacial and coupon failure. The failure is considered interlaminar when it occurs within the laminate (tearing of the laminate), in the heating element (tearing of the heating element), or within both of them. The failure is called interfacial when it occurs at the

interface between the laminate and the heating element. The coupon failure occurs when the tensile strength of the material is lower than its shear strength, and hence the materials fails before the bond does. The interlaminar mode yields to the highest shear strength, showing a good quality of the weld, while the interfacial mode is linked to lower strength and hence poorer bonding. The coupon failure mode does not give any information about the shear strength. These modes are represented schematically in Figure 39 in the case of a single-lap shear joint (the double-lap shear specimens fail in the same way, except the failure occurs on two surfaces).

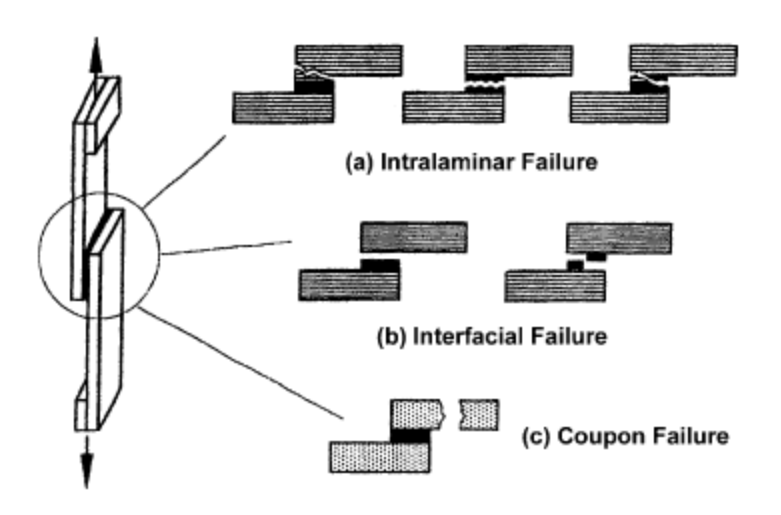


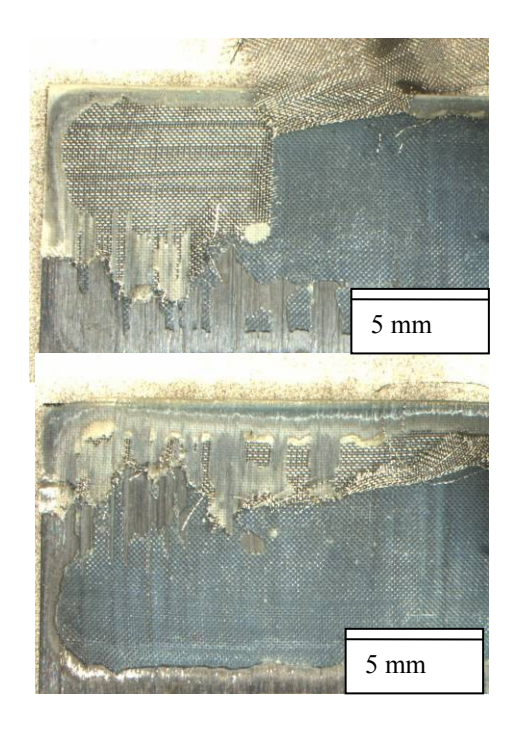
Figure 39: Schematic of the failure modes [9]

#### 4.3.2 Fracture surfaces from static tests

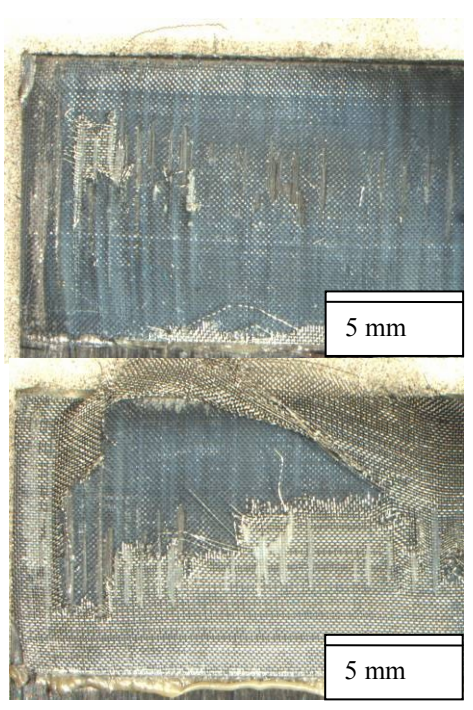
The fracture surfaces from static tests of PEEK/CF, PEKK/CF, PEI/CF and PEI/GF are shown in Figure 40, Figure 41, Figure 42 and Figure 43, respectively. The failure of both welds seemed to occur simultaneously. Except in the case of PEI/GF, which exhibited a coupon failure, all materials exhibited interlaminar failure on both welds, with tearing of both the heating element and the laminate. However, some differences could be observed: for PEI/CF, the heating element had very little damage and most of the deterioration occurred within the laminate, with many fibres being ripped off

the laminate. For PEEK/CF, the opposite could be observed, with most of the damage being done to the heating element and very few ruptured fibres. PEKK/CF's behaviour was in between, with damage equally shared between the heating element and the laminate.

This reveals the degree of adhesion between the heating element and the polymer: the interfacial bonding was certainly better between the heating element and PEI than PEEK, resulting on parts of the laminate ripping off and sticking to the heating element. On the other side, most of the heating elements used to weld PEEK samples are fully visible, and clearly most of the welded polymer remained stuck to the adherends, while the heating element was torn between the laminates. The detached parts of the mesh showed no visible sign of polymer impregnation. PEKK samples showed an intermediary behaviour.

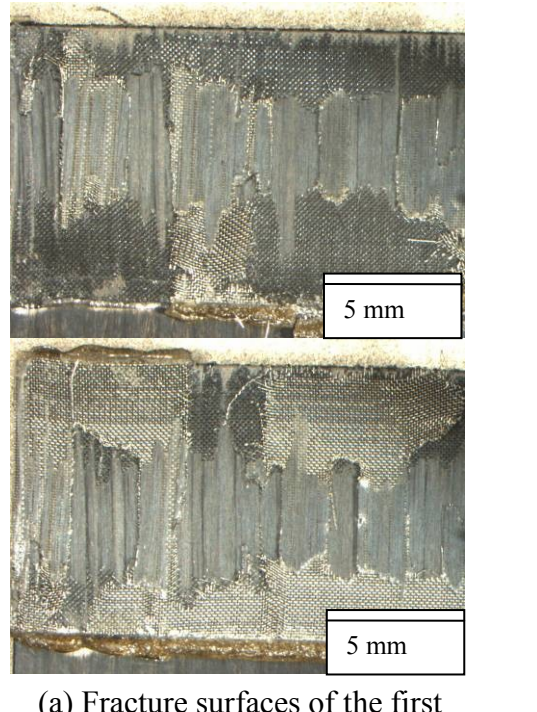


(a) Fracture surfaces of the first weld

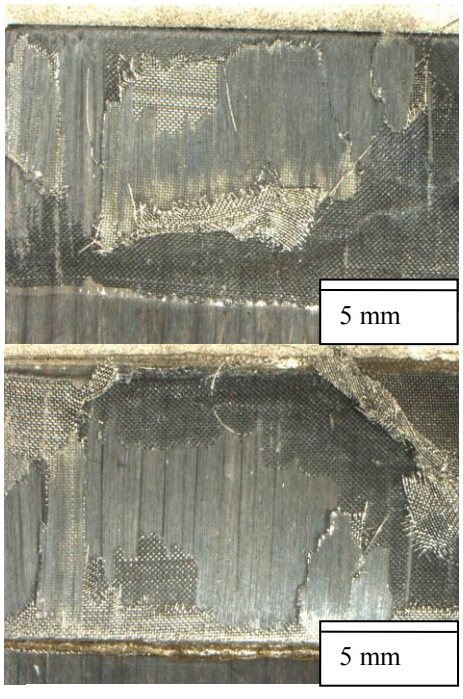


(b) Fracture surfaces of the second weld

Figure 40: Fracture surfaces from PEEK/CF static tests

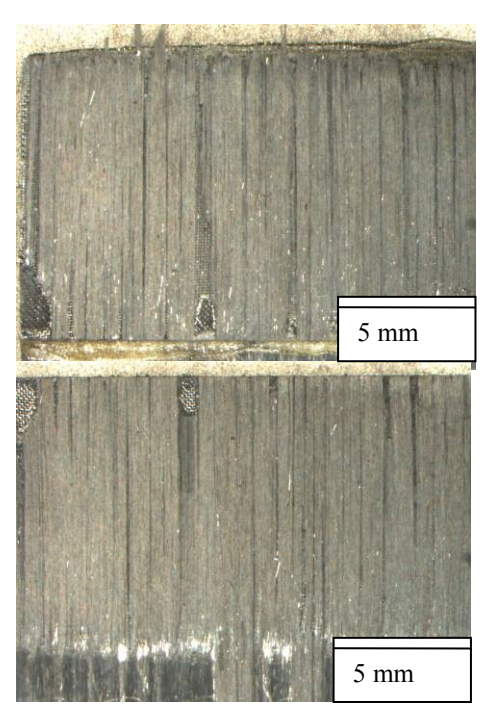


(a) Fracture surfaces of the first weld

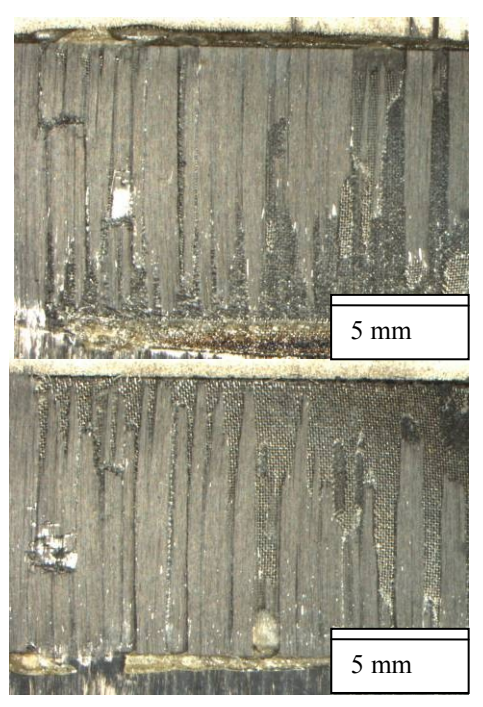


(b) Fracture surfaces of the second weld

Figure 41: Fracture surfaces from PEKK/CF static tests



(a) Fracture surfaces of the first weld



(b) Fracture surfaces of the second weld

Figure 42: Fracture surfaces from PEI/CF static tests



Figure 43: Fracture specimen of PEI/GF from static tests

## 4.3.3 Fracture surfaces from fatigue tests

Fracture surfaces from fatigue tests for each material are shown in Figure 45. Figure 44 explains the terminology used. The same modes of failure as in the static case were observed, except for the PEI/GF samples where weld failures could this time be observed, for lower applied loads. The PEI/GF also exhibited interlaminar failure, with considerable damage done to the laminates. Several layers were torn during the failure, indicating a very good adhesion of the joint. PEI/CF also showed major deterioration of the adherend, with fibres being ripped out along the length of the laminate even outside the weld interface as shown in Figure 45 (c), while PEEK/CF and PEKK/CF exhibited less adherend deterioration, like for the static failures.

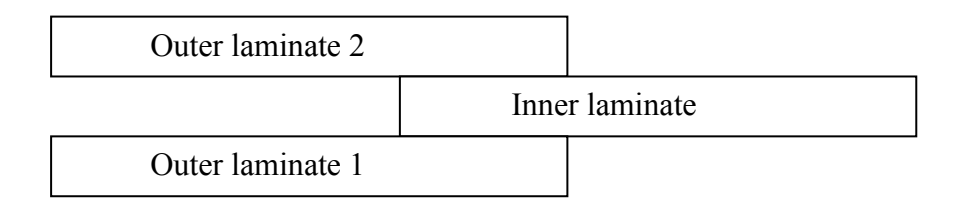
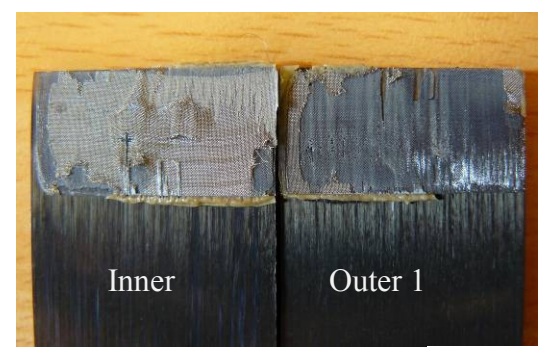
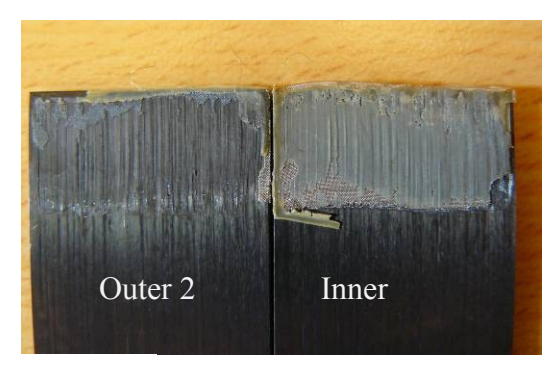
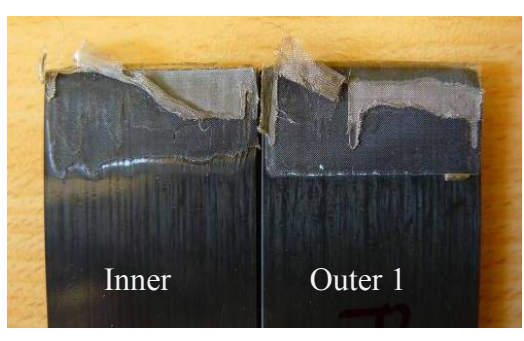


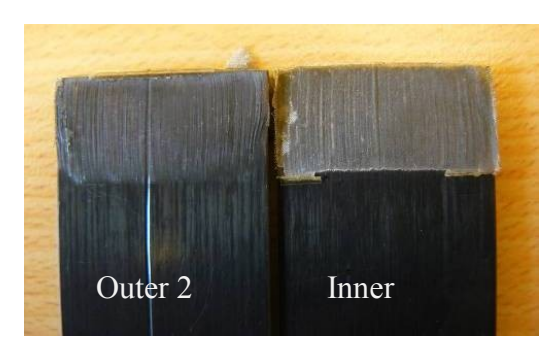
Figure 44: Schematics of the double-lap specimen



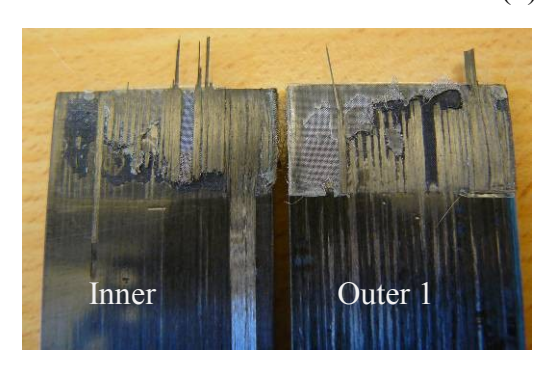


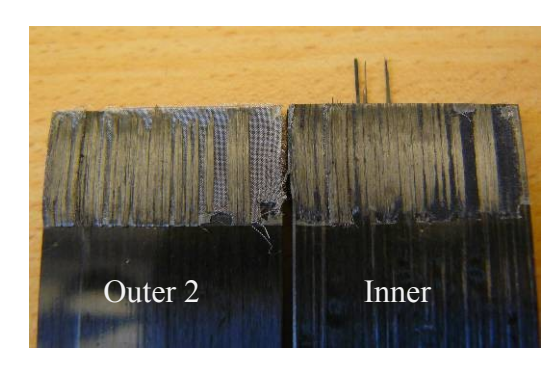
(a) PEEK/CF



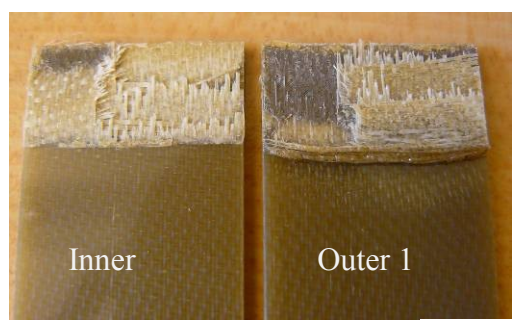


(b) PEKK/CF





(c) PEI/CF





(d) PEI/GF

Figure 45: Fracture surfaces from fatigue tests for the two welds for: (a) PEEK/CF, (b) PEKK/CF, (c) PEI/CF, (d) PEI/GF

Unlike in the static case where the welds seemed to have failed at the same time, the welds failures were not simultaneous and one weld failed before the other, resulting in the transfer of the entire load in the other weld, rapidly leading to the second failure. It was probably the case for static loading as well, but the failure was too rapid to be observed. This can be explained by the non-symmetry in the welding condition, as the second weld is performed between a laminate and the single-lap specimen obtained from the first weld. This is shown schematically in Figure 46: for the first weld the configuration is symmetric while for the second weld it is not and the through-thickness temperature should thus be different in the two cases (see section 3.1.3 for the welding procedure). To avoid this non-symmetry, a second laminate could be added on the top of the specimen for the second weld, as shown in Figure 47. This non-symmetry could also explain the difference observed between the fracture surfaces of the two welds, like in Figure 45 (a) and (b).

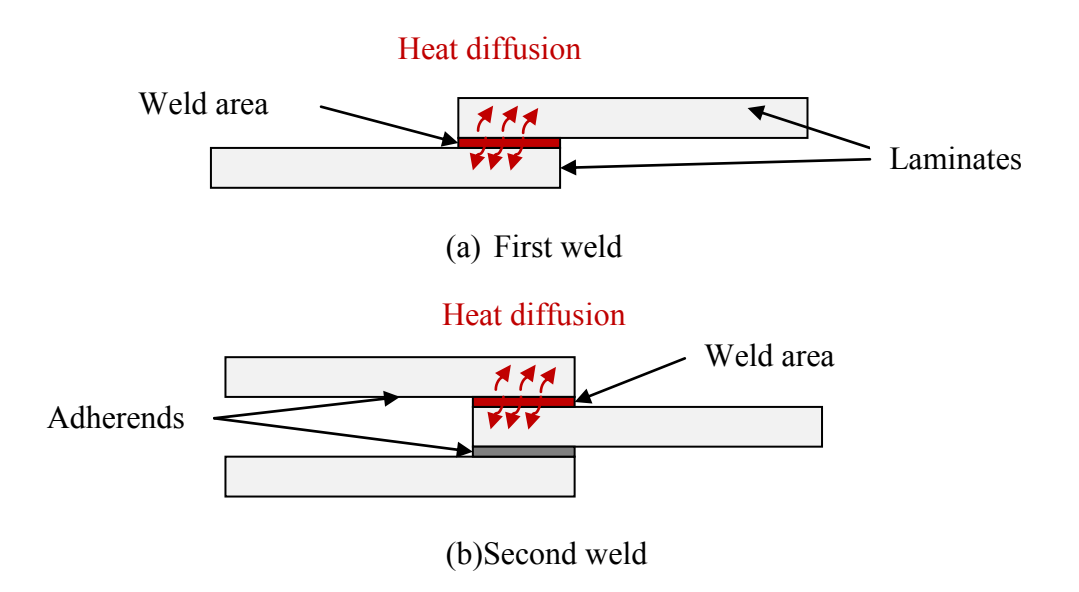


Figure 46: Schematics of the welding configuration for (a) the first weld and (b) the second weld

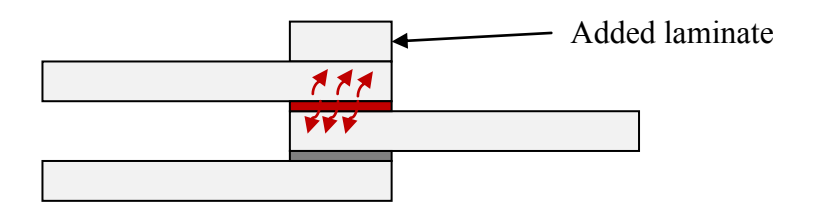


Figure 47: Schematics of the suggested welding configuration for the second weld

It is interesting to note that when the heating element is torn in two, the remaining parts stay generally stuck at the end of each laminate, like shown in Figure 48.

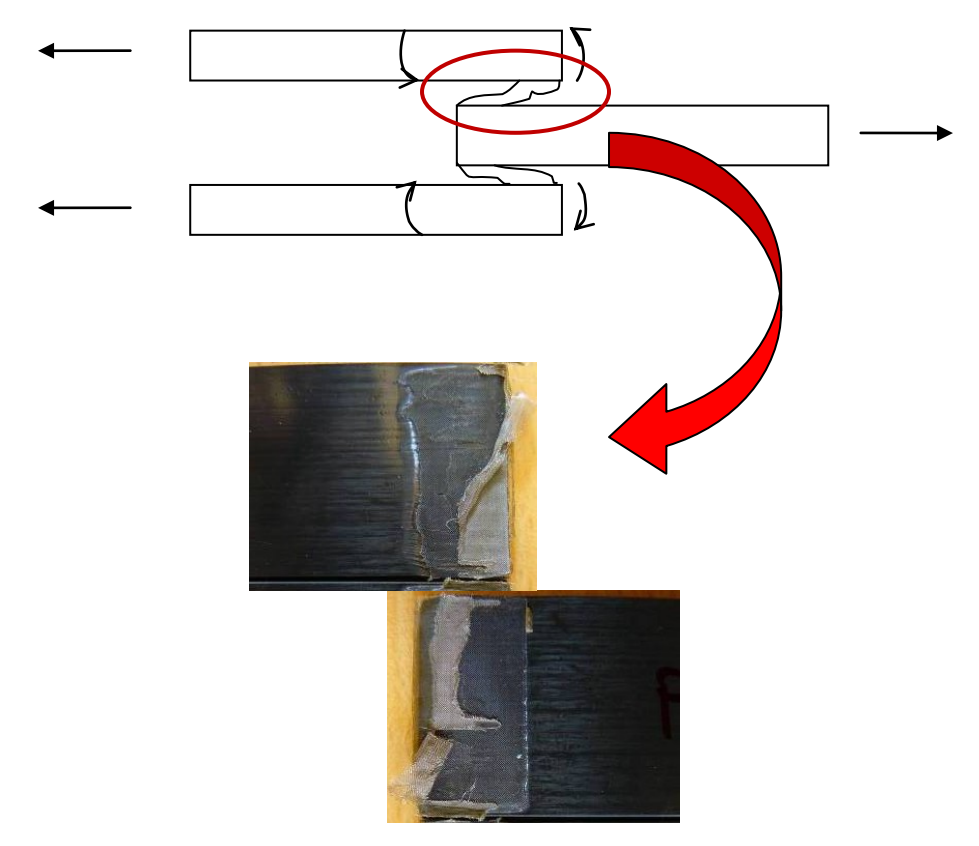


Figure 48: Heating element deterioration

Heat transfer modelling and analysis of the temperature distribution inside the weld can shed some light on this observation. Talbot [21] used 3D ANSYS model to investigate the temperature distribution along the length of the weld and showed that there is a drop of temperature on the end of the weld, specifically where the heating element adhesion is the poorest. This is illustrated in Figure 49, in the case of APC-2/AS4 laminates.

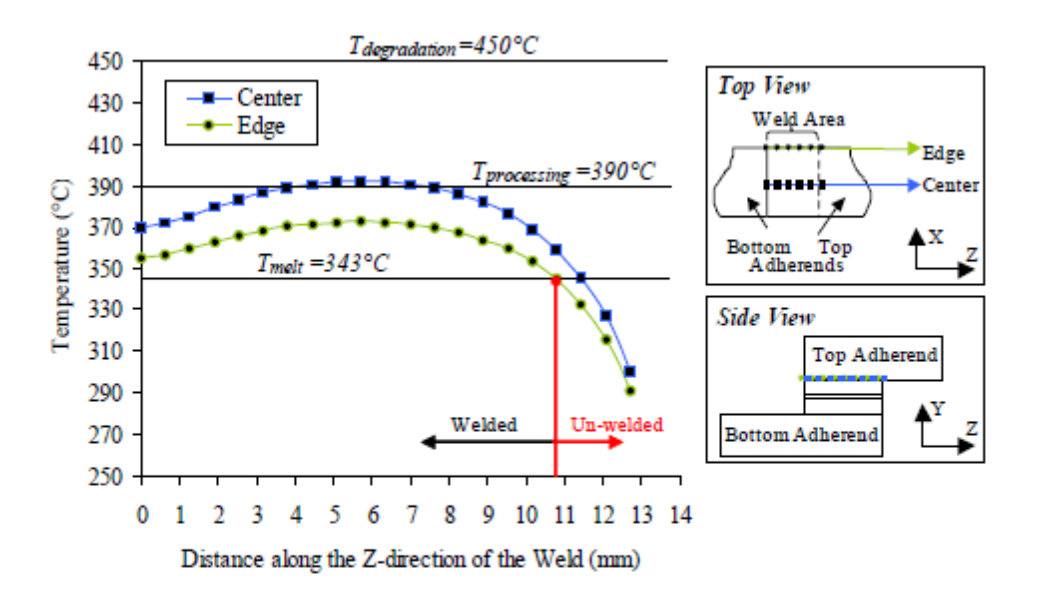


Figure 49: Temperature distribution along the length of the weld as predicted by 3D model[21]

Based on this model, it can be deducted that the quality of the weld will be poorer in the part of the interface where the temperature drop occurs, which is precisely where the heating element was observed to detach from the laminate. To avoid this problem, the processing temperature was increased in order to obtain a more uniform temperature distribution throughout the weld.

## 4.4 Interface quality characterization

#### 4.4.1 Scanning electron microscopy (SEM)

Scanning electron microscopy allows higher magnifications than optical microscopy to observe fibre breakage or adhesion of the polymer. A typical fracture surface is presented in Figure 50, for a PEKK/CF specimen. Various regions can be identified: fibres from the bottom laminate, resin-rich region, heating element and fibres from the top laminate. A closer look was taken in each of these regions, as shown in Figure 51 and Figure 52.

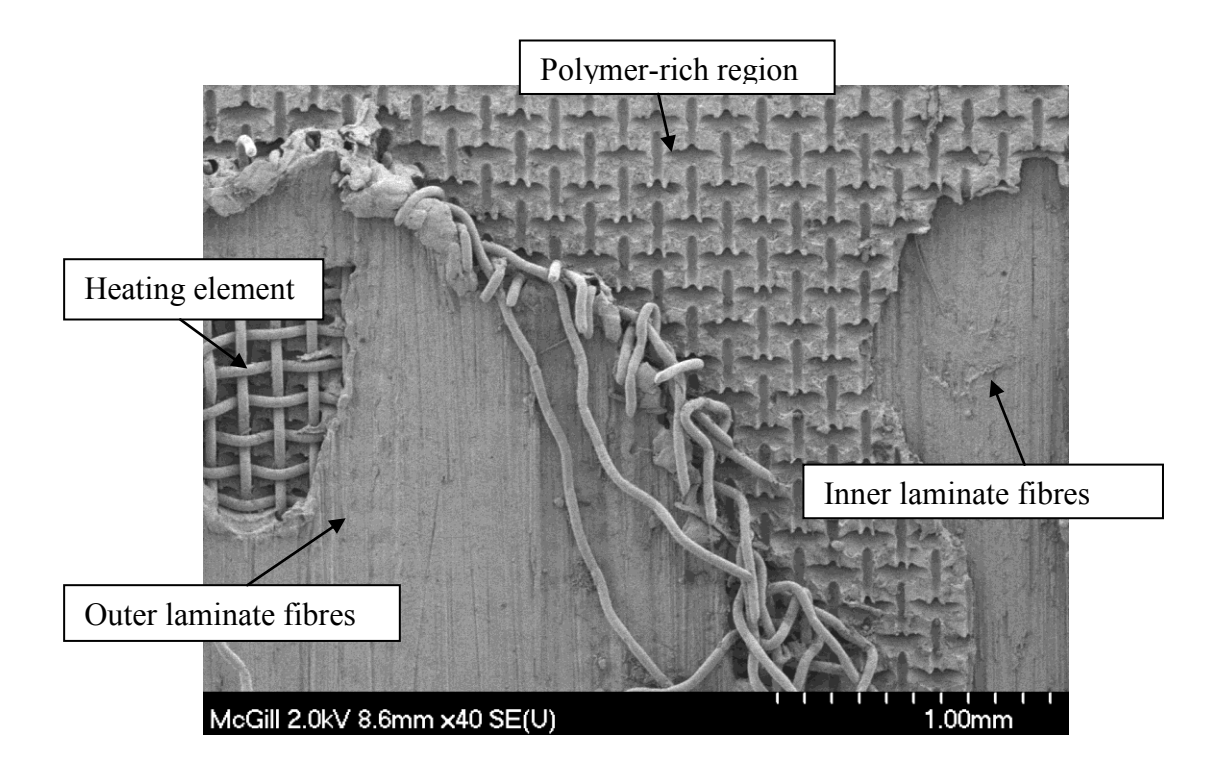


Figure 50: Fracture surface of fatigue tested PEKK/CF (SEM x40)

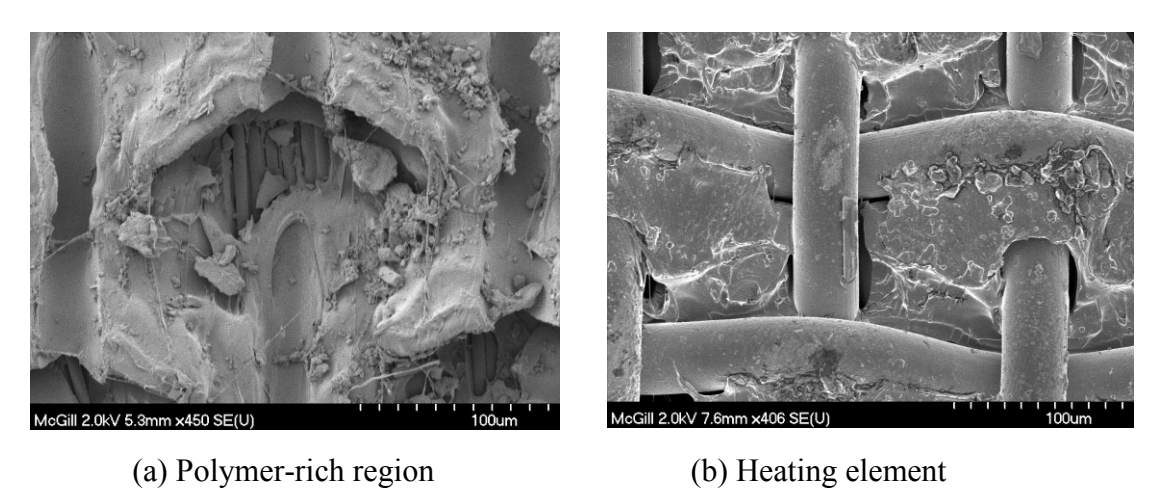


Figure 51: SEM image of (a): Polymer-rich region (450x), (b): Heating element (406x)

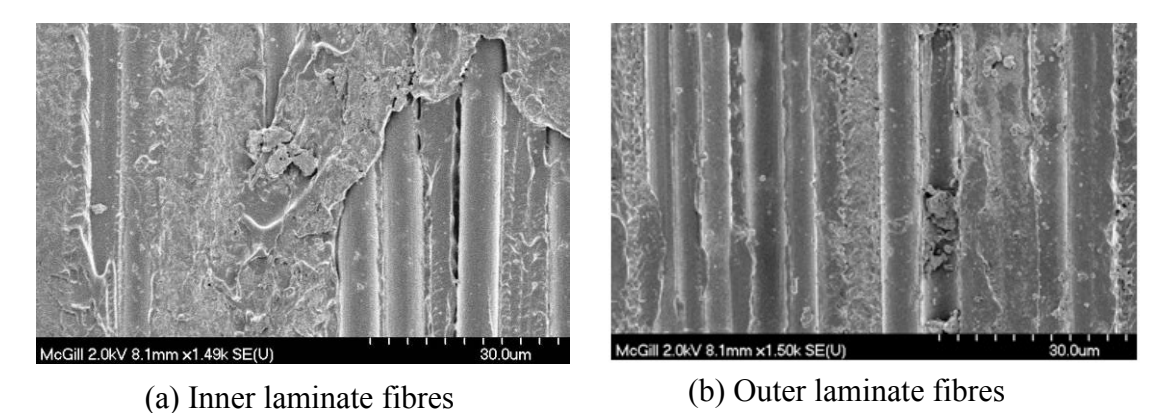


Figure 52: SEM image of (a): Inner laminate fibres (1490x) and (b): Outer laminate fibres (1500x)

SEM micrographs reveal a good adhesion between the polymer and the fibres, which were well impregnated by the resin. The wetting of the heating element was good as well; however the adhesion between the mesh and the polymer was weaker, showing that the bond strength was carried out mainly by mechanical interlocking rather than interfacial bonding between the polymer and the mesh. This was true for every material tested, as illustrated on Figure 53.

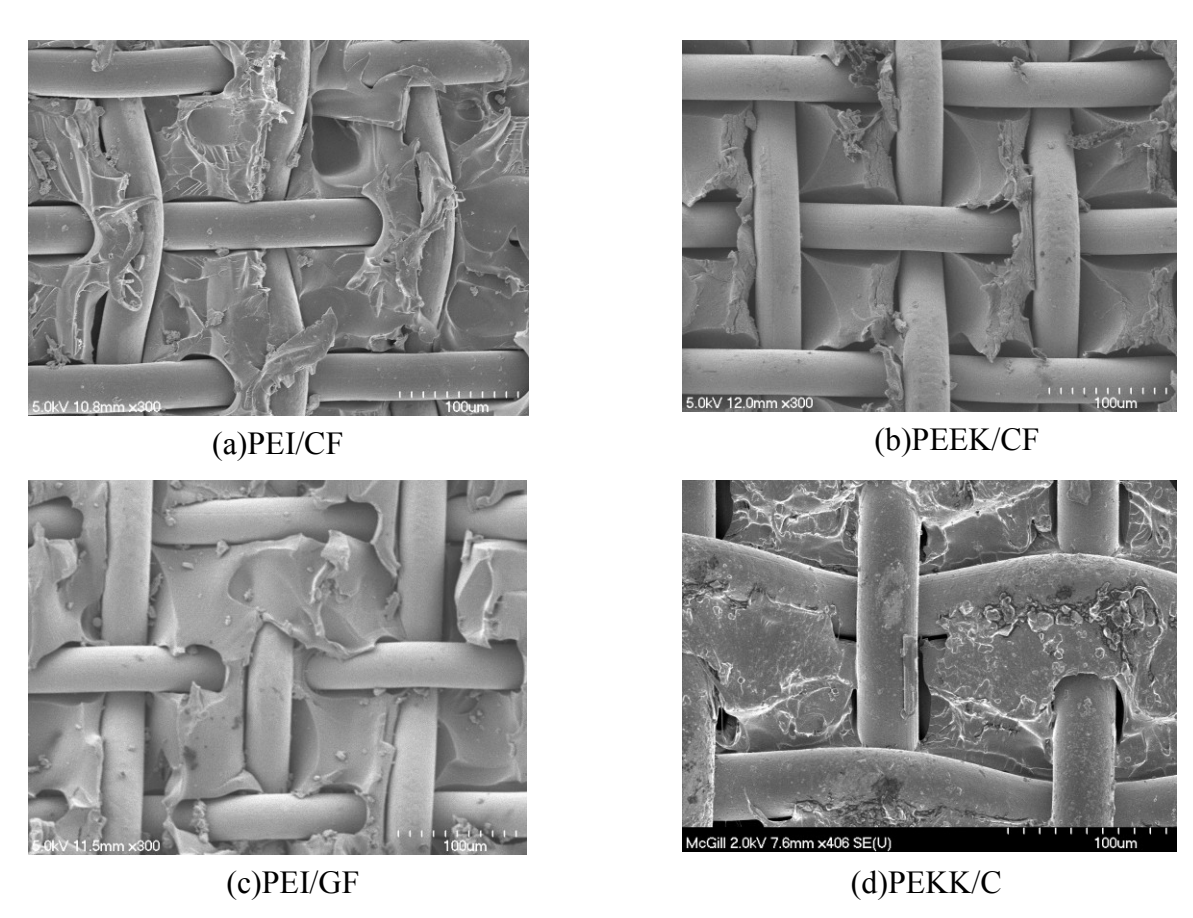


Figure 53: SEM pictures of the heating element impregnation for (a) PEI/CF, (b) PEEK/CF, (c) PEI/GF and (d) PEKK/CF

As the type of fibres and the lay-up was different for the PEI/GF specimens, the fracture surfaces were quite different from the other materials. A typical fracture surface for PEI/GF is presented in Figure 54.

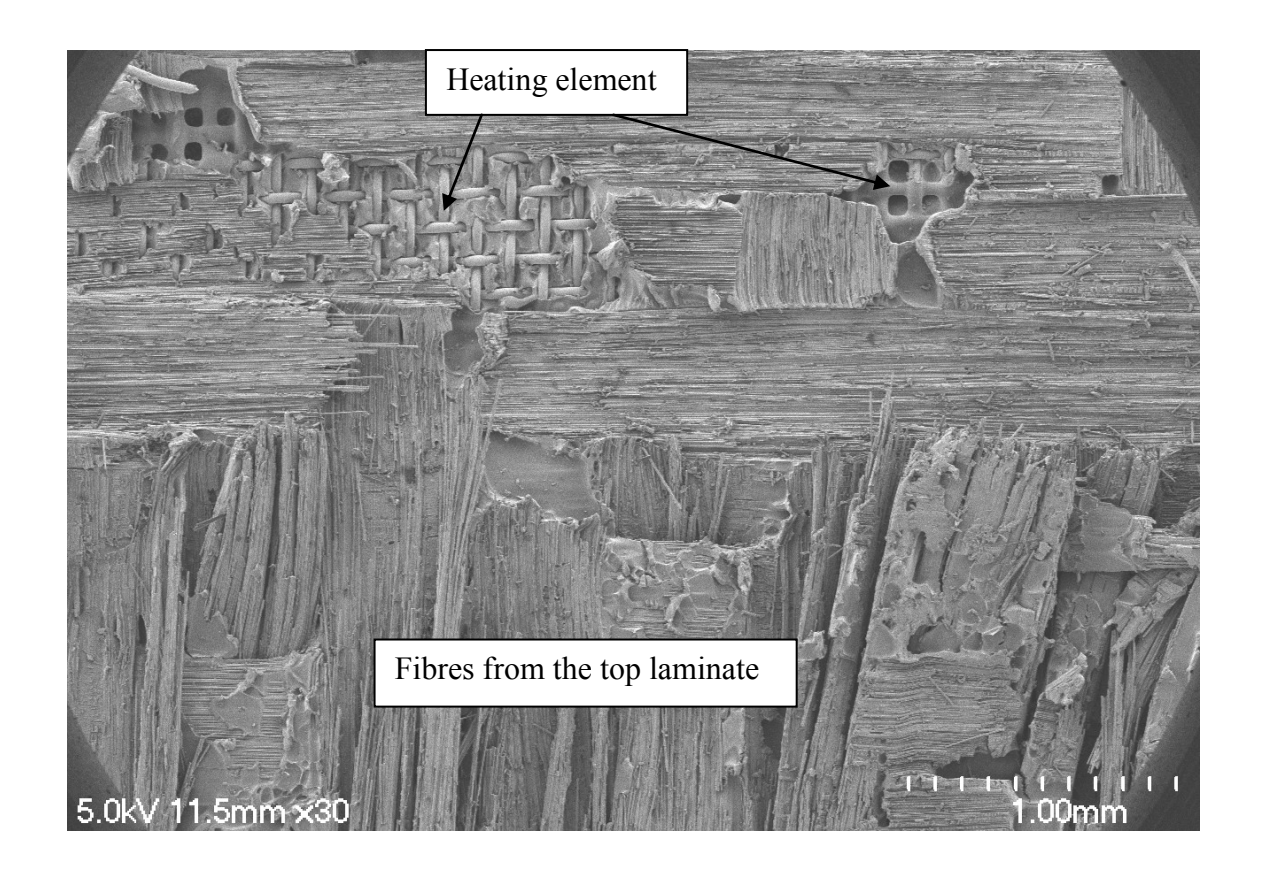


Figure 54: Typical fracture surface of fatigue tested PEI/GF (30×)

A lot more fibres than for the other materials were broken, due to the higher brittleness of glass fibres. Several layers of fibres could be observed on the fracture surfaces. Another difference with the other materials is the impregnation of the heating element: at some locations, it could be seen that the heating element had completely been impregnated with the polymer, with no visible wire, as shown in Figure 55. This is consistent with the lower viscosity of PEI than PEEK or PEKK. It also reveals a better interfacial bonding between the heating element and PEI than with PEEK or PEKK.

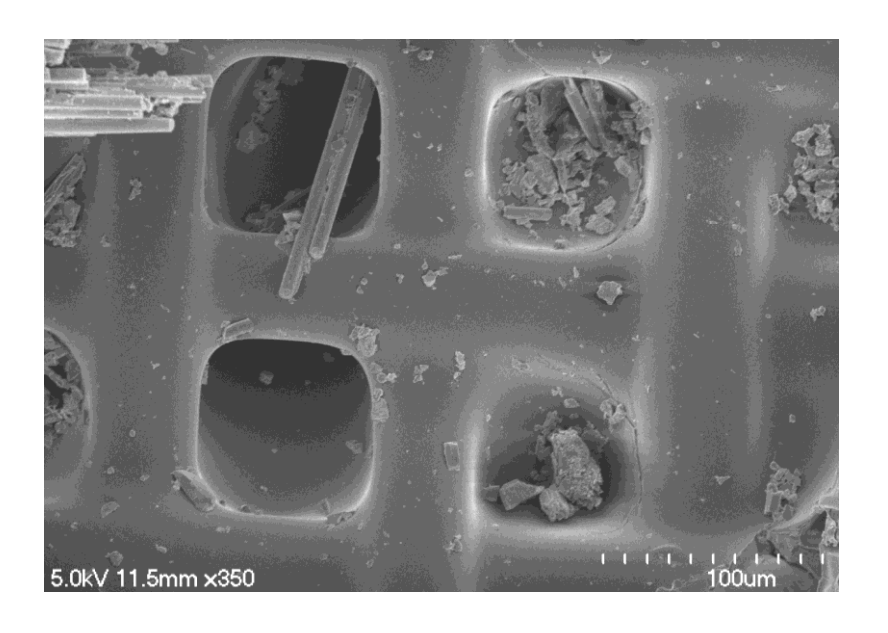


Figure 55: Heating element impregnation for a fatigue tested PEI/GF specimen (350×)

Figure 56 presents the fracture surface of a PEEK/CF specimen. Like the other materials, various areas could be identified: bottom laminate (welded or not), polymer, heating element (impregnated or not). The limit between the welded and the unwelded area confirms what was said previously about the temperature distribution: there is a temperature drop at the end of the weld area which results in a poorer bonding at that end, and explains why the heating element did not remain stuck on that side.

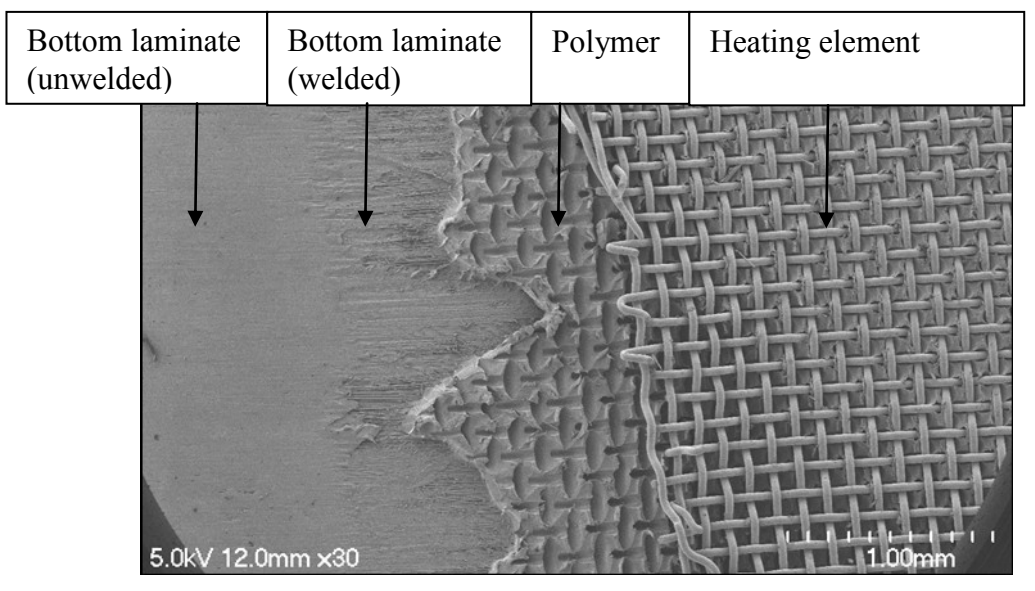
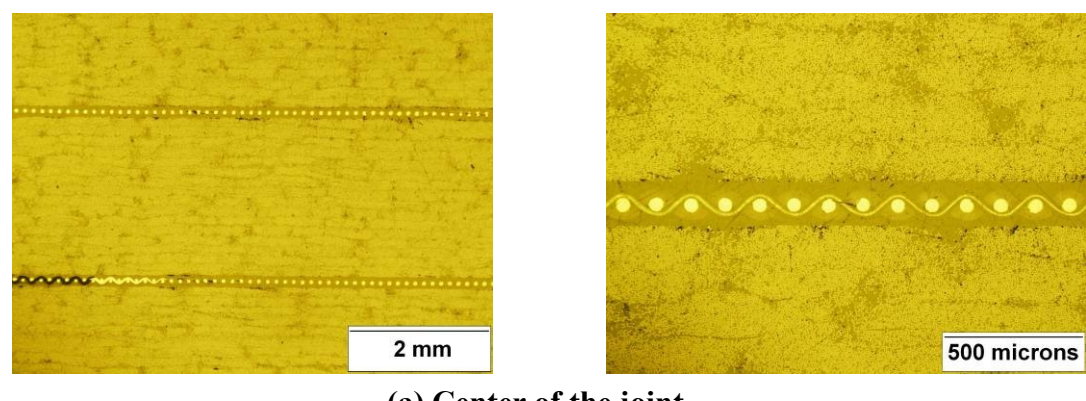


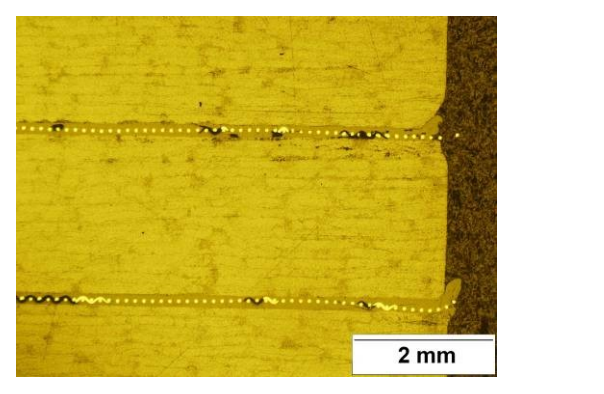
Figure 56: Fracture surface of fatigue tested PEEK/CF (30×)

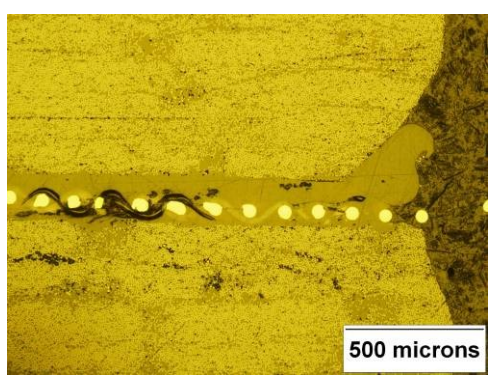
#### 4.4.2 Optical microscopy

Microscope observation was also used to examine the quality of the weld by looking at the cross-section of the joint. Observations were made at the centre and at the edges of the welds, with magnifications of 25× and 100×. Pictures of the edges and centre for both weld interfaces are shown for PEKK/CF in Figure 57 and for PEI/CF in Figure 58. The same general behaviour was observed for each material. No difference could be seen between the first and the second weld. At the centre of the joint, a uniform weld with no void or porosity was observed. The heating element was completely impregnated with the polymer, which led to development of mechanical interlocks thus a strong bond. At the edges of the joints, some signs of polymer squeezed out and over heating due to the local edge effects were observed. These observations are in good agreement with the ones made by Dubé et al [18] on the single-lap-shear configuration. PEI samples exhibited more voids at the edge of the joint than PEEK and PEKK. This could be explained by PEI lower environmental resistance; however in that case the defects would be located all over the joint and not only at the edge. Another explanation is the fact that molten PEI has a lower viscosity than PEEK and PEKK [82]. As a result, more polymer is being squeezed out of the weld area under the welding pressure and more voids are created. More deformation was also observed at the edge of the joint for PEI samples.



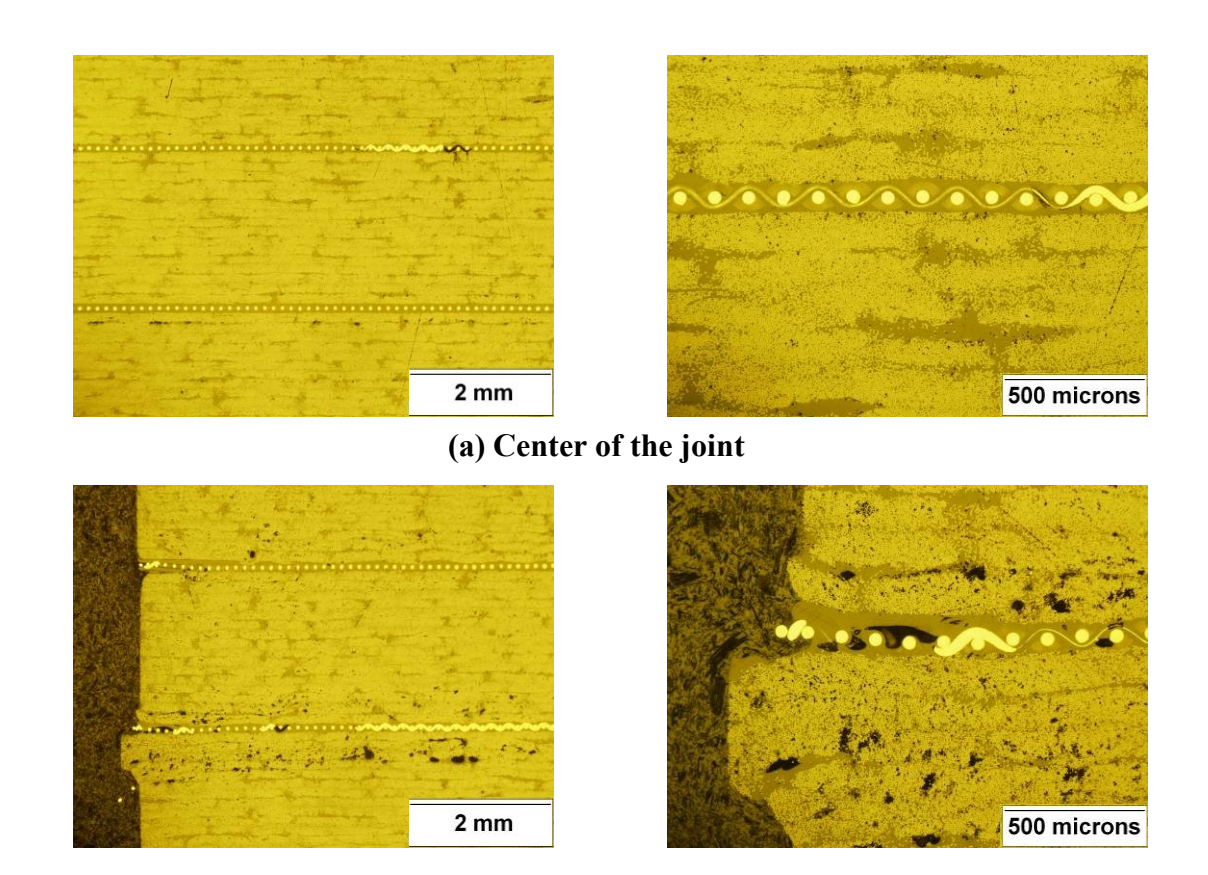
(a) Center of the joint





(b) Edge of the joint

Figure 57: Micrographs  $25\times$  and  $100\times$  of the cross-section at the center (a) and edge (b) of a double-lap PEKK/CF specimen



(b) Edge of the joint

Figure 58: Micrographs 25x and 100x of the cross-section at the center (a) and edge (b) of a double-lap PEI/CF specimen

### 5 Discussion and stress analysis

The mechanical performances of resistance-welded joints are the same whether the configuration is a single-lap or a double-lap joint. As these results were verified for different materials (amorphous and semi-crystalline), and even different fibre arrangements, they can probably be verified with other materials or structures. These results indicate that the mode of failure is probably not the same for adhesive bonding and resistance welding. In the case of adhesive bonding, for thick enough adherends, failure is controlled by peel stresses, which are far more significant for single-lap joints and lead to earlier failure than double-lap joints. For resistance welding, either the failure is not induced by peel stresses, or there is no such difference in the amplitude of peel stresses between the single-lap and the double-lap geometry.

A very simple analysis was performed to investigate the stress distribution at the interface for both configurations. ANSYS Finite Element Analysis software was used to model the stress distribution of the single-lap and double-lap configuration under tensile loading. Pre-processing, solving and post-processing of the model were performed with ANSYS workbench 11.0. In order to simplify the model, the weld interface was assumed to be of the same material as the adherends (the heating element was not taken into account). The joint was simulated using simple surface-to-surface contact between the welded parts. The joint was simulated using simple surface-to-surface contact between the welded parts. The analysis was a structural steady-state, non-linear analysis with small displacements. The element type is automatically chosen by ANSYS workbench and was set to SOLID186, a 20-node solid element. Element size was 0.5 mm.

### 5.1 Geometry and material properties

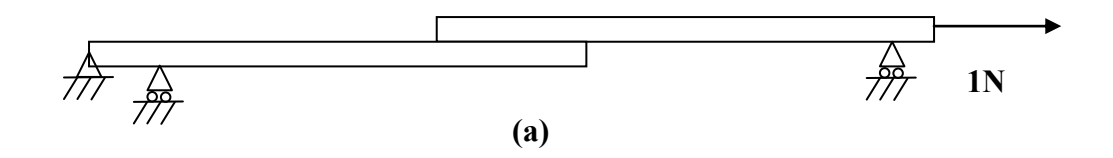
The adherends were two (for the single-lap joint) or three (for the double-lap joint) APC2/AS4 laminates, overlapping on each other. The laminates were 101.6 mm long, 25.4 mm wide and 2.3 mm thick. The overlap length was 12.7 mm. The material's properties are shown in Table 8.

Table 8: APC2/AS4 Mechanical properties [83]

Young's Modulus (GPa)	E <sub>11</sub>	$\mathbf{E}_{22}$	E <sub>33</sub>
	138	10.2	10.2
Shear Modulus (GPa)	G <sub>12</sub>	$G_{23}$	G <sub>13</sub>
	5.7	3.7	5.7
Poisson's Ratio	v <sub>12</sub>	V <sub>23</sub>	v <sub>13</sub>
	0.28	0.33	0.28

# **5.2 Boundary Conditions**

A 1N unit-load parallel to the direction of the length was applied to one end of the joints, while the other end was clamped. To simulate the clamping, no displacement was allowed in the transverse direction at both ends of the specimen. The boundary conditions are shown schematically in Figure 59.



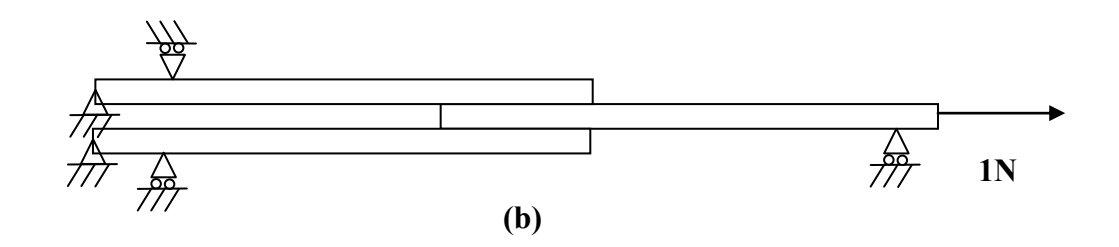


Figure 59: Boundary conditions for (a): single-lap joint and (b): double-lap joint

## 5.3 Results

Figure 60 and Figure 61 show the deformed shapes of the single-lap and the double-lap joint, respectively. The deformation is exaggerated by the software. As expected, there is some bending in both configurations, more significantly in the single-lap than in the double-lap one. In both configurations the order of magnitude is very small, compared with the size of the sample.

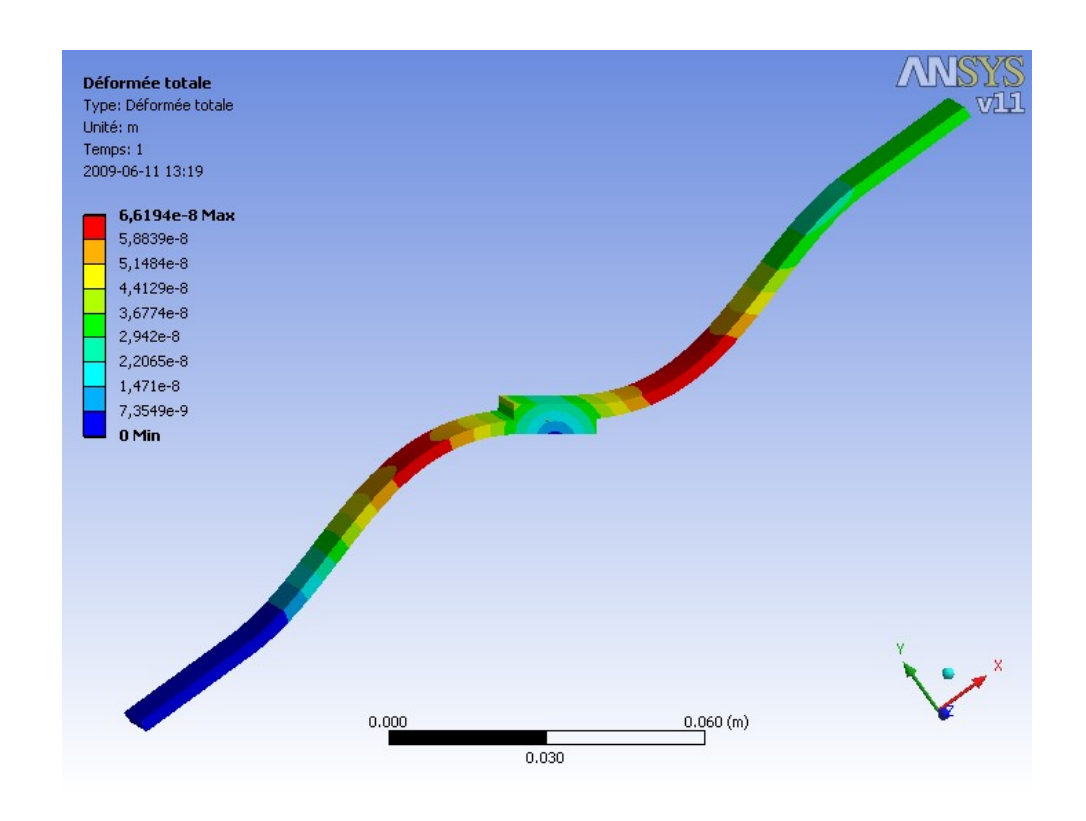


Figure 60: Deformed shape of single-lap joint

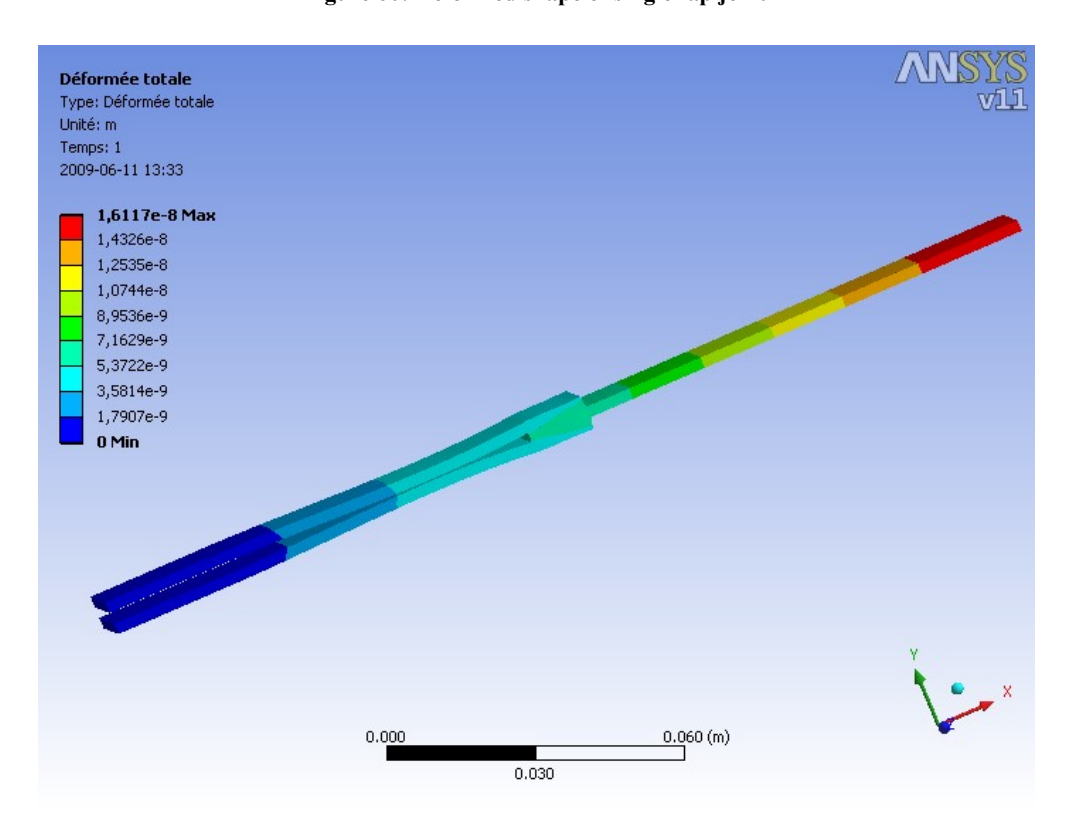
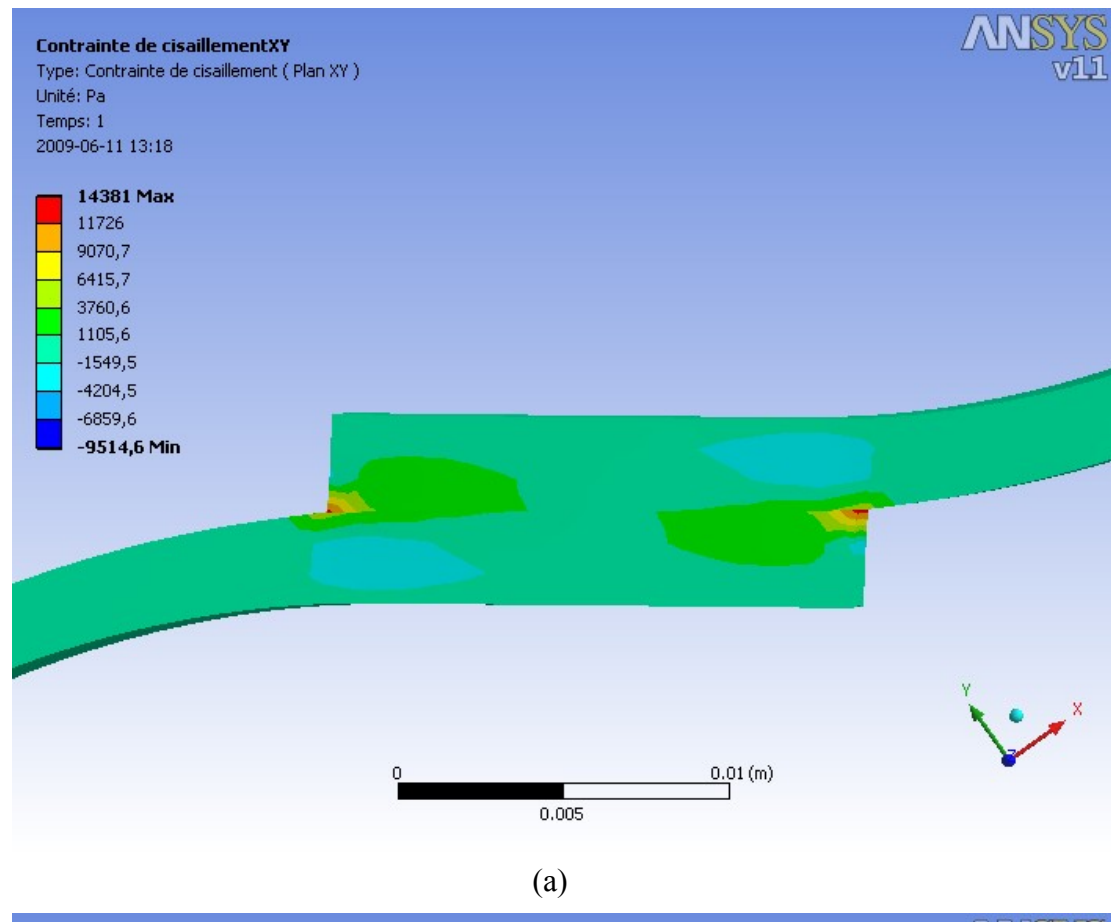


Figure 61: Deformed shape of double-lap joint



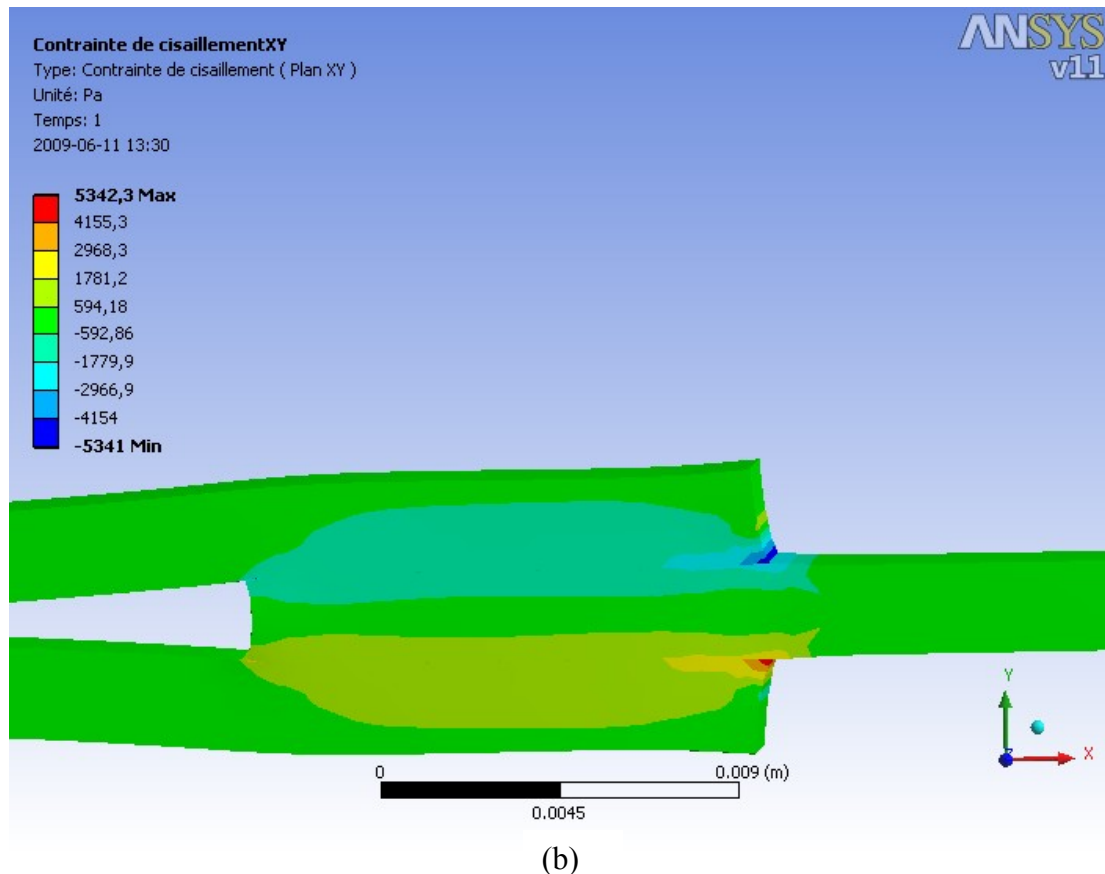
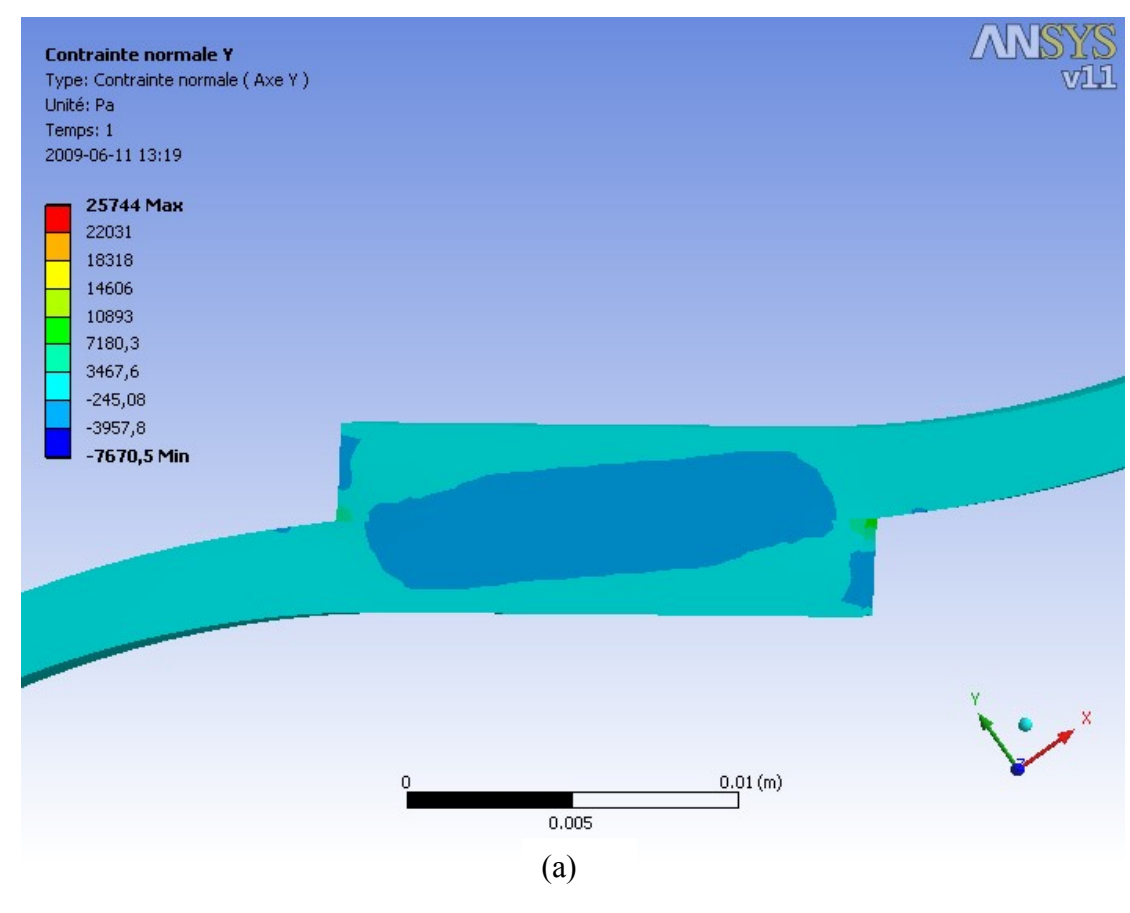


Figure 62: Shear stresses  $\tau_{xy}$  in (a) single-lap joint and (b) double-lap joint  $\,$ 



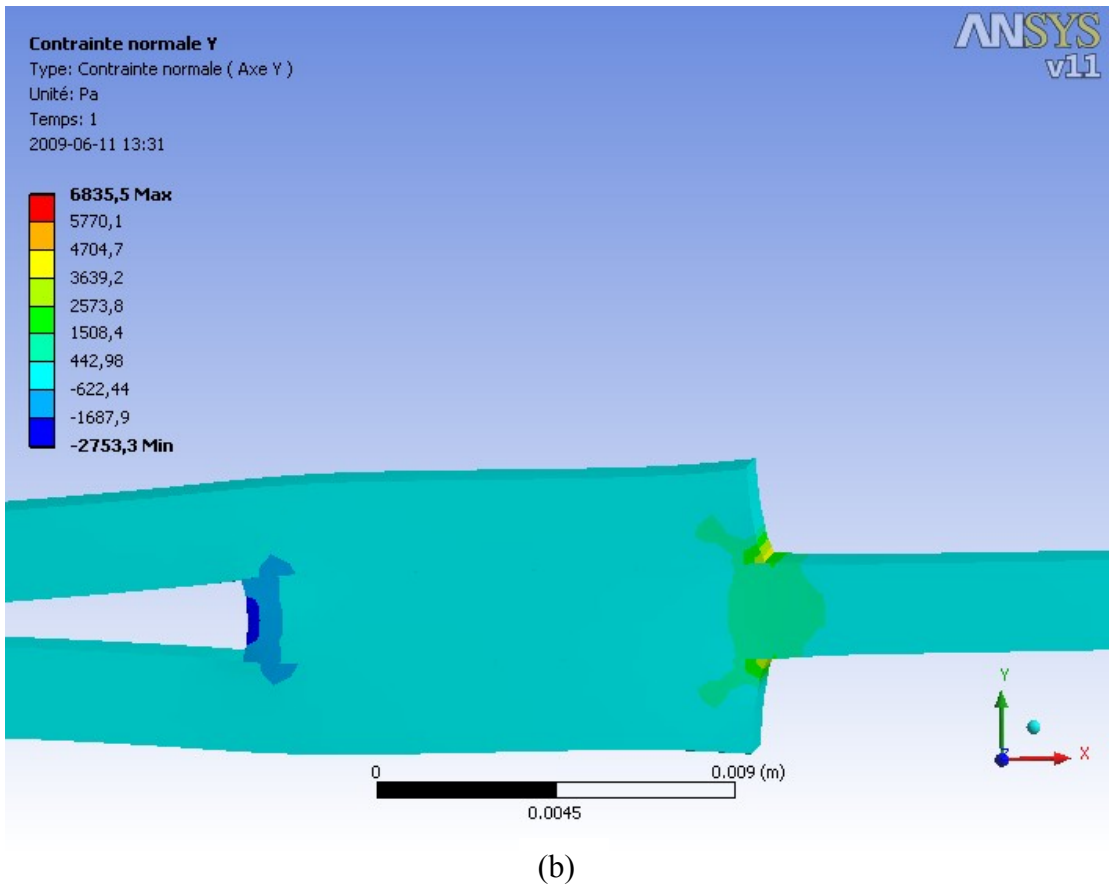


Figure 63: Normal stresses in (a) single-lap joint and (b) double-lap joint

Figure 62 and Figure 63 show the shear stresses and the normal stresses for both configurations. In each case, there is a stress concentration at the edges of the joint. For the single-lap joint, there is symmetry across the centre, while the symmetry is across the mid-plane for the double-lap joint. This is consistent with the geometry and the boundary conditions. The stresses along the overlap were plotted and are shown in Figure 64 and Figure 65, for single-lap and double-lap joints respectively. For normal stresses, in both cases there is a plateau away from the edges where the stresses are close to zero (for double-lap) or in small compression (for single-lap). A peak can be observed at the edges, larger in the case of single-lap joints. A similar plateau is observed for shear stresses away from the edges, where the values are very similar for single-lap and double-lap joint. At the edges they both exhibit a peak, which is again higher in the case of single-lap joint.

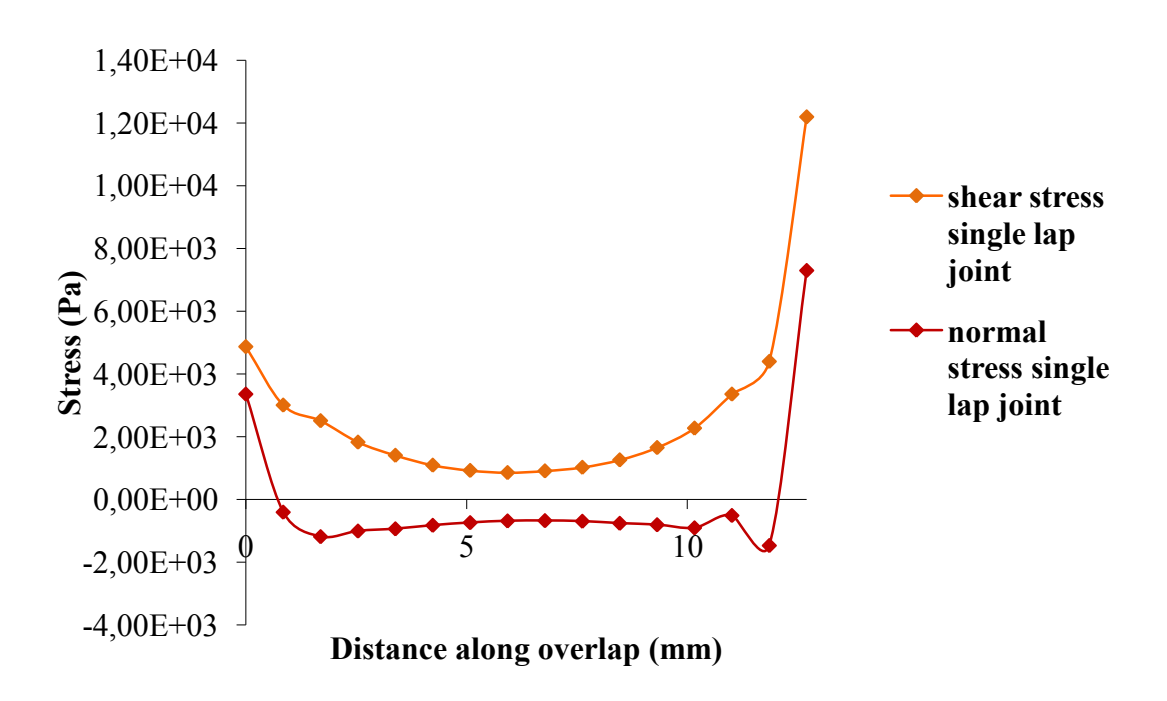


Figure 64: Stresses along the interface for the single-lap joint

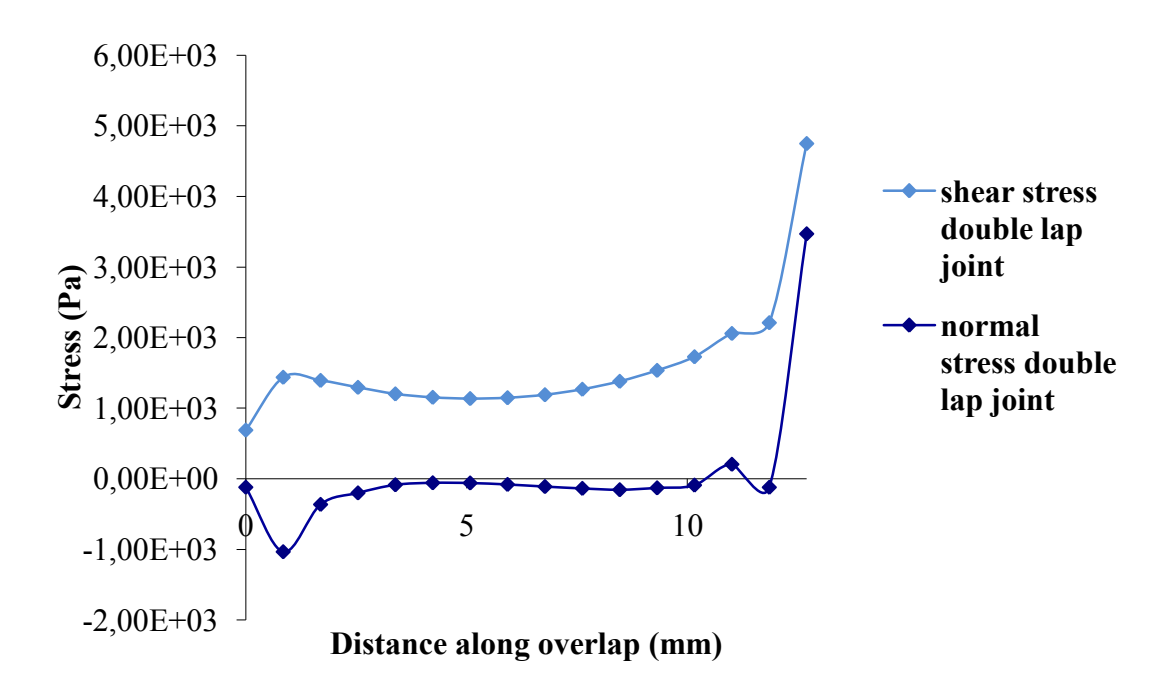


Figure 65: Stresses along the interface for the double-lap joint

These results show that the joint's configuration is critical mainly at the edges of the overlap, where the stresses are the highest and the difference between the two configurations is the largest. However, observations on the welded specimens have also shown that the edges are the place where the joint is the weakest, due to some defects induced by the welding process. The previous simulation assumes a perfect joint, and does not take into account those defects. Consequently, this analysis is not reliable for predicting the actual stress distribution in the resistance-welded joints, and can only give a general idea of the differences between the two configurations in ideal conditions. However, experiments have shown that those differences are not important in the mechanical behaviour of the joints, since both configurations exhibited similar results. The stress analysis was only performed at a macroscopic level, considering a uniform interface. This was acceptable for adhesive bonding, where the interface is an adhesive layer, but not for resistance welding. A much more sophisticated model would be necessary to predict the actual behaviour of the joint,

taking into account the non-uniformity of the weld. Because of the presence of the heating element, the bonding mechanism is very complex, as it relies on both interfacial bonding and mechanical interlocking. The temperature distribution should also be taken into account, as it greatly influences the quality of the bond.

Unlike adhesive joints, peel stresses do not seem to be dominating, even at the edges of the joint. Lower stresses are found for the double-lap configuration, which was to be expected due to the load transfer on the second weld. However, this reduction is of the same order for shear stresses and peel stresses, while in the case of adhesive bonding a significant reduction of the peel stresses would be observed. This could explain why no difference was observed in the mechanical behaviour of resistance-welded single-lap and double-lap joints. However, a more thorough analysis would be required to fully understand the stress distribution.

#### 6 Conclusions and future work

#### 6.1 Conclusions

The static and fatigue behaviour of resistance-welded thermoplastic composite double-lap joints was investigated, and the quality of the weld was characterized.

Observation of the fracture surfaces and the weld interface revealed a good quality of the weld, with good impregnation of the polymer at the interface. The fracture surfaces revealed a good adhesion between the polymer and the fibres, but a weaker one between the polymer and the heating element, showing that the main bonding mechanism was mechanical interlocking. Some samples exhibited unwelded areas at the edge of the overlap, where the bond quality was found to be the poorest.

Resistance-welded double-lap joints were found to have equivalent static and fatigue mechanical properties compared with single-lap joints, for all materials tested. Lap shear strengths of 53 MPa, 49 MPa, 45 MPa and an extrapolated value of 34 MPa were obtained for PEEK/CF, PEKK/CF, PEI/CF and PEI/GF, respectively. Infinite fatigue lives were obtained at 30% for PEEK/CF and PEKK/CF, 25% for PEI/CF and 20% for PEI/GF.

Under static loading, both joint surfaces exhibited interlaminar failure mode.

The only exception was for PEI/GF, where coupon failure was observed, and the material failed before the joint.

The fatigue loading caused one weld to fail first, while the other failure was due to the load redistribution. Like for the static loading, the fracture surfaces revealed an interlaminar failure mode.

**Experimental results from resistance welding were found to be very different from those from adhesive bonding**: in the adhesive case the mechanical performances of the single-lap joints could be improved by using double-lap joints instead. No such improvement could be observed for resistance welding, showing that the process itself influences greatly the failure mechanism.

#### **6.2** Future work

For future work, a more complex model should be developed for resistance-welded joints, taking into account the presence of the heating element and the weld defects due to the non-uniformity of the temperature distribution. This model could be compared with results obtained with adhesive joints.

Interfacial bonding between the heating element and the polymer should be studied and a method of improving it should be developed, in order to improve the joint's strength, which was shown to rely mainly on mechanical interlocking with the actual process.

The heating element being a metallic mesh, it is sensitive to corrosion. The influence of environmental conditions, such as humidity, on mechanical performances of resistance-welded joints should be investigated.

Finally, for semi-crystalline polymers, the influence of crystallinity on the mechanical performances of the joints should be studied. Various cooling rates should be tested and optimized to obtain the best weld's strength.

### References

- 1. Thermoplastic composites gain leading edge on the A380. Gardiner, G. s.l.: High-Performance Composites- Design and Manufacturing Solutions for Industry, 2006, pp. 50-55.
- 2. Methods for fusion bonding thermoplastic composites. Benatar, A. et Gutowski, T.G. 1, s.l.: SAMPE Quarterly, 1986, Vol. 18, pp. 35-42.
- 3. Repair of thermoplastic resin composite by fusion bonding. Xiao, X., Hoa, S.V. et Street, K.N. 1994, ASTM STP 1227, pp. 30–44.
- 4. Experimental investigation of the resistance welding for thermoplastic-matrix composites. Part I: heating element and heat transfer. Ageorges, C., Ye, L. et Hou, M. s.l.: Composites Sciences and Technologies, 2000, Vol. 60, pp. 1027-39.
- 5. Design and manufacture of an automated resistance welder for thermoplastic composites. Lambing, C.L.T., et al. s.l.: ANTEC '91, 1991, pp. 2527–31.
- Scaling Issues in Resistance- Welded Thermoplastic Composite Joints. McKnight,
   H., Holmes, S. T., Gillespie, J. W. JR., Lambing, C. L. T., Marinelli, J. M. 4,
   1998, Advances in Polymer Technology, Vol. 16, pp. 279-295.
- 7. Joining thermoplastic pipes. **Hunt, J.** Feb. 1990, Chemical Engineering, pp. 110-114.
- 8. Welding Processes for Plastics. **Grimm, R. A.** s.l.: Advance Materials and Processes, 1995.
- 9. Resistance welding of thermoplastic composites-an overview. Stavrov, D. et Bersee, H.E.N. s.l.: Composites: Part A, 2005, Vol. 36, pp. 39-54.

- 10. Resistance welding of continuous carbon fiber/polypropylene composites. **Hou, M. et Friedrich, K.** 4, 1992, Plastics rubber and composites processing and applications, Vol. 18, pp. 205-213.
- 11. Resistance welding of graphite polyetheretherketone composites An experimental investigation. Eveno, E. et Gillespie, J.W.J. s.l.: Journal of Thermoplastic Composite Materials, 1988;, Vol. 1, pp. 322-338.
- 12. An experimental study of resistance welding of carbon fibre fabric reinforced polyetherimide (CF fabric/PEI) composite material. **Hou, M., Ye, L. et Mai, Y.W.** 1, s.l.: Applied Composite Materials, 1999, Vol. 6, pp. 35-49.
- 13. Experimental investigation of the resistance welding for thermoplastic-matrix composites. I. Heating element and heat transfer. **Ageorges, C., Ye, L. et Hou, M.** 7, s.l.: Composites Science and Technology, 2000, Vol. 60, pp. 1027-39.
- 14. Resistance welding of carbon fibre reinforced thermoplastic composite using alternative heating element. **Hou, M., et al.** 1-4, 1999, Composite structures, Vol. 47, p. 414.
- 15. The Influence of the Heating Element on Resistance Welding of Thermoplastic Composite Materials. **Stavrov, D., Bersee, H.E.N., Beukers, A.** San Diego , USA : s.n., 2003. Proceedings of the ICCM-14 Conference.
- 16. Experimental Investigation of Resistance Welding of Thermoplastic Composites with Metal Mesh Heating Element. Stavrov, D., Bersee, H.E.N. 2004.
- 17. Resistance Welding of Continuous Fibre Reinforced PPS Composites with Metal Mesh Heating Element. Stavrov, D., Bersee, H.E.N., Beukers, A. Belfast, Northern

- Ireland, UK: s.n., 2005. International Conference on Innovation and Integration in Aerospace Sciences.
- 18. Metal mesh heating element optimisation in resistance welding of thermoplastic composites. **Dubé, M., et al.** s.l.: Composites Part A: Applied Science and Manufacturing, 2007.
- 19. Experimental characterization of processing-performance relationships of resistance welded graphite/polyetheretherketone composite joints. Don, R.C., Gillespie, J.W. Jr. et Lambing, C.L.T. 9, s.l.: Polymer engineering and science, 1992, Vol. 32.
- 20. Experimental investigation of large-scale welding of carbon fiber thermoplastic composite materials. **Stavrov, D.**, **Bersee**, **H.E.N.**, **Beukers, A.** San Diego: Proceedings of ICCM-14 Conference, July (2003). ID-1552.
- 21. **Talbot, E.** *Manufacturing process modelling of thermoplastic composite resistance welding.* s.l.: McGill University. Dept. of Mechanical Engineering. Thesis, 2005.
- 22. Handbook of plastics joining: a practical guide. s.l.: Plastic Design Library, 1997.
- 23. **Xiao, X. R., Hoa, S. V., and Street, K. N.** Processing Modelling of Resistance Welding of APC-2 Composite. *Journal of Composite Materials*. 1992, Vol. 26, 7.
- 24. Experimental investigation of the resistance welding for thermoplastic-matrix composites. Part II: optimum processing window and mechanical performance.

  Ageorges, C., Ye, L. et Hou, M. s.l.: Compos Sci Technol, 2000, Vol. 60, pp. pp. 1191–1202.

- 25. Progress in joining advanced materials. Fernie, J.A., Threadgill, P.L. et Watson, M.N. s.l.: Welding Metal Fabricat, 1991, pp. pp. 179–184.
- 26. Resistance welding of continuous carbon fibre/polypropylene composites. **Hou, M. et Friedrich, K.** s.l.: Plast, Rubber, Compos Process Appl, 1992, Vol. 18.
- 27. Resistance welding of continuous glass fiber-reinforced polyethylene composites. **Hou, M. et Friedrich, K.** 3, s.l.: Compos Manufact, 1992, Vol. 3.
- 28. Resistance welding of graphite-polyarylsulfone/polysulfone dual-polymer composites. **Howie, I., Gillespsie, Jr. J.W. et Smiley, J.** 205±25, s.l.: J Thermoplast Compos Mater, 1993, Vol. 6.
- 29. A New approach for joining plastics and composites to metals. Wise RJ, Watson MN. s.l.: Proceedings of the 50th Annual Technical Conference, ANTEC'92, 1992. p. p. 2113±6.
- 30. *Joining thermoplastic lined steel pipe*. **Taylor, NS.** s.l.: Proceedings of the 52nd Annual Technical Conference, ANTEC'94, 1994. p. p. 1356±9.
- 31. Strength of aluminum and glass reinforced polypropylene sandwich single lap joints. **McKnight SH, McBride M, Gillespie Jr. JW.** s.l.: Proceedings of the Eighth Technical Conference of the American Society for Composites, 1993. pp. p. 419-30.
- 32. Resistance heated fusion bonding of carbon fibre/PEEK composites and 7075-T6 aluminium. McKnight SH, Holmes ST, Gillespie Jr. JW, Lambing CLT, Marinelli. s.l.: Proceedings of the 51st Annual Technical Conference, ANTEC'93, 1993. pp. p. 1474-9.

- 33. Resistance Welding of Metal/Thermoplastic Composite Joints. Ageorges, C. et Ye, L. 6, s.l.: Journal of Thermoplastic Composite Materials, 2001, Vol. 14, pp. 449-475.
- 34. Application of thermoplastic resistance welding techniques to thermoset composites. **Don, R.C., et al.** s.l.: Proceedings of the 52nd Annual Technical Conference, ANTEC 94, 1994. pp. p. 1295-7.
- 35. Resistance welding of thermosetting composite/thermoplastic composite joints.

  Ageorges, C. et Ye, L. 11, s.l.: Composites. Part A, Applied science and manufacturing, 2001, Vol. 32, pp. 1603-1612.
- 36. Resistance welding of thermoplastic composites skin/stringer joints. **Dubé, M., et al.** 12, s.l.: Composites Part A: Applied Science and Manufacturing, 2007, Vol. 38, pp. Pages 2541-2552.
- 37. Fatigue failure characterisation of resistance-welded thermoplastic composites skin/stringer joints. **Dubé, M., et al.** 4, s.l.: International Journal of Fatigue, 2009, Vol. 31, pp. 719-725.
- 38. Processing and performance of resistance welded thermoplastic composites. **Bastien, L., Don, R.C., Gillespie, J.W.** Washington DC, USA: Proceedings of the 45th Annual Conference, 1990.
- 39. Fusion bonding of thermoplastic composites by resistance heating. Don, R.C., Bastien, L., Jakobsen, T.B., Gillespie, J.W. s.l.: SAMPE Journal, 1990. Vol. 26, pp. 59-66.

- 40. Process Optimization of Resistance-Welded Thermoplastic Composites Using Metal Mesh Heating Elements. Yousefpour, A., et al. Long Beach, USA: SAMPE, 2005.
- 41. The resistive implant welding of thermoplastic composite materials. . Taylor, N.S., Davenport, R. Montreal, Canada: Proceedings of the 49th Annual Technical Conference, 1991.
- 42. Joining Methods for Graphite/PEEK Thermoplastic Composites. Silverman, E.M., Griese, R.A. s.l.: SAMPE Journal, 1989. Vol. 25, pp. 34-38.
- 43. Fatigue performance characterisation of resistance-welded thermoplastic composites. **Dubé, M., et al.** 7-8, s.l.: Composites Science and Technology, June 2008, Vol. 68, pp. 1759-1765.
- 44. The torque transmission capabilities of the adhesively-bonded tubular single lap joint and the double lap joint. **Ho Choi, J. et Gil Lee, D.** 3, s.l.: The Journal of adhesion, 1994, Vol. 44, pp. 197-212.
- 45. Fatigue behaviour and damage evolution of single lap bonded joints in composite material. Quaresimin, M. and Ricotta, M. s.l.: Composites Science and Technology, 2006, Vol. 66, pp. pp. 176–187.
- 46. Techniques to reduce the peel stresses in adhesive joints with composites.

  Adams, R. D., Lucas da Silva F. M. 3, s.l.: International journal of adhesion & adhesives, 2007, Vol. 27, p. 227.
- 47. The effect of geometry on the fracture of adhesive joints. Papini, M., Fernlund, G. et Spelt, J.K. 1, s.l.: International Journal of Adhesion and Adhesives, 1994, Vol. 14.

- 48. **Kalpakjian, S.** *Manufacturing Engineering and Technology.* New York: Addison-Wesley, 1992.
- 49. Strength of joints involving composites. Adams, R. D., Davies, R. Yokohama, Japan: Adhesion science and technology: proceedings of the International Adhesion Symposium, November 6-10, 1994.
- 50. Investigation of Joints in Advanced Fibrous Composites for Aircraft Structures.

  Hawley, A. V. et Lehman, G. M. s.l.: AFFDL-TR-69-43, 1969, Vol. 1.
- 51. Influence of environmental and geometric parameters on the behavior of fastener joints in advanced composites. Parida, B. K., Prakash, R. V., Mangalgiri, P. D., Vijayaraju, K. s.l.: Composite Materials: Fatigue and Structure, 1997, Vol. 6.
- 52. Adhesive Bonding of Polymer Composites. Vinson, J. R. 19, s.l.: POLYMER ENGINEERING AND SCIENCE, 1989, Vol. 29.
- 53. Designing to Minimize Peel Stresses in Adhesive-Bonded Joints. Hart-Smith, L J. Pittsburgh, Pennsylvania; USA: Delamination and Debonding of Materials, 8-10 Nov. 1983.
- 54. **Hollaway, L.** *Polymers and Polymer Composites in Construction.* s.l.: Thomas Telford, 1990.
- 55. **Minford, J. Dean.** Handbook of aluminum bonding technology and data. 1993: CRC Press.
- 56. **HANDBOOK, DEPARTMENT OF DEFENSE.** *COMPOSITE MATERIALS HANDBOOK.* Vol. VOLUME 3. POLYMER MATRIX COMPOSITES
  MATERIALS USAGE, DESIGN, AND ANALYSIS.

- 57. Adhesive-bonded double-lap joints. Hart-Smith, L. J. s.l.: NASA, CR-112235, 1973.
- 58. Adhesive-bonded single-lap joints. **Hart-Smith, L. J.** s.l.: NASA, CR-112236., 1973.
- 59. **Tong, L., Steven, G. P.** *Analysis and Design of Structural Bonded Joints.* s.l.: Kluwer Academic Publishers, 1999.
- 60. Die Niektraftverteiling in Zugbeanspruchten mit Konstanten Laschenquerschritten. Volkersen, O. s.l.: Luftfahrtforschung, 1938, Vol. 15, pp. 41-47.
- 61. Adams, R.D. and Wake, W.C. Structural adhesive joints in engineering. s.l.: Elsevier Applied Science Publishers, 1984.
- 62. The strength of glued joints. **De Bruyne, N. A.** s.l.: Aircraft Engineering, 1944, Vol. 16, pp. 115-118.
- 63. The stresses in cemented joints. Goland, M. et Reissner, E. s.l.: Journal of Applied Mechanics, 1944, Vol. 11, pp. A17-A27.
- 64. *Improved theoretical solutions for adhesive lap joints.* **Tsai, M.Y., Oplinger, D.W. et Morton, J.** 12, s.l.: International journal of solids and structures, 1998, Vol. 35, pp. 1163-1185.
- 65. Analysis and design of advanced composite bounded joints . Hart-Smith, L. J. s.l.: NASA-CR-2218, 1974.
- 66. Critical joints in large composite aircraft structure. Nelson, W. D., Bunin, B. L. et Hart-Smith, L. J. s.l.: NASA-CR-3710, 1983.

- 67. Optimized Bolted Joint. Hart-Smith, L. J., Bunin, B. L. et Watts, D. J. s.l.: NASA LAR-13250, 1986.
- 68. Adhesive-bonded scarf and stepped-lap joints . **Hart-Smith, L. J.** s.l. : NASA, CR-112237, 1973.
- 69. **W., Oplinger. D.** *A layered beam theory for single lap joints.* s.l.: Army Materials Technology Laboratory Report MTL TRY 1-23., 1991.
- 70. Stress analysis of adhesive-bonded lap joints. Adams, R.D., Peppiatt, N. A. 3, s.l.: The Journal of Strain Analysis for Engineering Design, 1974, Vol. 9.
- 71. A finite element model of single-lap adhesive joints. Lin, C. C. et Lin, Y. S. 12, s.l.: International Journal of Solids and Structures, 1993, Vol. 30, pp. 1679-1692.
- 72. An evaluation of analytical and numerical solutions to the single-lap joint. **Tsai, M. Y. and Morton, J.** 18, s.l.: International Journal of Solids and Structures, 1994, Vol. 31, pp. 2537-2563.
- 73. Improved theoretical solutions for adhesive lap joints. Tsai, M.Y., Oplinger, D.W. et Morton, J. 12, s.l.: International journal of solids and structures, 1998, Vol. 35.
- 74. *Analysis of overlaminated double-lap joints*. **Osnes, H., McGeorge, D.** 6-7, s.l.: Composites Part B: Engineering, 2005, Vol. 36, pp. 544-558.
- 75. **Béland, S.** High performance thermoplastic resins and their composites. s.l.: Park Ridge, N.J.: Noyes Data Corp.,, 1990.
- 76. Polymers, High Temperature. *Ulmann's Encyclopedia of Industrial Chemistry*. s.l.: Wiley, 2003.

- 77. **Biron, M.** Thermoplastics and thermoplastic composites: technical information for plastics users. s.l.: Butterworth-Heinemann, 2007.
- 78. The Enthalpic Relaxation of Amorphous Poly(Aryl Ether Ketone)s. **Browne, M. M. et Goodwin, A. A.** 1, s.l.: High Performance Polymers, 1997, Vol. 9.
- 79. Carbon molecular sieve membranes from polyetherimide. Fuertes, A.B. et Centeno, T.A. s.l.: Microporous and Mesoporous Materials, 1998, Vol. 26, pp. 23–26.
- 80. Cooling rate influences in carbon fibre/PEEK composites. Part 1. Crystallinity and interface adhesion. **Gao, S. et Kim, J-K.** 2000, Composites: Part A, Vol. 31, pp. 517–530.
- 81. Fatigue performance characterization of resistance-welded thermoplastic composites. **Dubé, M., et al.** 7-8, s.l.: Composites Science and Technology, June 2008, Vol. 68, p. 1759.
- 82. *High-Performance Polymers*. **Herold, F. et Schnelle, A.** 3, s.l.: Advanced Materials, 2004, Vol. 4, pp. 143 152.
- 83. Thermoplastic Composite Materials Handbook. s.l.: CYTEC Fiberite Inc, Anaheim, CA, 1999.
- 84. **Strong, A. Brent.** *High performance and engineering thermoplastic composites.* s.l.: Lancaster, Pa.: Technomic Pub. Co., 1993.
- 85. Carlsson, Leif A. Thermoplastic composite materials. s.l.: Amsterdam; New York: Elsevier; New York, NY, USA: Distributors for the U.S. and Canada, Elsevier Science Pub. Co., 1991.

- 86. **Mallick, P. K.** Fiber-reinforced Composites: Materials, Manufacturing, and Design. s.l.: CRC Press, 1993.
- 87. **Aström, B.T.** *Manufacturing of Polymer Composites.* s.l.: Chapman & Hall, 1997.
- 88. Welding of High-Performance Thermoplastic Composites. Rudolf, R., Mitschang, P., Neitzel, M. and Rueckert, C. 5, s.l.: Polymer and Polymer Composites, 1999, Vol. 7, pp. 309–315.
- 89. **Rajiv S. Mishra, Murray W. Mahoney.** Friction Stir Welding and Processing. s.l.: ASM International, 2007.
- 90. Benefits of Induction Welding of Reinforced Thermoplastics in High Performance Applications. Nichols, Val A. Kagan and Russell J. 13, 2005, Journal of Reinforced Plastics and Composites, Vol. 24, pp. 1345-1352.
- 91. Microwave Joining and Repair of Composite Materials. Varadan, V.K. and Varadan, V.V. 7, 1991, Polymer Engineering and Science, Vol. 31, pp. 470–486.
- 92. Adhesive bonding of polymer composites. Vinson, J.R. 19, s.l.: Polymer engineering and science, 1989, Vol. 29, pp. pp. 1325-1331.
- 93. McGrath, G. Materials Information Service, edited by Justin Furness.
- 94. *Microwave welding of thermoplastics*. **Wise, R. J., Froment, I. D.** 2001, JOURNAL OF MATERIALS SCIENCE, Vol. 36, pp. 5935 5954.
- 95. Friction stir welding: Recent developments in tool and process technologies. Thomas, W.M., Johnson, K. I. et Wiesner, C. S. 6, 2003, Advanced engineering materials, Vol. 5, pp. 485-490.

- 96. Fusion Bonding/Welding of Thermoplastic Composites. Yousefpour, A., i Hojjati, M. et Immarigeon, J-P. 2004, Journal of Thermoplastic Composite Materials.
- 97. **Ageorges, C. et Ye, L.** Fusion bonding of polymer composites: from basic mechanisms to process optimisation. s.l.: Springer, 2002.
- 98. Impulse resistance welding: a new technique for joining advanced thermoplastic composite parts. Arias, M. et Ziegmann, G. s.l.: 41st International SAMPE Symposium and Exhibition., 1996. pp. 41(2): 1361–1371.
- 99. Friction-stir welding of a beryllium-aluminum powder metallurgy alloy. Contreras, F., Trillo, E. A. et Murr, L. E. s.l.: Journal of materials science, 2002, Vol. 37, pp. 89-99.
- 100. Grewell, David A., Benatar, Avraham et Park, Joon B. Plastics and composites welding handbook. s.l.: Hanser, 2003.
- 101. Joining and repair of a carbon fibre-reinforced thermoplastic. Davies, P., et al.6, s.l.: Composites, November 1991, Vol. 22.
- 102. Current leakage prevention in resistance welding of carbon fibre reinforced thermoplastics. **Dubé, M., et al.** 6, s.l.: Composites Science and Technology, May 2008, Vol. 68, pp. Pages 1579-1587.
- 103. Fusion Welding Techniques for Plastics. **Grimm, R. A.** s.l.: Welding Journal, 1990, pp. pp. 23-28.
- 104. RF Welding of PVC and Other Thermoplastic Compounds. Leighton, J., Brantley, T. et Szabo, E. 3, September 1993, Journal of vinyl technology, Vol. 15.

105. Induction welding of thermoplastic composites—an overview. Ahmed, T.J., et al. 2006, Composites: Part A, Vol. 37, pp. 1638–1651.

106. Joining Methods for Plastics and Plastic Composites: An Overview. **Stokes, V. K.** No. 19, Mid-October 1989, Polymer engineering and science, Vol. 29.